

**AN INVESTIGATION INTO 5-LOBE LUNG
MODELLING**

By

VUONG Xuan Tung

**A Thesis Submitted in Partial Fulfilment of the Degree of
Master of Engineering**



Auckland University of Technology

Auckland, New Zealand

June, 2005

ACKNOWLEDGEMENTS

I would like to thank my supervisor Professor Ahmed Al-Jumaily for his guidance and assistance during the preparation of this thesis. I really appreciate his consistently helpful attitude and being such a patient supervisor. In particular, I would like to thank Professor Al-Jumaily again for providing valuable support, encouragement and knowledge during my time to study this course. I also wish to thank his great teaching during two years in my Master study. I have learnt so much from this course.

I wish to thank all the lecturers, students and all people who take part in the Master of Engineering programme. Especially I wish to thank Jennie Walters, Heather Stonyer and Benneth Gilbert for their support and help during my hard time in New Zealand. I would like to thank Dr Pui Ming Au and Prasika Inderjeeth Manilal and Youhua Du for their helpful support. All people in the Diagnostic & Control Research Centre, I also want to thank you all for being such good friends to me.

I wish to give my most sincere appreciation to my family at home and overseas. Without their support, I will not have the strength to go this far in my life. Thank you, Father, Mum, Uncle Tony Thang Vuong, Uncle Binh Vuong, Auntie Julie Phuong Vuong, and Auntie Hong Vuong who always stay behind me for everything. Finally, I would wish to thank my dear girlfriend for her support and contribution to this thesis. Without you I would not be the person as I am right now.

ABSTRACT

To understand how the input impedance of the respiratory system relates to pressure and volume airflow of the airway branched structure, this thesis focuses on developing a mathematical model of the branched airway including trachea and branching airways. The 5-Lobe lung model is developed mathematically and experimentally. A computer model is constructed in the MatlabTM programming environment. It accounts for the effects of airways with varying cross-sectional area, flexible wall properties, and the bronchial tree within the lung using the mathematical methods developed in previous researches. The terminal impedances are determined by proposed idealized lobe models. A range of frequencies up to 256 Hz are tested on this model. Cases of study on obstructions by varying lung stiffness from healthy to unhealthy conditions are investigated.

Mathematical model is validated by experiment investigations on the mechanical lung simulator, which is built in Diagnostic & Control Research Centre at Auckland University of Technology. The results conclude that mathematical methods used in this research are capable to produce predictable results of the input impedance.

TABLE OF CONTENTS

ACKNOWLEDGEMENTS	iii
ABSTRACT	iv
LIST OF FIGURES	viii
LIST OF TABLES	x
STATEMENT OF ORIGINALITY	xi
NOMENCLATURE	xii
1. INTRODUCTION	1
1.1 Background.....	1
1.2 Motivation.....	1
1.3 Mechanics of Breathing.....	3
1.4 General Consideration	3
1.5 Overview of Various Approaches	4
1.5.1 <i>Forced Oscillation Technique</i>	4
1.5.2 <i>Acoustic Reflection Methods</i>	5
1.5.3 <i>Dynamic of the Airway Modelling</i>	6
1.5.4 <i>The Electrical Transmission-line Approach</i>	7
1.5.5 <i>Summary</i>	7
1.6 Overview of Modelling Approach Implemented in this Research.....	8
1.7 Aims and Outline of the Thesis.....	8
2. MATHEMATICAL MODELLING	10
2.1 Introduction.....	10
2.2 Airways Dynamic.....	12
2.3 5- Lobe Lung Model.....	14
2.4 Idealized Lobe Model.....	15
2.5 The Conducting Airway Dynamic Model	18
2.6 Case Study - Obstruction Investigations	22
2.7 Physical Parameters for the Mathematical Simulations	23
2.8 Summary.....	23
3. EXPERIMENT INVESTIGATION	24
3.1 Introduction.....	24
3.2 Lung Simulator.....	24
3.2.1 <i>Lung Simulator Setup</i>	26

3.2.2	<i>5-Lobe Lung Simulation</i>	28
3.2.3	<i>Equipment and Instrumentation</i>	29
3.3	Experimental Procedure.....	33
3.4	Sample Results of Experiment Procedure	33
3.5	Effects on the Lung Simulator at Different Operation Frequencies.....	34
3.6	Obstruction Effects on the Lung Simulator	34
3.7	Comments about Experimental Equipment	45
3.8	Summary.....	45
4.	INPUT IMPEDANCE RESULTS	46
4.1	Introduction.....	46
4.2	Input Impedance Results.....	47
4.2.1	<i>Mathematical Input Impedance at Normal Conditions</i>	47
4.2.2	<i>Experimental Input Impedance at Normal Conditions</i>	48
4.2.3	<i>Experimental Input Impedance at Different Exciting Frequencies</i>	49
4.2.4	<i>Summary</i>	49
4.3	Obstruction Investigations	53
4.3.1	<i>One-Lobe Obstruction</i>	53
4.3.2	<i>Two- Lobe Obstruction</i>	54
4.3.3	<i>Three -Lobe Obstruction</i>	56
4.3.4	<i>Four- Lobe Obstruction</i>	57
4.3.5	<i>Five- Lobe Obstruction</i>	58
4.4	Experiments on Obstruction Investigation	64
4.5	Summary.....	66
5.	OVERALL DISCUSSION	67
5.1	Introduction.....	67
5.2	Comparison at healthy condition	68
5.3	Obstruction Investigation.....	71
5.4	Summary.....	74
6.	CONCLUSIONS AND FUTURE WORK	75
6.1	Conclusion	75
6.2	Future Work	76
	REFERENCES	77
	APPENDICES	81
	APPENDIX A MATHEMATICAL EQUATIONS	82
	APPENDIX B MATLAB PROGRAM	85

APPENDIX C	FFT TRANSFORM	93
APPENDIX D	EXPERIMENT RESULTS	95
APPENDIX E	EXPERIMENT INPUT IMPEDANCE RESULTS.....	130

LIST OF FIGURES

Figure 2.1: Single Compartment Lung Model	11
Figure 2.2: The two compartment Lung Model	11
Figure 2.3: A single compliant tube	12
Figure 2.4: 5-lobe Lung Model	14
Figure 2.5: Idealised Mass-Spring-Dashpot Lobe Model.....	15
Figure 3.1: Schematic Diagram of the Lung Simulator.....	25
Figure 3.2: A picture of the Lung Simulator.....	25
Figure 3.3: Mechanical Lung Simulator	27
Figure 3.4: A schematic of the tested-airways.	28
Figure 3.5: Picture of five-lobe airways is used in the lung simulator	28
Figure 3.6: Pressure transducer is used in the Lung Simulator.....	29
Figure 3.7: The actual setup of the Pressure Sensors in the Lung Simulator.....	30
Figure 3.8: The custom made Thermal Flow Meter is used in the Lung Simulator.....	30
Figure 3.9: Electronic Cards setup to obtain air velocity at 5-Lobe Lung Model.....	31
Figure 3.10: The in-house custom made Wheatstone Bridge is used in the Lung Simulator.	31
Figure 3.11: Power Spectrum of measured impedance up to 256 Hz	35
Figure 3.12: Power Spectrum of the impedance at lobe R1 measured at different exciting frequencies up to 1 Hz	36
Figure 3.13: Power Spectrum of the impedance at lobe R2 measured at different exciting frequencies up to 1 Hz	37
Figure 3.14: Power Spectrum of the impedance at lobe R3 measured at different exciting frequencies up to 1 Hz	38
Figure 3.15: Power Spectrum of the impedance at lobe L1 measured at different exciting frequencies up to 1 Hz.....	39
Figure 3.16: Power Spectrum of the impedance at lobe L2 measured at different exciting frequencies up to 1 Hz.....	40
Figure 3.17: Power Spectrum of the experiment impedances of the lung simulator measured by increasing stiffness of each lobe respectively	41
Figure 3.18: Power Spectrum of the Impedance of 5-lobe lung simulator when increasing stiffness at lobe R1 and R2	42
Figure 3.19: Power Spectrum of the Impedance of the 5-lobe lung simulator when increasing stiffness at lobe R1, R2 and R3.....	43

Figure 3.20: Power Spectrum of the Impedance of the 5-lobe lung simulator when increasing stiffness at lobe R1, R2, R3 and L1.....	44
Figure 4.1: Normalized Input Impedance of the mathematical model determined for normal conditions.....	50
Figure 4.2: Normalized Input Impedance of the experiment investigations determined for normal conditions	51
Figure 4.3: Normalized Input Impedance of the experiment investigations determined at varied exciting frequencies up to 1 Hz.....	52
Figure 4.4: Normalized Input Impedance determined by increasing stiffness to unhealthy condition at each lobe respectively	59
Figure 4.5: Normalized Input Impedance determined by increasing stiffness to unhealthy condition at every two lobes respectively	60
Figure 4.5 (Continues): Normalized Input Impedance determined by increasing stiffness to unhealthy condition at every two lobes respectively	61
Figure 4.6: Normalized Input Impedance determined by increasing stiffness to unhealthy condition at every three lobes respectively	62
Figure 4.7: Normalized Input Impedance determined by increasing stiffness to unhealthy condition at every four lobes respectively.....	63
Figure 4.8: Normalized Input Impedance determined by increasing stiffness to unhealthy condition at all five lobes.	64
Figure 4.9: Normalized Input Impedance of the experiment investigations determined by increasing stiffness at each lobe respectively	65

LIST OF TABLES

Table 2.1: Geometric and Mechanical Properties of the Simulated Lung Model	23
Table 3.1: Equipment's details of the lung simulator	32
Table 5.1: Comparison between the predicted resonances for the mathematical model simulated by different range of frequencies	69
Table 5.2: Comparison between measured resonances for the experiment five-lobe model recorded by different sampling rates	69
Table 5.3: Comparison between resonances of the lung simulator measured at different exciting frequency	70
Table 5.4: Comparison between predicted and measured resonances of the five-lobe models as measured at normal breath cycle.	70
Table 5.5: Comparison between predicted and measured resonances of the five-lobe models as measured at different exciting frequencies.....	71
Table 5.6: Summary and Comparison between the resonances for one-lobe obstruction and predicted models.....	72
Table 5.7: Summary and Comparison between the resonances for the two-lobe obstruction and predicted simulations.....	73
Table 5.8: Summary and Comparison between the resonances for three-lobe obstruction and predicted simulations	73
Table 5.9: Summary and Comparison between the resonances for four-lobe obstruction and predicted models.....	74
Table 5.10: Summary and Comparison between the resonances for five-lobe obstruction and predicted models.....	74

STATEMENT OF ORIGINALITY

'I hereby declare that this submission is my own work and that, to the best of my knowledge and belief, it contains no material previously published or written by another person nor material which to a substantial extent has been accepted for the qualification of any other degree or diploma of a university or other institution of higher learning, except where due acknowledgment is made in the acknowledgments.'

..... (signed)

..... (date)

NOMENCLATURE

A_i	Cross-sectional area of the airway [m^2] where $i=1:9$ is airway number.
A_o	Airflow cross-sectional area [m^2]
B	Damping ratio of the lobe material [N/m^2]
C	Compliance of the lung wall [m^3/Pa]
E	Elasticity of the balloon [N/m^2]
$F(t)$	Exciting force [N]
$H(s)$	Laplace transfer function
ρ_o	Initial steady-state fluid mass density [kg/m^3]
I	Inertance of the lung wall [kg/m^2]
K	Lobe stiffness [N/m^2]
K_w	Tube wall elastance [N/m^2]
L	Tube length [m]
L_i	airway length [m], where $i=1:9$ is airway number.
M_B	Fluid bulk modulus [N/m^2]
M	Mass of the lobe [kg]
$P(t)$	Pressure change in time of one compartment model [N/m^2]
P_a	Initial steady-state pressure or atmosphere pressure [N/m^2]
p_o	Atmosphere pressure at room temperature [N/m^2]
P_L	Output pressure [N/m^2]
P_o	Input pressure [N/m^2]
$P_{pleural}$	Pressure exerted by motion of thoracic [N/m^2]
Q	Volume flow rate [m^3/s]
r_o	inside radius of the airway [m]
R	Resistance of the pipe wall [N/m^2]
s	Laplace transform variable
t_w	Tube wall thickness [m]
V	Volume of the lung [m^3]
V_L	Output velocity [m^2/s]
V_o	Input velocity [m^2/s]
x	Displacement [m]
Z	Impedance of the lobe [Pa/m^3s^{-1}]
Z_L	Output Impedance [Pa/m^3s^{-1}]

Z_o	Input Impedance [$\text{Pa}/\text{m}^3\text{s}^{-1}$]
\overline{Z}_o	Normalized Input Impedance [$\text{Pa}/\text{m}^3 \text{s}^{-1}$]
\overline{z}_s	Characteristic impedance [$\text{Pa}/\text{m}^3 \text{s}^{-1}$]
ω	Exciting frequency [rad/s]
ω_n	Tube wall natural frequency [rad/s]
ω_1	Tube wall natural frequency when air-filled [rad/s]

CHAPTER 1

1. INTRODUCTION

1.1 Background

Measurement of the input impedance of the lung system helps to identify the dynamic characteristics of the respiratory system. Based on those characteristics, scientists can determine whether the lung is healthy or not. An example of an unhealthy respiratory is asthma. It is a breathing disorder that arises from conditions where the airway passages are obstructed by either inflammation or allergy, which results in very large input impedance. The airway constriction causes airflow restriction and breathing difficulties.

In addition to its usefulness in modelling and simulation, this research focuses on developing appropriate measuring techniques to determine the input impedance of the respiratory system. This chapter covers a brief literature review that forms the backbone of this paper. First, a brief overview of studies of the respiratory system is provided. Second, the specific modelling approaches undertaken by researchers are summarised. Last but not least, this chapter will also give a synthetic overview of the literature on acoustic impedance measurement of the respiratory system and the methods which have been used recently.

1.2 Motivation

The study of the human respiratory system has attracted a lot of attention from science in response to many diseases which relate to respiratory disorders. Research on the lung system in terms of changing airflow or pressure in and out the human body; or in terms of dynamic behaviours of the properties of the wall tissues and smooth muscles, have led researchers in several directions. For many years, researchers used different approaches to gain a better understanding of the acoustic impedance processes within

the lung system. Early research on the modelling of the respiratory system focused on the flow resistance and pressure drop characteristics across the airway passages but did not include airway narrowing into the models [1-3]. Several researchers have attempted to model the respiratory system as branching networks and analysed the dynamics of input impedance response [4-20]. Al-Jumaily and Mithraratne [4] have developed a theoretical acoustical model for the respiratory system based on the Weibel's symmetric model [21]. They found a significant influence of the dynamic characteristics and response of an elastic tube on analysing occlusions in the lung system. Al-Jumaily and Al-Saffar [5] have also extended the model developed by Fredberg [6] to study the dynamic of the lung system. They included the effect of the wall inertia to study the dynamic response of the respiratory system measured at the trachea. In addition, Al-Jumaily and Al-Fakhri [7, 8] have developed a mathematical model to study the influence of elastance variation on the respiratory system dynamics. In their paper, they used the acoustical approach to determine the impedance at the throat using impedance recursion formulas for both symmetric and asymmetric structure to consider the response of the lung system when wall properties vary. They cited that "*the overall normalised input impedance frequency spectrum could be used to give a reasonable signature for identifying such abnormality*", [8]. Al-Jumaily and Du [9] have modelled and simulated the airways for identifying and detecting obstruction. The results demonstrated that the input impedance resonant frequencies are associated with the locations of the obstruction with its degree of severity in any of the airway branches. Previously, Fredberg and Hoenig [10] developed an efficient method for computing the input impedance and resonant frequency of asymmetrically branching networks. They computed the input impedance and resonant frequencies to simulate the dynamic response of the normal lung of adult humans up to 10,000 Hz. The results showed that in the high frequency range, there were differences between the input impedance of symmetric and asymmetric models. There were, however, similarities in the lower frequency range. Fredberg and Moore [6] presented a distributed model of the complex branching networks to simulate the response of asymmetric branching networks. The simulations were carried out to investigate the characteristic response of the airway models with regard to input impedance, frequency, lung pressure and volume. The results were later verified by Fredberg *et al* [11] on excised canine lungs.

The above literature shows that it is very important to study and recognize behaviours of the dynamics of a tube system or in other words, the airway system. However, the

various models mentioned above have their own limitations. As a result, until now no comprehensive acoustic model of the complete respiratory system has been fully understood.

In the physical aspect, airways are a series of branched tubing from the main tube or the trachea goes down to the bronchioles [22]. It ends with the alveolar sacs where gas exchange takes place. Science convinces that the airway network should act or behave similar to any physical system and has its own natural frequencies of vibration at which it responds spontaneously once excited. Therefore, it is logical to comprehend that identifying the natural frequency characteristics of the complex branching structure based on measuring the input impedance is an important speculation of perhaps utilising mechanical relaxation for relief airway disorders [23]. However, it is necessary to study the physical structure of the lung to get a better understanding of the lung during its operation.

1.3 Mechanics of Breathing

In breathing, the mechanical system energies are generated by the respiratory muscles movements, which in turn are controlled by the higher central nervous system via the intercostals and phrenic nerves [24]. Although most breathing is involuntary, it may be voluntarily by taking “a *deep breath, hold the breath, cough, sneeze, speak, sing or use the chest muscles to lift heavy objects*” [24].

During inspiration, the diaphragm contracts and the rib cage expands, these motions increase the volume of the thorax. By Boyle’s law, this causes pressure at the alveoli to fall below atmospheric pressure [25]. And since airflow occurs when there is a difference in pressure, air flows in through the nose or mouth. The air travels down the trachea into the bronchial tree filling and expanding the alveolar sacs. During exhalation, the opposite process occurs. Beginning with a relaxation of the inspiratory muscles, the volume of the thorax decreases and the alveolar pressure increases. When the alveolar pressure exceeds the atmospheric pressure at the mouth, expiration starts.

1.4 General Consideration

Impedance can be considered as the response of a specific passive system to a harmonic excitation [26]. In acoustics the particular impedance is defined as the ratio of the pressure and the particle velocity at a given point. As the particle velocity is a quantitative vector, the impedance depends on the direction of this vector. This quantity

is mainly used in a free field or in cavities. In tubes, the following definition is preferred: “*the acoustical impedance at any cross-section of the tube is the ratio of the mean pressure and the volume flow rate at the cross-section.*” [26].

$$Z = \frac{P}{V} \quad (1.1)$$

One may distinguish between input impedances, for which both quantities are considered at the same point, and transfer impedances for which the two quantities are considered at two different points. An example is a resonator, which can be seen as a one-port passive linear acoustic system. The input impedance is sufficient to describe its behaviour. In a passive linear N- element there is a relation between the pressure P_i on each side and the volume flow rate V_j , where i and j are port numbers ($i,j=1$ to N), which can be written in a matrix form:

$$[Z_{i,j}] = \frac{\{P_i\}}{\{V_j\}} \quad (1.2)$$

Where: $\{P_i\}$ and $\{V_j\}$ are N-vectors containing the pressures and volume flow rate at each point.

1.5 Overview of Various Approaches

Several techniques have been used to measure respiratory properties, such as the Forced Oscillation Technique, Acoustic Reflection technique, Dynamics of the airway modelling and Transmission- line method. In this section, an overall discussion of the various methods and applications are presented.

1.5.1 Forced Oscillation Technique

The Forced Oscillation Technique (FOT) is a non-invasive method which is to measure respiratory mechanics [27]. The technique employs low-amplitude pressure oscillations superimposed on the normal breathing to study the mechanical properties of the respiratory system [28]. Respiratory resistance and elastance are then computed from pressure and flow recorded at the airway opening under the assumption that the contribution of the patient’s respiratory muscles is zero, so that airway pressure coincides with transpulmonary pressure. This technique is again based on the application of a small pressure oscillation

(about 2 cmH₂O) at the airway opening by means of an external generator [29]. Otis et al [30] use an alveolar capsule oscillation technique to measure the input impedance, lobe volume and trans-pulmonary pressure. Using the results, they were able to determine the lobe pressure and volume at the airways closure and reopening.

1.5.2 Acoustic Reflection Methods

In the acoustic study of the human respiratory system, several types of acoustic reflection measurements have proved practically valuable. It also is a non-invasive approach and is commonly known as the acoustic reflection method using either one or two microphones scheme [31-35]. This method is based on the principle of acoustic wave propagation and reflection in a duct which involves sound waves. This acoustic reflection method gives the longitudinal cross-sectional area profile along the airway. This is a useful method in understanding the structure and function of the airways. Jackson et al [36] used this method to conduct a research of area profiles of excised dog tracheas and lungs measured. They modelled the airway as a series of discontinuously joined cylindrical segments of equal length but differing cross-sectional area and hence, differing impedance. They designed a reflector-meter where a sound pulse created by a spark discharge was applied to the airway via source tube. Reflections were generated at the boundaries between the cylindrical segments. It then returned from the airway and reflected signals were recorded by a microphone which is embedded in the wall of the source tube. After the first reflected sound pulse passed the microphone, they carried on up the source tube. At this point, they were reflected by the sound source and again returned to the microphone. The distance between the source tube and location of the microphone ensured that at the microphone the airway reflections and source reflections did not overlap. The input impulse response of the airways was determined by de-convoluting the airway reflection with the input pulse shape. (The de-convolution was carried out by performing a frequency analysis). Fredberg et al [37] were believed to be the first to measure human patients. They used a measurement system that was more complicated compared to the system used by Jackson et al [36]. In this system, a sound pulse produced by a loudspeaker was applied to the airway via a five meter long source tube. At this time, the tube was filled with a gas mixture of He and O₂. The reflected signals

returned from the airways were recorded through a microphone in the wall of the source tube.

1.5.3 Dynamic of the Airway Modelling

Simulation models have been extensively used in breathing mechanics in order to develop a new model or technique to study static and dynamic properties of the lung system. Studies of the input impedance of the complex airway networks, which depends on pressure change over volume flow rate, are mainly used to reveal dynamic characteristic of the airway system. However, since breathing is an unsteady process that varies in pressure, flow rate and volume due to inspiration and expiration, therefore, an appropriate simulation model is needed to study dynamic behaviour of the respiratory system. Schmid-Schoenbein and Fung [17, 18] developed a distributed model with multi degree of freedom to study the respiratory system as a continuous elastic body. The lung dynamic characteristics were simulated as a simple lumped mass-spring-dashpot model. This model consists of dynamic airways, lung parenchyma, chest wall, diaphragm and abdomen. They concluded from this study that a continuum model is more realistic and dynamic characteristics of the respiratory system could be obtained to interpret various pulmonary diseases. Fredberg and co workers [6, 10-15] investigated the dynamic characteristics of the trachea-bronchial tree under various conditions. Fredberg and Moore [6] presented a mathematical model to simulate the distributed response of asymmetric branching networks. Simulations were carried out on the human lung to investigate the response of pressure with frequency, path and position. The model included mechanical in-homogeneities from origin to terminations as well as parallel ways. Some other researchers have focused on modelling constrictions in the respiratory system. For example, Tang *et al* [38] designed a mathematical function to specify the shape of a contraction and developed Navier-Stokes equations for fluid flow in constricted tubes. They used the boundary iteration numerical method to get the dynamic response of a system and justified the results experimentally. Elad *et al* [39] developed a semi-empirical equation of a pressure –area relationship for the bronchial airways. Halpern and Grotberg [40, 41] used the Navier-Stokes equations and associated lubrication theory to investigate the thin film of Newtonian fluid coating the inner surface of an elastic circular tube. They analysed the effects of initial film thickness, surface tension of the air-liquid interface and modulus of elasticity of

the wall on meniscus formation and compliant collapse. The results showed that the airway closure occurs more rapidly with increasing unperturbed film thickness, surface tension, wall flexibility and decreasing wall damping. Margolis and Tabrizi [42] presented a method to investigate dynamics of the lung using ‘bond graphs’. The model included the distributed dynamics of the proximal airway such as trachea and main bronchi, while the distal generations are represented by lumping of resistance and compliance effects. The model was capable of simulating dynamic characteristics of the system for frequencies as high as 8500 Hz. They also claimed that “*with some modifications the model can predict the input-output relation between the mouth and any desired lung segment location*” [42].

1.5.4 The Electrical Transmission-line Approach

Many researchers have chosen this method to study the airway dynamic or to understand how respiratory sounds relate to pulmonary anatomy and respiratory airflow or to determine respiratory parameter properties. For many years, speech researchers have used this method to have a better understanding of the acoustical processes within the vocal tract during speech [43]. Ginaluca Nucci and colleagues [44] developed the model in time domain to evaluate the impact of different ventilator strategies as well as constrictive pathologies on the time course of acinar pressures and flows. They simplified the original Horsfield structure [45] to model a binary tree structure including a trachea, wall compliance, laminar resistance, small airways and alveolar compartments. They concluded that this model is capable to investigate realistically the effect of homogeneous versus heterogeneous constrictive pathologies and the impact of different ventilatory patterns on pressure and flow distribution at the acinar level in the mechanically ventilated patient.

1.5.5 Summary

In summary, all these techniques discussed above have shown very positive signals to scientist in terms of modelling of trachea-bronchial tree. A number of mathematical models have been proposed to describe the airway mechanics in healthy airways as well as unhealthy airway networks. Experimental investigations also reported that simplified model of the lung can be modelled based on measurement of dynamic characteristics of the respiratory system such

as input impedance, pressure-volume relationship by either fitting data methods or empirical correlations between variables. Even though the airway mechanical properties have been included in some acoustical models to determine the dynamic characteristics of the airways, none of these studies have made an attempt to a complete simulation model that can be used to determine healthy and unhealthy lungs. In particular, none of the above references have modelled as a 5-Lobe lung model, which reflects to a realistic lung. This indicates that the study of the respiratory system is still a potential area in the future.

1.6 Overview of Modelling Approach Implemented in this Research

To understand how the impedance of the respiratory system relates to pressure and airflow of the airway branched structure, this thesis focuses on developing a mathematical model of the branched airway including trachea and branching airways within the lung. The model accounts for the effects of airways with varying cross-sectional area, flexible wall properties, and the bronchial tree within the lung using the mathematical methods that have been developed in some previous researches [4, 5, 7, 8 and 9]. The research focuses on developing a realistic 5-Lobe model of the respiratory system. The results are then compared with some experimental investigations on a mechanical lung simulator developed for the purpose of validation.

1.7 Aims and Outline of the Thesis

The aims of the present thesis are:

1. To develop a mathematical 5- Lobe Model representing the actual lung.
2. To use a mechanical 5-Lobe Lung Simulator to accurately measure the input impedance of a tested bronchial tree.
3. To compare the measured values to the theoretical values to validate the lung simulator.
4. To investigate the effects of changing lung properties on the input impedance response.

The structure of this research is as follows. Chapter 2 contains a detailed discussion of the basic theory behind the techniques. The information of the input impedance

response of the compliant tube is described, along with various mathematical equations for calculating input impedance.

A practical lung simulator is presented in Chapter 3. The experimental determination of impedance response of each lobe is described. An experimentally determined input impedance response in various parameters is also described and discussed. In Chapter 4, the results of input impedance calculated from the mathematical model and experimental investigations are presented, together with a brief discussion of the effect of change in lung wall parameters. Chapter 5 analyses the results obtained in Chapter 4 in more depth.

Finally, Chapter 6 will make the concluding remarks in light of the completed work and provide some ideas for future development.

CHAPTER 2

2. MATHEMATICAL MODELLING

2.1 Introduction

The respiratory system can be considered as a physical model, which consists of a collection of physical components interacting with one another and with the environment. In reality, most real life systems, such as the respiratory system in this case, are complex and non-linear, but they can be simplified to linear models under certain conditions. A linear model has useful properties that make analysis easier. The simplest model of the complex respiratory system is assumed as a single compartment connected to a pipe representing the trachea [46] as shown in figure 2.1.

The relationship between the pressure applied at the opening of the model $P(t)$ and the volume in the model $V(t)$ during emptying of this balloon can be described as a first order equation as follows [46]:

$$P(t) = EV(t) + R\dot{V}(t) \quad (2.0)$$

Where E is the elastance of the balloon, R is the resistance of the pipe and $\dot{V}(t)$ is the flow rate through the opening. Using regression analysis one can calculate E and R from $P(t)$, $V(t)$ and $\dot{V}(t)$. If this model is considered as the respiratory system, the values of R and E reflect the resistance of the airways and the elasticity of the respiratory system, whereas $V(t)$ is the volume increase from functional residual capacity i.e. where $P(t)$ at mouth opening is zero. In other words, the passive deflation of the respiratory system is characterised by a volume-time profile determined by E and

R. However, many in-vivo measurements show that modelling the respiratory system as a single compartment is too crude and require further improvement.

Many investigations have modelled the lung with more than one compartment as it is shown in figure 2.2. This model can be found in many research papers. For example, Otis [47] had used this model to study the relationship between the compliance and frequency. Wanner *et als* [48] used this model to study the relationship between the frequency and the lung compliance. He claimed that “*the non-invasive N_2 washout test is capable of predicting the ratio of dynamic compliance and static compliance and at the same time gives a direct measure of gas distribution*”, [48]. However, 5-Lobe lung model has not been found in the previous literature and seems more logical due to the fact that an actual lung consists of five lobes, two in the left and three in the right.

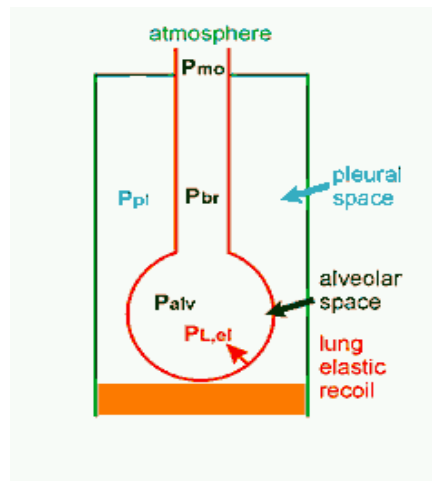


Figure 2.1: Single Compartment Lung Model

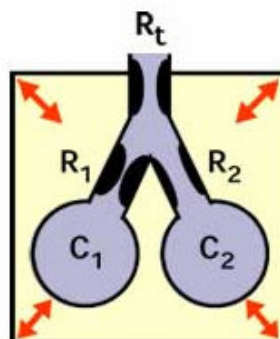


Figure 2.2: The two compartment Lung Model

In the following sections a 5-Lobe lung model is developed. The model consists of two important components: the airways dynamic and the lung dynamic.

2.2 Airways Dynamic

Figure 2.3 shows a compliant tube which resembles an airway passage conveying an acoustic wave travelling alongside the tube with an input pressure P_o and velocity V_o , respectively. The wave undergoes partial reflection and partial transmission at each change in cross-sectional area along the tube's bore, creating a reflection sequence and transmission sequence. The transmission sequence picked up by measurement instrument at the terminal point results in a pressure P_L and velocity V_L . The input and output impedance Z_o and Z_L can be defined respectively as:

$$Z_o = \frac{P_o}{A_o V_o} \quad (2.1)$$

$$Z_L = \frac{P_L}{A_o V_L} \quad (2.2)$$

Where A_o is the air flow cross-sectional area.

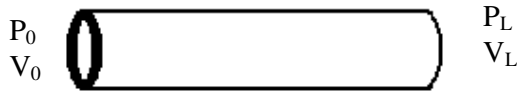


Figure 2.3: A single compliant tube

To understand how the input impedance of the system can be calculated from its pressure and volume flow rate, it is first necessary to understand how the pressure and volume flow rate transmit inside the tube.

In studying the dynamic characteristic of each branch of the respiratory system, one is interested in correlating between the impedance at the inlet and outlet of the branch. Consider a compliant tube with the input and output impedance as defined by equation 2.1 and 2.2. Implementing the following assumptions:

1. One-dimension flow, since the tube radius is much less than the tube length;

2. The fluid is conveyed in an adiabatic environment without friction and work;
3. The tube has constant area in sections other than that at contraction location, except for radial elastic deformation;
4. The tube is not allowed to deform in the longitudinal direction except for perturbation;
5. The radial deformation is very small compared to the tube dimensions.

This will lead to the fact that an acoustic wave is propagating in a compliant tube, transmits to the other end. Applying conservation of mass and energy along the conductive tube with some mathematical manipulations lead to the following relationship [4] (see Appendix A for more details)

$$\begin{bmatrix} V_L \\ P_L \end{bmatrix} = \begin{bmatrix} a_{11} & a_{12} \\ a_{21} & a_{22} \end{bmatrix} \begin{bmatrix} V_0 \\ P_0 \end{bmatrix} \quad (2.3)$$

This matrix generates two equations which correlate between the outlet pressure and velocity with the inlet pressure and velocity, where a_{ij} are elements depending on the fluid and wall properties and given as:

$$\begin{aligned} a_{11} &= \cosh(s \cdot \sqrt{M} \cdot L) \\ a_{12} &= -\frac{\sqrt{M}}{\rho_0} \sinh(s \cdot \sqrt{M} \cdot L) \\ a_{21} &= -\frac{\rho_0}{\sqrt{M}} \sinh(s \cdot \sqrt{M} \cdot L) \\ a_{22} &= \cosh(s \cdot \sqrt{M} \cdot L) \end{aligned} \quad (2.4)$$

The value of parameter M is given by

$$M = \frac{\rho_0 [K_w \cdot s^2 + (K_w + M_B) \cdot \omega_n^2]}{K_w M_B (s^2 + \omega_n^2)} \quad (2.5)$$

Where K_w is the tube wall elastance which is given by [4]

$$K_w = \frac{r_0}{2K} = \frac{E \cdot t_w - p_0 \cdot r_0}{2r_0} \quad (2.6)$$

Where ρ_0 is fluid initial steady-state mass density, M_B is fluid bulk modulus, ω_n is the tube wall natural frequency under initial steady-state pressure, s is Laplace transform variable, r_o is inside radius of a airway, E is wall elasticity of tube material, t_w is wall thickness of the tube and p_o is pressure at initial steady-state boundary.

To determine the relationship between the input and the output impedance in the tube, equation (2.3) can be manipulated to get:

$$Z(0,s) = \frac{P_p(0,s)}{A_0 V_p(0,s)} = \frac{\frac{\rho_0}{\sqrt{M}} \sinh(s\sqrt{M}L) + A_0 Z_L \cosh(s\sqrt{M}L)}{A_0 \left[\cosh(s\sqrt{M}L) + A_0 Z_L \frac{\sqrt{M}}{\rho_0} \sinh(s\sqrt{M}L) \right]} \quad (2.7)$$

Where Z_L is output impedance measured at $x=L$

Equation (2.7) can be used as a governing equation to determine the relationship between the input impedance at $x=0$ and the output impedance at $x=L$.

2.3 5- Lobe Lung Model

An actual human lung consists of five lobes, three to the right and two to the left. To fulfil this resemblance, in this thesis the lung is assumed to be made of five lobes, three to the right R1, R2, R3 and two to the left L1, L2 with conducting airway passage from 1 to 9, see figure (2.4). The basic principle of derivation is based on determining the input impedance in terms of the output impedance for each segment using equation (2.6).

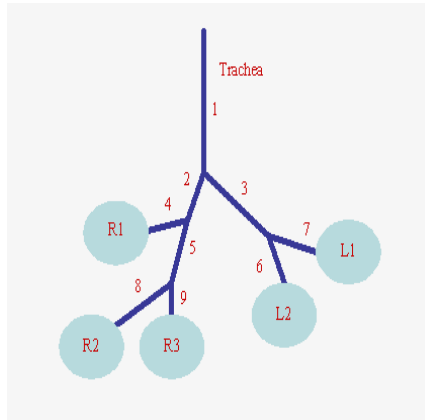


Figure 2.4: 5-lobe Lung Model

The airways model in this thesis is developed from basic principles using the input impedance equations (2.7). Figure 2.4 is the proposed model for the lung. To determine the input impedance at the throat, one has to follow the following procedure:

1. Determine an equivalent impedance at the outlet of each lobe;
2. Use equation (2.7) to determine the impedance at the inlet of each conducting segment in terms of that at the outlet of the segment;
3. Whenever there is a junction, use the parallel law to find the equivalent impedance, namely $Z_L = \frac{Z_1 Z_2}{Z_1 + Z_2}$;
4. Continue to use the recursion format (equation 2.7) until one can get the overall input impedance at the throat.

It is worthy to note that the main reason for determining the main input impedance at the throat is the fact that physically this is the point where measurement is feasible.

2.4 Idealized Lobe Model

Consider an idealized 5-Lobe lung simulator to replicate an actual lung. Each lobe is simulated by an elastic balloon which can be modelled as a mass-spring-dashpot system. During uninterrupted mechanical ventilation, respiratory gas is moved in and out of the lobes. The lobe's mechanics deal with the pressures acting on the lobe and the concomitant changes in pulmonary gas volume produced. The static and dynamic behaviour of the lobe is mathematically described by the equation of motion. Figure 2.5 shows a mechanical system with M, B and K as the equivalent mass, damping and stiffness of the lobe respectively with an application force F, which generates the displacement x . The equation of motion for this lobe is:

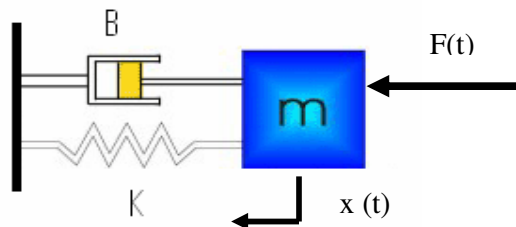


Figure 2.5: Idealised Mass-Spring-Dashpot Lobe Model

$$F(t) = Kx(t) + B \dot{x}(t) + M \ddot{x}(t) \quad (2.8)$$

Equation 2.8 shows that the force F has to overcome three opposition forces related to spring or elasticity, damping factor and inertia. Transferring this model of the linear mechanical system to a three-dimensional mechanical analogue of the lobe in Figure 2.4, position x (or displacement) is expressed as volume V of the lobe gas and force as pressure. The pressure ΔP applied to the lobe is the net pressure exerted by the motion of the lung. The simulated lobe analogue changes its volume when pressure ΔP is applied. In analogy to the linear mechanical system, ΔP has to overcome three opposing pressures related to elasticity, damping and inertia according to Hook's Law, Stoke's Law and Newton's Law respectively. This can mathematically be described by the modifying equation of motion (2.8) to its general form of a lung with one degree of freedom as:

$$A^2 P = KV + B \frac{dV}{dt} + M \frac{d^2V}{dt^2} \quad (2.9)$$

The pressure change in equation 2.9 is equal to pressure difference across the lobe's wall as a driving pressure of the lobe model, it can be determined from the difference between the external pressure and the internal pressure as follows:

$$P = P_a - P_{pleural} \quad (2.10)$$

Where: P_a is atmosphere pressure and $P_{pleural}$ is the pressure exerted by motion of thoracic.

Rearranging equation 2.9, one can get

$$P = I \frac{d^2V}{dt^2} + R \frac{dV}{dt} + \frac{1}{C} V \quad (2.11)$$

Where

- $I =$ inertance of the lung wall $= \frac{M}{A^2} \text{ kg/m}^2$.

- R= resistance of the lung wall = $\frac{B}{A^2}$.
- $\frac{1}{C} = \frac{K}{A^2}$ is elastance of the lung wall.

Equation 2.11 can be rewritten as

$$\frac{V}{P} = \frac{1}{ID^2 + RD + 1/C} \quad (2.12)$$

The Laplace transformation of this time domain equation (2.12) into the corresponding frequency domain ($s = j\omega$) expression is

$$V(s) = \frac{P(s)}{Is^2 + Rs + 1/C} = H(s)P(s) \quad (2.13)$$

$$\text{Where } H(s) = \frac{1}{Is^2 + Rs + 1/C}$$

This is second order system, with the frequency response expressed as

$$H(s) = \frac{1}{\sqrt{\left(1 - \frac{\omega^2}{\omega_n^2}\right)^2 + \left(2\zeta \frac{\omega}{\omega_n}\right)^2}} \quad (2.14)$$

Where ω is exiting angular frequency; ω_n is natural frequency of the lobe's wall properties and ζ is damping factor of the lobe's properties. The values of natural frequency and damping factor are given by

$$\omega_n = \frac{1}{2\pi} \sqrt{\frac{1/C}{M}} \quad (2.15)$$

$$\zeta = \frac{R}{2M\omega_n} \quad (2.16)$$

The volume flow rate is defined as the volume change in time. Therefore, derivation of volume change can be used to determine the volume flow of the lobe as expressed in equation (2.17).

$$Q = \frac{dV}{dt} \quad \text{Or } Q = sV \quad \text{in Laplace Transformation} \quad (2.17)$$

$$V = \frac{Q}{s} \quad (2.18)$$

Substitute equation 2.18 into equation 2.13

$$Q(s) = H(s) * P(s) * s \quad (2.19)$$

The Impedance is defined as a ratio between pressure and volume flow rate

$$Z(s) = \frac{P(s)}{Q(s)} \quad (2.20)$$

Substituting this into equation 2.19, the impedance transfer function is determined as

$$Z(s) = \frac{1}{H(s) * s} = Is + R + \frac{1}{Cs} \quad (2.21)$$

$$\text{Or } Z = \frac{Ms^2 + Bs + K}{A^2s} \quad (2.22)$$

Equation 2.22 is used in MatlabTM programming to calculate the terminal impedance. For lobes R1, R2, R3, L1 and L2, the impedances at the inlet of the lobes are defined by Z_{R1} , Z_{R2} , Z_{R3} , Z_{L1} and Z_{L2} respectively. These input impedances are calculated in the following section.

2.5 The Conducting Airway Dynamic Model

The airway simulation system in this thesis is shown in figure 2.4, which includes a trachea passage (1) which is branched into two daughter bronchia tubes, one on the right (2) and one on the left (3). The one on the right (2) branches to conducting tubes (4) and (5). The conducting airway (5) then branches into termination airways, which are numbered (8) and (9). However, conducting passage (3) on the left of the airway,

branches to termination airways number (6) and (7). The terminal impedance can be determined by equation 2.22. Using equation 2.7, for each individual passage at the termination of the airways, the input impedance may be expressed as follows:

Input impedance of segment number 4 in terms of the impedance of lobe R1 can be expressed as

$$Z_{o,4} = \frac{\frac{\rho_0}{\sqrt{M_4}} \sinh(s\sqrt{M_4}L_4) + A_4 Z_{L,4} \cosh(s\sqrt{M_4}L_4)}{A_4 \left[\cosh(s\sqrt{M_4}L_4) + A_4 Z_{L,4} \frac{\sqrt{M_4}}{\rho_0} \sinh(s\sqrt{M_4}L_4) \right]} \quad (2.23)$$

Where $Z_{L,4} = Z_{R1}$ is the terminal impedance according to equation 2.22.

Similarly, Input impedances of tube number 6, 7, 8, 9 are expressed as

$$Z_{o,6} = \frac{\frac{\rho_0}{\sqrt{M_6}} \sinh(s\sqrt{M_6}L_6) + A_6 Z_{L,6} \cosh(s\sqrt{M_6}L_6)}{A_6 \left[\cosh(s\sqrt{M_6}L_6) + A_6 Z_{L,6} \frac{\sqrt{M_6}}{\rho_0} \sinh(s\sqrt{M_6}L_6) \right]} \quad (2.24)$$

$$Z_{o,7} = \frac{\frac{\rho_0}{\sqrt{M_7}} \sinh(s\sqrt{M_7}L_7) + A_7 Z_{L,7} \cosh(s\sqrt{M_7}L_7)}{A_7 \left[\cosh(s\sqrt{M_7}L_7) + A_7 Z_{L,7} \frac{\sqrt{M_7}}{\rho_0} \sinh(s\sqrt{M_7}L_7) \right]} \quad (2.25)$$

$$Z_{o,8} = \frac{\frac{\rho_0}{\sqrt{M_8}} \sinh(s\sqrt{M_8}L_8) + A_8 Z_{L,8} \cosh(s\sqrt{M_8}L_8)}{A_8 \left[\cosh(s\sqrt{M_8}L_8) + A_8 Z_{L,8} \frac{\sqrt{M_8}}{\rho_0} \sinh(s\sqrt{M_8}L_8) \right]} \quad (2.26)$$

$$Z_{o,9} = \frac{\frac{\rho_0}{\sqrt{M_9}} \sinh(s\sqrt{M_9}L_9) + A_9 Z_{L,9} \cosh(s\sqrt{M_9}L_9)}{A_9 \left[\cosh(s\sqrt{M_9}L_9) + A_9 Z_{L,9} \frac{\sqrt{M_9}}{\rho_0} \sinh(s\sqrt{M_9}L_9) \right]} \quad (2.27)$$

Where $Z_{L,6}=Z_{L2}$ is terminal impedance at lobe L2; $Z_{L,7} = Z_{L1}$ is terminal impedance at lobe L1, $Z_{L,8} = Z_{R2}$ is terminal impedance at lobe R2 and $Z_{L,9}= Z_{R3}$ is terminal impedance at lobe R3.

The impedance at the junction for tube number 8 and 9 is determined by following equation:

$$\frac{1}{Z_{0,5}} = \frac{1}{Z_{0,8}} + \frac{1}{Z_{0,9}} \quad \text{or} \quad Z_{L,5} = \frac{Z_{0,8} * Z_{0,9}}{Z_{0,8} + Z_{0,9}} \quad (2.28)$$

The input impedance of tube 5 is considered using equation 2.7:

$$Z_{0,5} = \frac{\frac{\rho_0}{\sqrt{M_5}} \sinh(s\sqrt{M_5}L_5) + A_5 Z_{L,5} \cosh(s\sqrt{M_5}L_5)}{A_5 \left[\cosh(s\sqrt{M_5}L_5) + A_5 Z_{L,5} \frac{\sqrt{M_5}}{\rho_0} \sinh(s\sqrt{M_5}L_5) \right]} \quad (2.29)$$

At the junction between tubes 4 and 5, the equivalence impedance is obtained from equation 2.30:

$$Z_{L,2} = \frac{Z_{0,4} * Z_{0,5}}{Z_{0,4} + Z_{0,5}} \quad (2.30)$$

At the junction between tubes 6 and 7, similar approach to calculate the equivalence impedance to get

$$Z_{L,3} = \frac{Z_{0,6} * Z_{0,7}}{Z_{0,6} + Z_{0,7}} \quad (2.31)$$

Using equation 2.7, the input impedances at tube 2 and 3 is determined by

$$Z_{0,2} = \frac{\frac{\rho_0}{\sqrt{M_2}} \sinh(s\sqrt{M_2}L_2) + A_2 Z_{L,2} \cosh(s\sqrt{M_2}L_2)}{A_2 \left[\cosh(s\sqrt{M_2}L_2) + A_2 Z_{L,2} \frac{\sqrt{M_2}}{\rho_0} \sinh(s\sqrt{M_2}L_2) \right]} \quad (2.32)$$

$$Z_{o,3} = \frac{\frac{\rho_0}{\sqrt{M_3}} \sinh(s\sqrt{M_3}L_3) + A_3 Z_{L,3} \cosh(s\sqrt{M_3}L_3)}{A_3 \left[\cosh(s\sqrt{M_3}L_3) + A_3 Z_{L,3} \frac{\sqrt{M_3}}{\rho_0} \sinh(s\sqrt{M_3}L_3) \right]} \quad (2.33)$$

The impedance at the junction for the trachea is determined by:

$$Z_{L,1} = \frac{Z_{o,2} * Z_{o,3}}{Z_{o,2} + Z_{o,3}} \quad (2.34)$$

Finally, use equation 2.7 again to obtain the input impedance of the airways system

$$Z_{o,1} = \frac{\frac{\rho_0}{\sqrt{M_1}} \sinh(s\sqrt{M_1}L_1) + A_1 Z_{L,1} \cosh(s\sqrt{M_1}L_1)}{A_1 \left[\cosh(s\sqrt{M_1}L_1) + A_1 Z_{L,1} \frac{\sqrt{M_1}}{\rho_0} \sinh(s\sqrt{M_1}L_1) \right]} \quad (2.35)$$

The frequency spectrum of equation 2.35 can be determined by replacing s with $j\omega$. For general applications, as for this research, the normalized input impedance is calculated as [4]:

$$\bar{Z}_0 = \frac{Z_0}{z_s} \quad (2.36)$$

Where \bar{z}_s is the tube characteristic impedance, which can be calculated by [4]:

$$\bar{z}_s = \frac{1}{A_0} \sqrt{\frac{M_B \rho_0}{|H|}} \quad (2.37)$$

Which

$$H = \frac{\omega_1^2 - \omega^2}{\omega_0^2 - \omega^2} \quad (2.38)$$

ω_0 is tube's wall natural frequency, ω_1 is the tube's wall natural frequency when air-filled and ω is exciting frequency. The following equations express the value of the tube's wall natural frequency in terms of mechanical properties.

$$\omega_0^2 = \frac{K_w}{M_w} \quad \text{and} \quad \omega_1^2 = \frac{K_w + M_B}{M_w} \quad (2.39)$$

Where M_w is the tube wall linear density (kg/m), K_w is tube wall elastance and M_B is fluid bulk modulus.

A MatlabTM computer program is developed to calculate the input impedance of the 5-Lobe lung model (see Appendix B). The results are given in Chapter 4.

2.6 Case Study - Obstruction Investigations

Equation 2.22 shows that the impedance is depending on the material properties such as inertance, elastance and resistance. Any change of these properties variable will introduce the changes in calculating the terminal impedance. The aim of this section is to determine the effect of an introduced occlusion by changing the lung wall stiffness. The lung wall stiffness was varied from healthy value $k=6$ KPa to unhealthy value of 110 MPa [49]. The results are used to compare with the experiment investigation in Chapter 3.

The simulation is performed at different lobe of the mathematical 5-Lobe model. The effective terminal impedance is calculated in MatlabTM programming software and saved as M.fig file for further inspection. The results of this investigation are later presented in Chapter 4. The steps of setting in this investigation as follows:

1. One-Lobe Obstruction: each lobe is set to be obstructed respectively at each experiment, otherwise is assumed to be at normal conditions;
2. Two-Lobe Obstruction: by introducing obstruction at every two lobes at the same time, the rests are assumed to be at normal conditions;
3. Three-Lobe Obstruction: increasing occlusion by three lobes at the same time, the rests are assumed to be at normal conditions;
4. Four-Lobe Obstruction: four lobes are made to be occlusive, only one lobe is left at normal conditions;

5. Five-Lobe Obstruction: total five lobes are obstructed.

2.7 Physical Parameters for the Mathematical Simulations

Researches of modelling the terminal impedance have taken different approaches from the one described in section 2.4. They assumed that the terminal impedance is a combination of the lung impedance and thoracic impedance [4-9]. However, in this research, a simple modal analysis for each lobe described in section 2.4 is used. Formulas for these parameter values are summarized in section 2.4 with the material properties for soft tissues and airway wall given in Table 2.1. Here, in this case, experiment is taken the value from measurement and the fact that the lobe is made of rubber. Therefore, parameter's values of the lobe are provided as follow [9]:

- $M=0.04$ Kg: mass of the lobe, taken from measurement.
- $\zeta =0.4$: damping factor of the rubber [49]
- $R=20$ Kg/s [49].

Table 2.1: Geometric and Mechanical Properties of the Simulated Lung Model [9]:

Airways Number	Length (m)	Radius (m)	Elastance (kN/m ²)
1	0.12	0.01	6000
2	0.10	0.008	6000
3	0.1	0.006	6000
4	0.08	0.005	6000
5	0.08	0.004	6000
6	0.08	0.003	6000
7	0.08	0.002	6000
8	0.07	0.002	6000
9	0.07	0.002	6000

2.8 Summary

Mathematical equations have been developed for the 5-Lobe Model. The experiment investigations are set up in the following chapter for 5-Lobe practical model using a lung simulator to determine the system dynamic behaviours at every lobe stiffness variation of the lung model and to study the effect of terminal impedance at different breathing conditions. Comparisons will be made in Chapter 4 and 5 to validate the results between the mathematical and experiment investigations.

CHAPTER 3

3. EXPERIMENT INVESTIGATION

3.1 Introduction

The theoretical method described in Chapter 2 clearly cannot be validated in vivo. The use of the input impedance needs to be verified in order to support this theoretical model. Therefore, to measure the input impedance of the actual lung, a practical lung simulator is developed and built. The construction and operation of such a lung simulator is described in this chapter. A clear validation methodology in measuring the input impedance is discussed and samples of the results are presented.

The aim of this experiment is to collate and obtain the necessary data for validation of the mathematical model. The lung model has been built at the Diagnostic and Control Research Centre of Auckland University of Technology [50]. The model is aimed to scrutinise the volume flow and pressure change in the airway when the lung simulator is operating. Therefore, the impedance at each individual branch assumed to be terminal impedance is calculated. The spectrum of the terminal impedances are then presented in this chapter.

3.2 Lung Simulator

In order to validate the theoretical modelling, an experimental lung simulator is needed to include as many realistic factors as possible. The lung simulator is designed, calibrated and ready to use. The system allows to measure air velocity and pressure at desired locations (terminal locations). The air velocity value can be used to determine the volume flow rate by multiply with cross-sectional area of the tube. It also allows measuring the compliance of the tested lung. Figure 3.1 and Picture 3.2 show a simple

schematic diagram and a picture of the lung simulator used in this study. The main components of the simulator are:

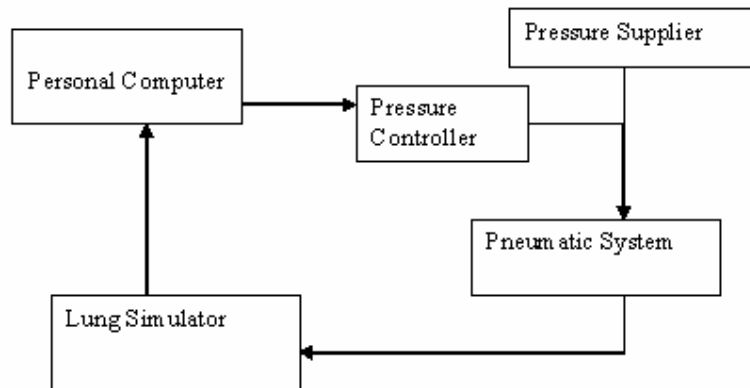


Figure 3.1: Schematic Diagram of the Lung Simulator

A personal computer is to communicate with the lung simulator and to supply the input breathe cycle as well as to receive the information from each individual sensor. A pressure control valve is used to supply the required air pressure from the air supply to the simulator. A pneumatic cylinder is used as the main driving force of the lung simulator. The simulator itself resembles the actual lung environment in pressure and elasticity content.

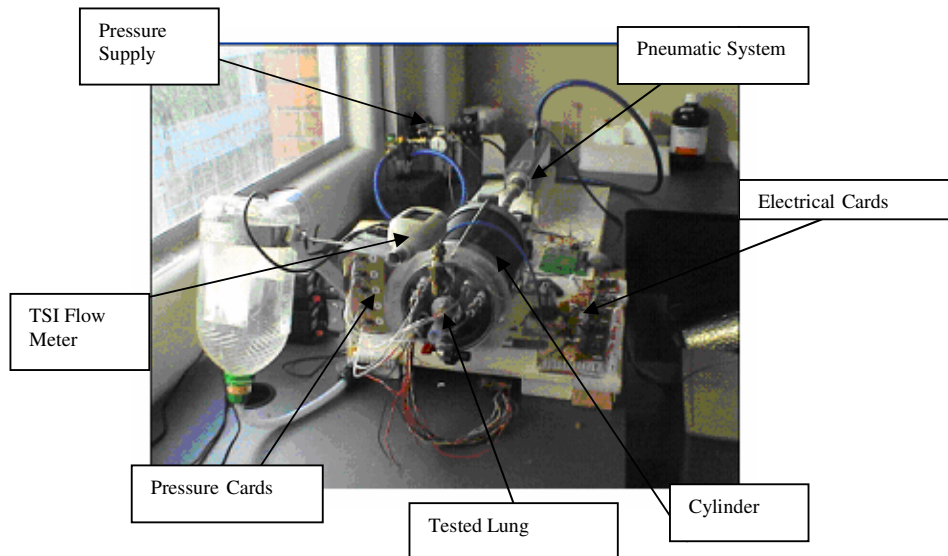


Figure 3.2: A picture of the Lung Simulator

3.2.1 Lung Simulator Setup

The basic principle of operation of the lung simulator (Figure 3.2) is to issue a breath cycle command from the computer using LabView™ to a control valve, which allows air to enter a pneumatic drive in accordance with certain modes. Once the actuator starts, it will drive the piston inside the cylinder which resembles the lung. The cylinder is filled with water to replicate the lung environment. Figure 3.3 gives a schematic representation of the mechanical system together with the actuators, interface electronics, low-level position controllers and the controlling computer. The real-time controller of the entire system has been implemented in LabView 6.1(National Instrument, New Zealand) installed on a Personal Computer. The Computer Control (1)* with a Data Acquisition (2) generates the analogue output signals with a volume reference (V_{ref}). The pneumatic system (3) is then driven by the output signals and its motion dynamically changes the volume inside the pneumatic cylinder (5). The piston position is measured using the encoder as a feedback to the system (4). The change in volume of the cylinder creates a negative pressure inside the chamber, which is the driving force to generate the pressure change and airflow in the tested-lung (6). This pressure change is measured by the pressure sensor (7). The flow is measured by TSI flow- meter (model 4043) (8) as pressure drops over the tested-lung. The accuracy of the TSI flow-meter is recorded as 2% of the reading or 0.05 Std l/min. It also monitors the temperature and the static pressure. In-house designed of electrical cards (9) and pressure transducers (10) are used to measure air velocity and pressure drop respectively at the terminal locations inside the tested-lung.

The output signals from the tested-lung, together with the signals representing the changes of the airways pressure are recorded via a LabView™ program and stored on the computer hard disk. All the data is given in time domain and will be ready for analysis.

* Numbers refer to elements in Figure 3.3

3.2.2 5-Lobe Lung Simulation

The tested-lung is in-house custom made. It includes five balloons (Figure 3.5) are connected to the terminal link of the airways. The tree-like airways (figure 3.4) consist of a trachea (1) branches into two daughter branches to simulate the primary bronchi (tubes 2 and 3). The two daughters again branch into two as it shows in the figure (3.4).

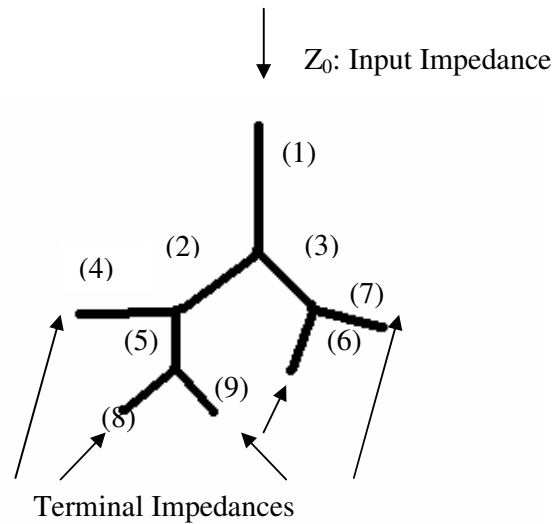


Figure 3.4: A schematic of the tested-airways.

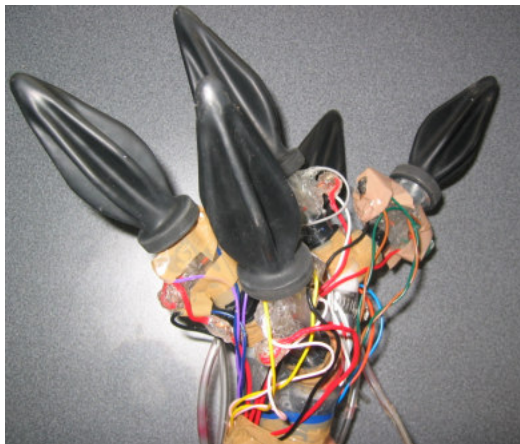


Figure 3.5: Picture of five-lobe airways is used in the lung simulator

A realistic lung has five lobes, three in the right side and two in the left. To simulate that, five balloons with the specifications given are used. These balloons are normally manufactured to simulate lungs and were supplied by

Fisher & Paykel Healthcare Ltd. They have the necessary stiffness and elasticity for resemblance. Each one of the balloons is connected to a tube (4, 8, 9, 6, and 7) which simulates a conducting airway. Each two of the airways is joined to form a parent (3, and 5), then parent (5) is joined with airway (4) to form a new parent (2). This process continues until the airway reaches to the main stem (1) which representing the trachea. See Figure 3.4.

3.2.3 Equipment and Instrumentation

The test lung simulator is equipped with in-house custom designed and built measurement devices. These devices measure the values of air flow and pressure in both directions at terminal link of the test-airways. The lung simulator is connected to a Personal Computer, through a control system. A pressure transducer is connected to the cylinder to measure the values of the lung pressure changes against the room pressure. TSI Flow meter is used to measure the total flow in and out of the tested-lung. In-house custom designed electrical cards are used to capture the air velocities at five lobes as well as five pressure transducers are used to measure the pressure change inside each one of the lobes. A detailed list of the equipment used to conduct the experimental investigation is listed in Table 3.1.

The pressure change is measured using a pressure transducer connecting to the cylinder. As the system operates, the sensor detects a change in pressure from inside of cylinder. This is used to calculate the total volume flow in and out of the cylinder. Figure 3.6 shows the pressure transducer used in this investigations and Figure 3.7 shows the actual setup of the actual pressure measurement in the lung simulator.



Figure 3.6: Pressure transducer is used in the Lung Simulator

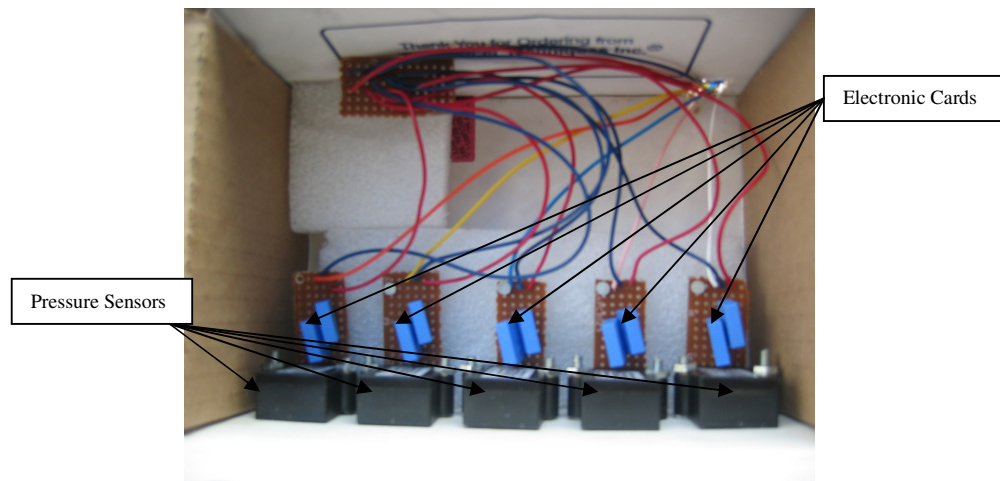


Figure 3.7: The actual setup of the Pressure Sensors in the Lung Simulator

Figure 3.8 shows the in-house custom made thermal flow meter which is used to measure the air velocity at the terminal link. The measurement principle is based on a heating wire which creates a uniform gradient temperature in the tube. The temperature is then detected by the two thermal resistors, which are placed on two sides of the heating wire. When there is no air flow, there is no difference in temperature between the two thermal resistors. When there is air flow in the tube, there is a difference between the two thermal resistors. This difference is proportional to the air velocity. Figure 3.9 shows the actual setup in the lung simulator.

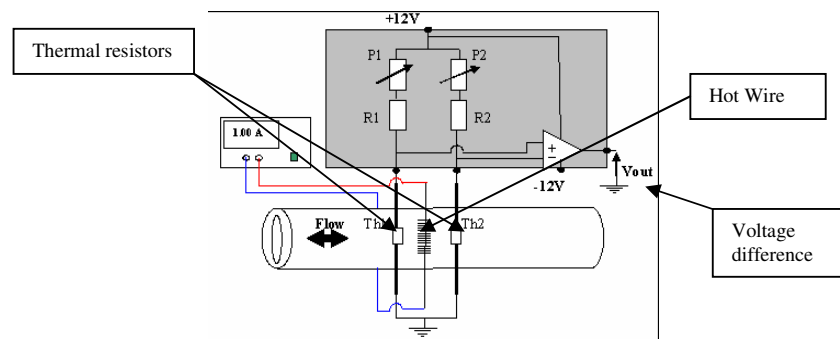


Figure 3.8: The custom made Thermal Flow Meter is used in the Lung Simulator

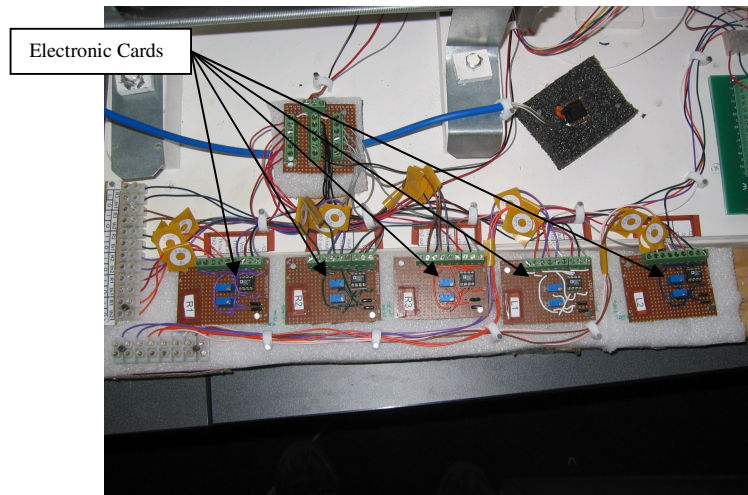


Figure 3.9: Electronic Cards setup to obtain air velocity at 5-Lobe Lung Model

Although there are several options to read the thermal meter output, a Wheatstone Bridge is chosen in order to give high sensitivity and accuracy. The output from the Wheatstone Bridge is connected to the instrumental differential amplifier to amplify the signal which then is saved in the Personal Computer in text file format. During an operation, the Wheatstone Bridge is set to be balanced and no current flow in either direction. It means there is no voltage difference. When the flow occurs which causes the thermal resistors to change, the Bridge becomes unbalance. This change causes the current flow in the circuit leading to a voltage difference. The difference of voltage is then recorded into the PC representing the changes in air velocity with time. Figure 3.10 shows the custom made Wheatstone bridge used in the lung simulator.

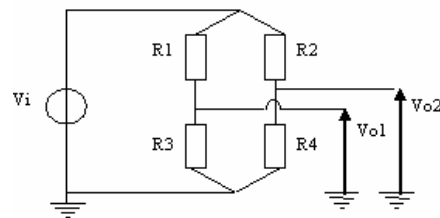


Figure 3.10: The in-house custom made Wheatstone Bridge is used in the Lung Simulator.

Table 3.1: Equipment Details for the Lung Simulator

Description	Purpose	Identification Details
Pneumatic system	To create the pressure-volume change	Custom made at AUT
Five thermal flow meter	To measure the flow rate at each terminal link	Custom made at AUT
Five balloons	To act as 5 alveolar and connect to the terminal link	Fisher&Paykel provided
Pressure regulator	To control pressure generate at the pneumatic system	Festo-MPPE3-1/8-1-010B
Five pressure sensors	To measure the pressure generated at terminal link	DC005NDC4
Electronic Cards	To control the pressure regulator	Custom made at AUT
Personal Computer	To process and control the data	AUT Serial Number
Matlab Software	Converts text file into relevant format for further analysis	Version 6.5.1
LabView Software	control program and store data	Version 6.1

3.3 Experimental Procedure

The following procedure is set for each operation:

1. The lung simulator is set to operate at normal conditions and tested-data results are recorded at different sampling rate up to 512 Hz. This rate is set up to 512 Hz to allow a Nyquist frequency up to 256 Hz upon of a Fast Fourier Transform (FFT);
2. For each experiment, 60 seconds length of data is acquired and saved in the Personal Computer. The waveforms are then exported to an ExcelTM file and are stored in the computer hard-drive for further analysis in MatlabTM software;
3. The recorded data is divided into short recordings depending on the sample rate of each file; as such each short recording had different time data points. For instance, if the data is recorded at 20 points per second and the system is operating at 6 seconds per cycle, the short recording file will contain 120 time points at 20 Hz sampling rate;
4. The next step is to transform the recorded data into the frequency domain to obtain a frequency analysis. The M-file is given in Appendix C is created in MatlabTM to produce an FFT function and obtain a useful signal power against frequency for each experiment. The graphs are then saved as M-figure file for further analysis.

3.4 Sample Results of Experiment Procedure

The following figures are the results obtained after the pressure and air velocity readings were transformed into the frequency domain. The measured impedance is then calculated and plotted into graphs in the frequency domain. The graphs of all experiments are presented in this section. Although the experiments are done for several tests, only a typical sample is presented in this chapter. The rest of the pre-experiment results are shown in Appendix D. MatlabTM programming to calculate impedance is presented in Appendix C.

Measurements are performed to investigate the effect of changes in the sampling rates on the estimate spectral amplitude of the lung simulator. The initial data collection

consisted of terminal impedance measurements at different sampling rates. Simulations are then performed to predict the input impedance of the lung simulator as a function of pressure and volume flow rate using the distributed lumped parameter models described in Chapter 2.

Figure 3.11 shows samples of the power spectral density of the terminal impedance measured in lobe R1 of the tested-lung simulator. Similar results have found in lobe R2, R3, L1 and L2. The plots have higher magnitude in the lower frequency range than in the higher frequency. It shows the presence of the particular frequency that the system operated during the experiment; in this case the system is set to operate at 6 seconds per breath cycle. The experimental measured impedance at lobes R2, R3, L1 and L2 are shown in Appendix D.

3.5 Effects on the Lung Simulator at Different Operation Frequencies

In order to obtain more accurate results, the lung simulator is set to operate at different frequencies up to 1 Hz according to the breath cycle. Series of experiments are made to obtain data from the lung simulator that is set to operate at different breath cycle from 1 second to 6 seconds respectively. Data again is recorded at 20 Hz sampling rate. The results are analysed and stored for further analysis. After transforming into frequency domain, data is used to calculate the terminal impedance and samples of the results are presented in Figures 3.12 to 3.16, the rest is shown in Appendix D.

3.6 Obstruction Effects on the Lung Simulator

The procedures are set up to study the effect of obstructed lung simulator at different location at terminal airways. By introducing more stiffness at each lobe of the tested lung, the lung simulator is then set to operate at normal breathing cycle. The steps of setting in this experiment are similar to that described in Chapter 2.

The results is then recoded and stored in the computer's hardware for further analysis. Data is recoded at 60 seconds length and is analysed using MatlabTM software to obtain the frequency analysis. Power Spectrum versus Frequency is created for each experiment and saved as M-figure file for later inspection. The sample results obtained after transforming the measurements into power spectrum in frequency domain are shown in Figures 3.17 to 3.20.

Power Spectrum Magnitude (dB)

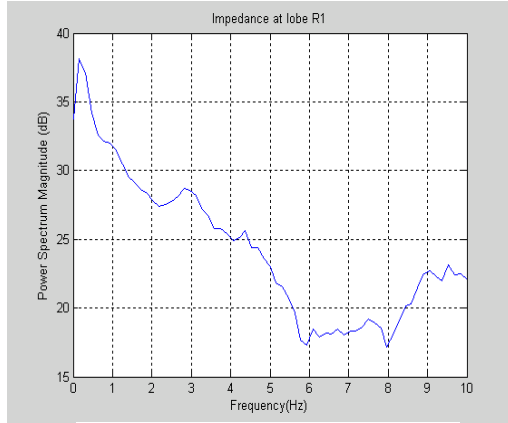


Figure 3.11(1): measured up to 10 Hz

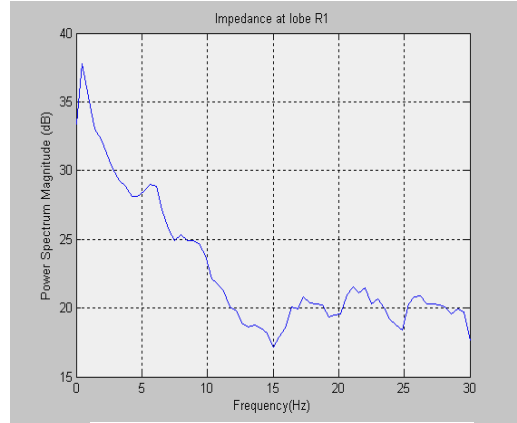


Figure 3.11(2): measured up to 30 Hz

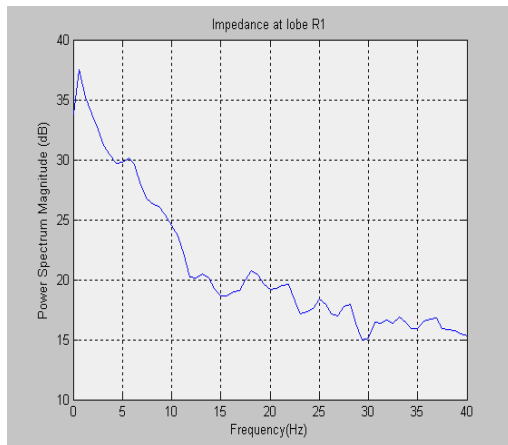


Figure 3.11(3): measured up to 40 Hz

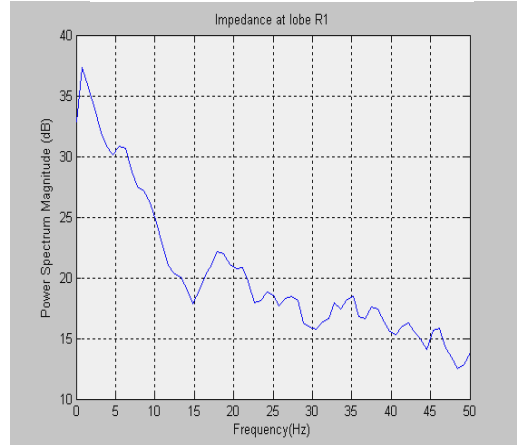


Figure 3.11(4): measured up to 50 Hz

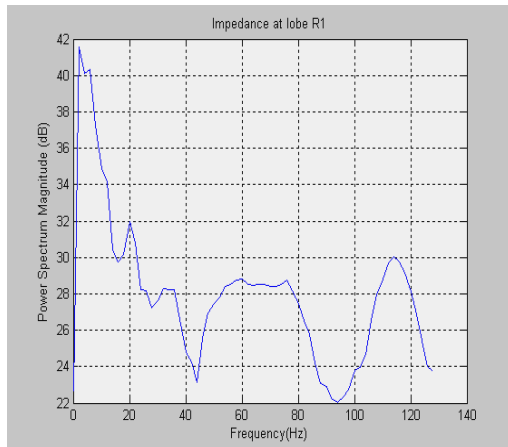


Figure 3.11(5): measured up to 128 Hz

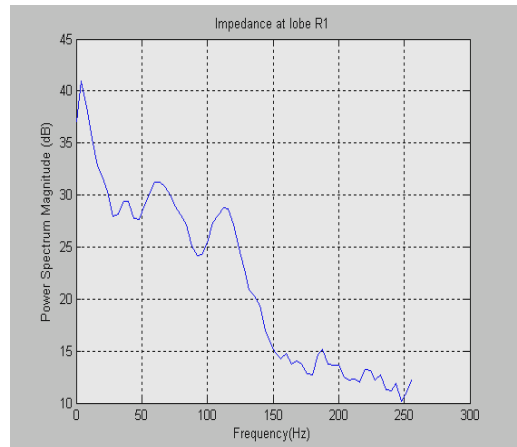


Figure 3.11(6): measured up to 256 Hz

Frequency (Hz)

Figure 3.11: Power Spectrum of measured impedance up to 256 Hz

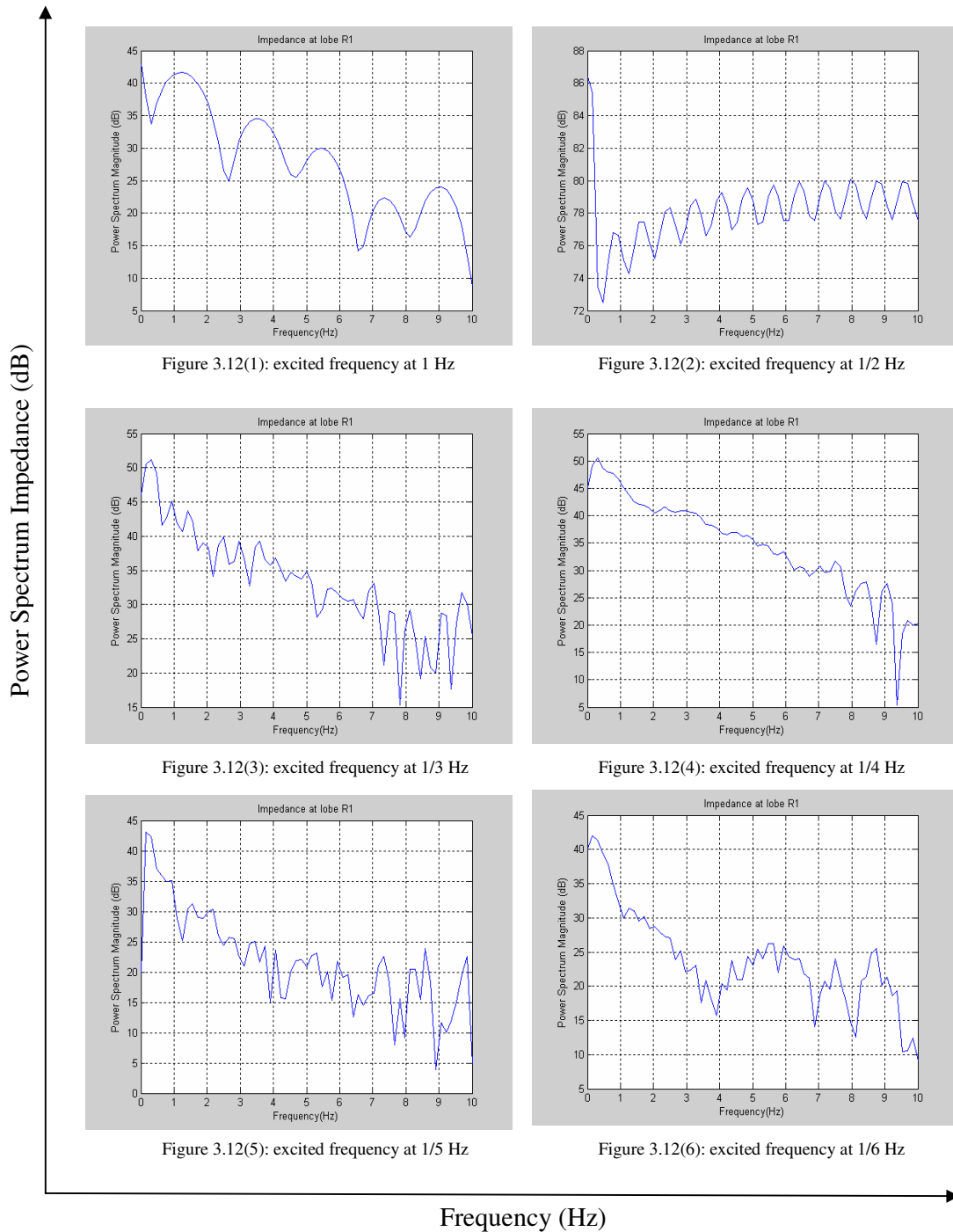


Figure 3.12: Power Spectrum of the impedance at lobe R1 measured at different exciting frequencies up to 1 Hz

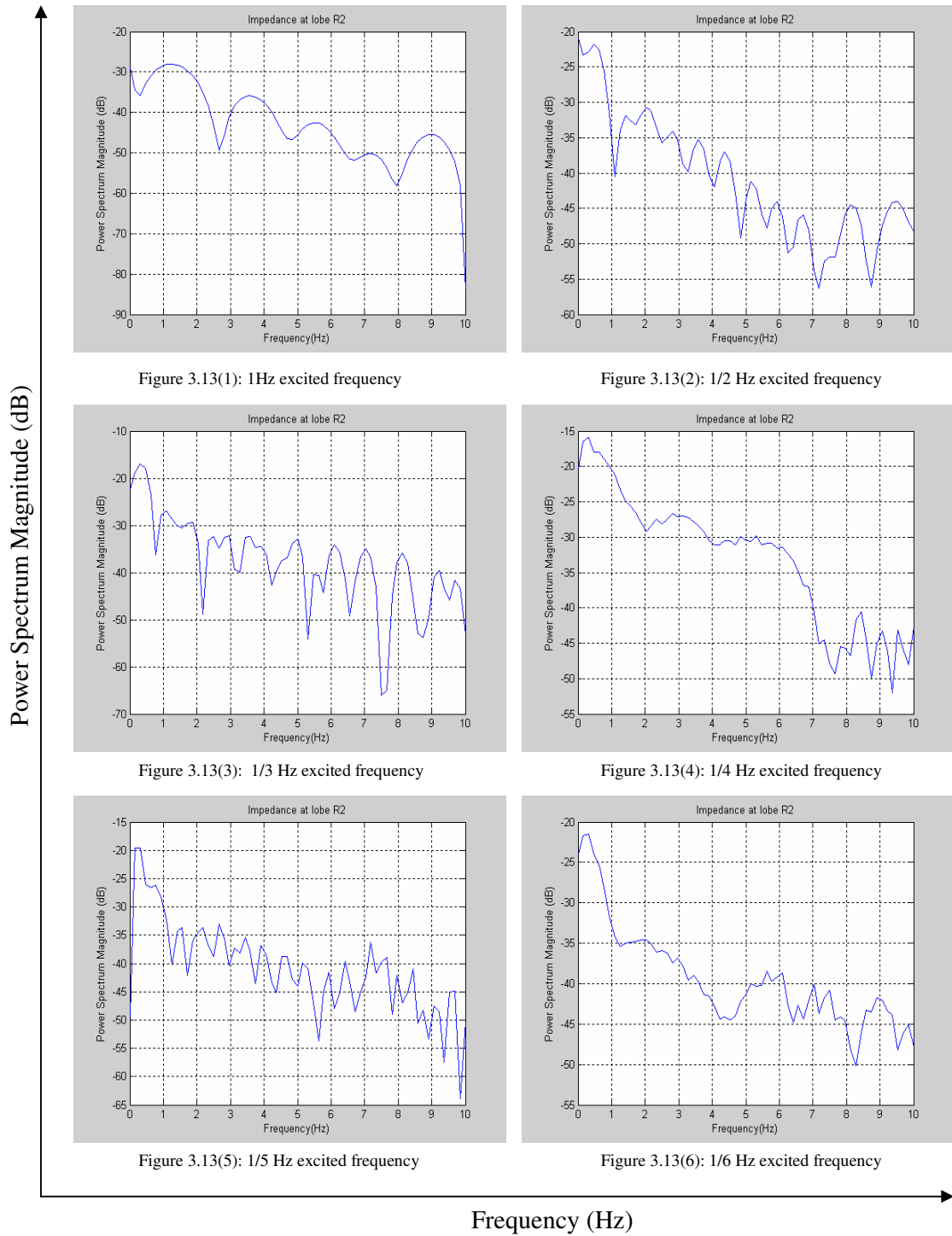


Figure 3.13: Power Spectrum of the impedance at lobe R2 measured at different exciting frequencies up to 1 Hz

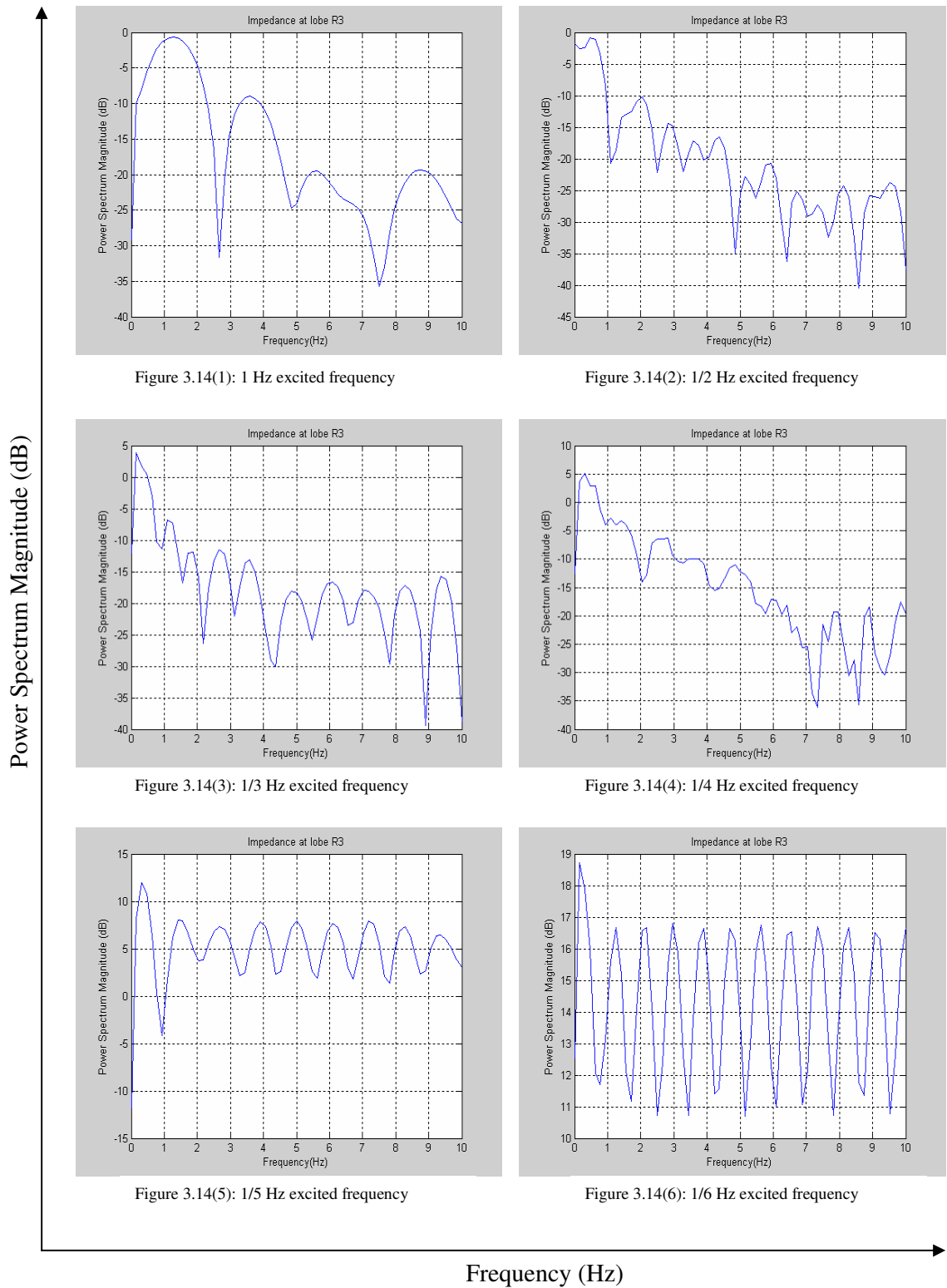


Figure 3.14: Power Spectrum of the impedance at lobe R3 measured at different exciting frequencies up to 1 Hz

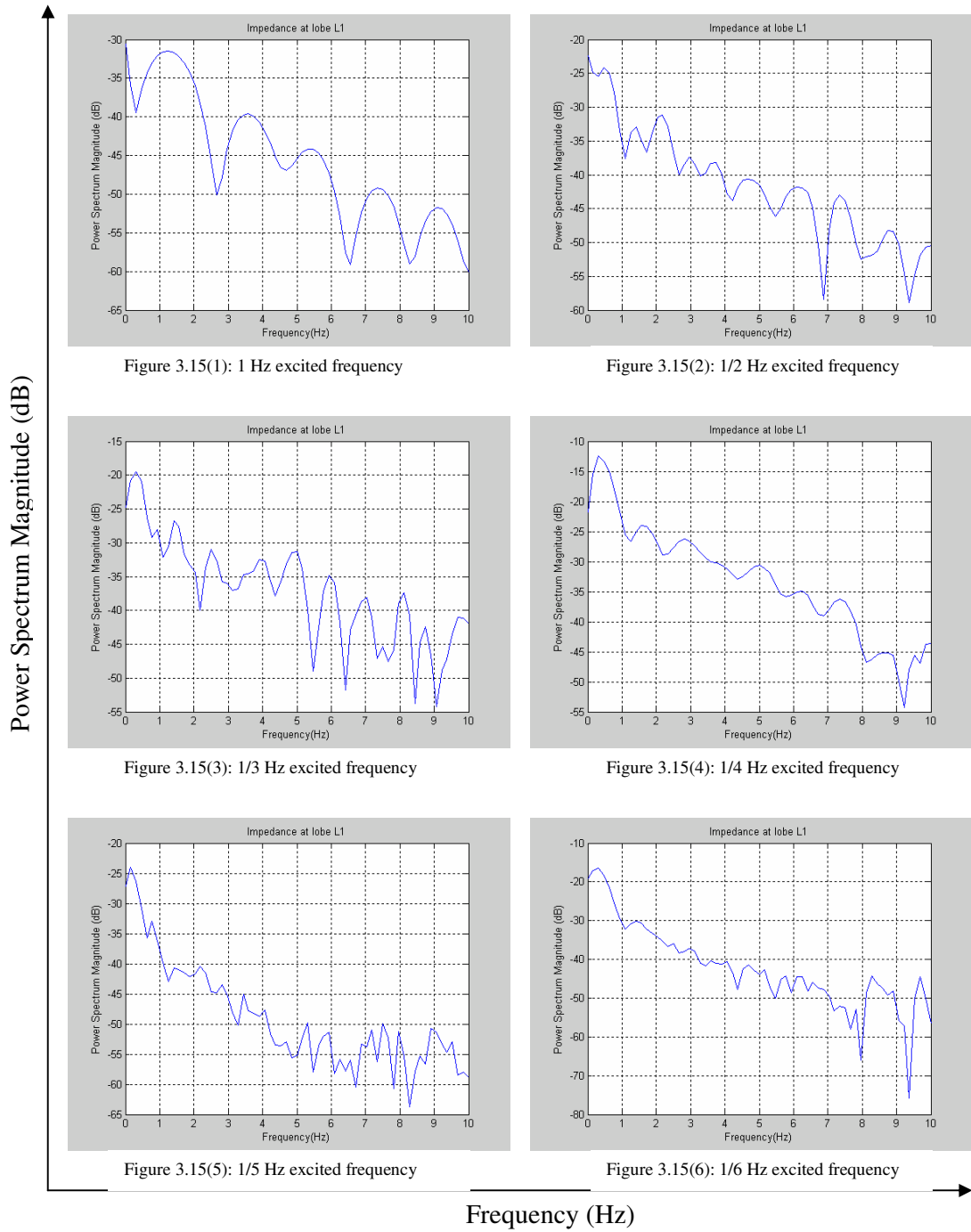


Figure 3.15: Power Spectrum of the impedance at lobe L1 measured at different exciting frequencies up to 1 Hz

Power Spectrum Magnitude (dB)

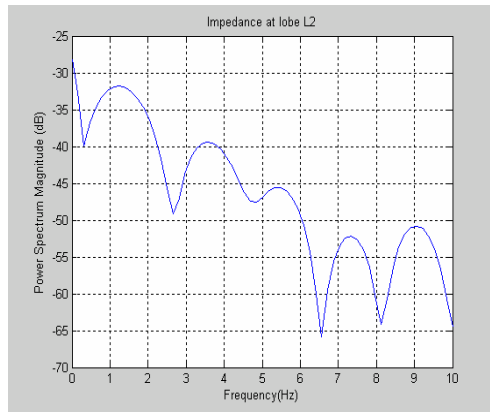


Figure 3.16(1): 1 Hz excited frequency

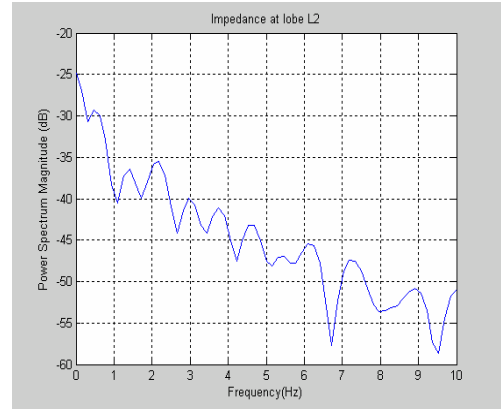


Figure 3.16(2): 1/2 Hz excited frequency

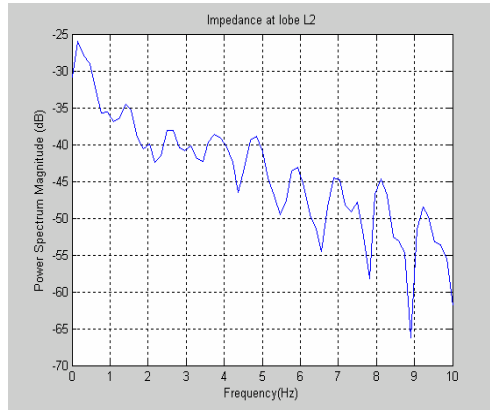


Figure 3.16(3): 1/3 Hz excited frequency

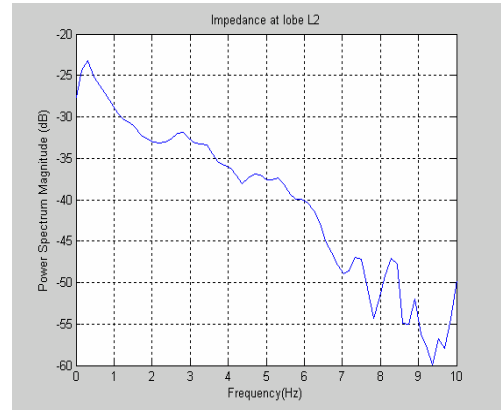


Figure 3.16(4): 1/4 Hz excited frequency

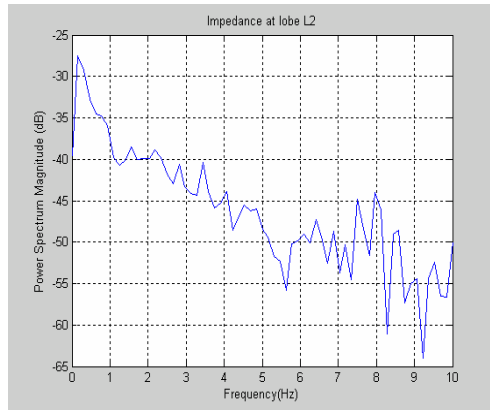


Figure 3.16(5): 1/5 Hz excited frequency

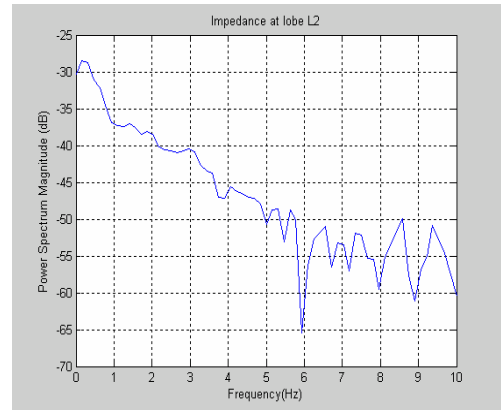


Figure 3.16(6): 1/6 Hz excited frequency

Frequency (Hz)

Figure 3.16: Power Spectrum of the impedance at lobe L2 measured at different exciting frequencies up to 1 Hz

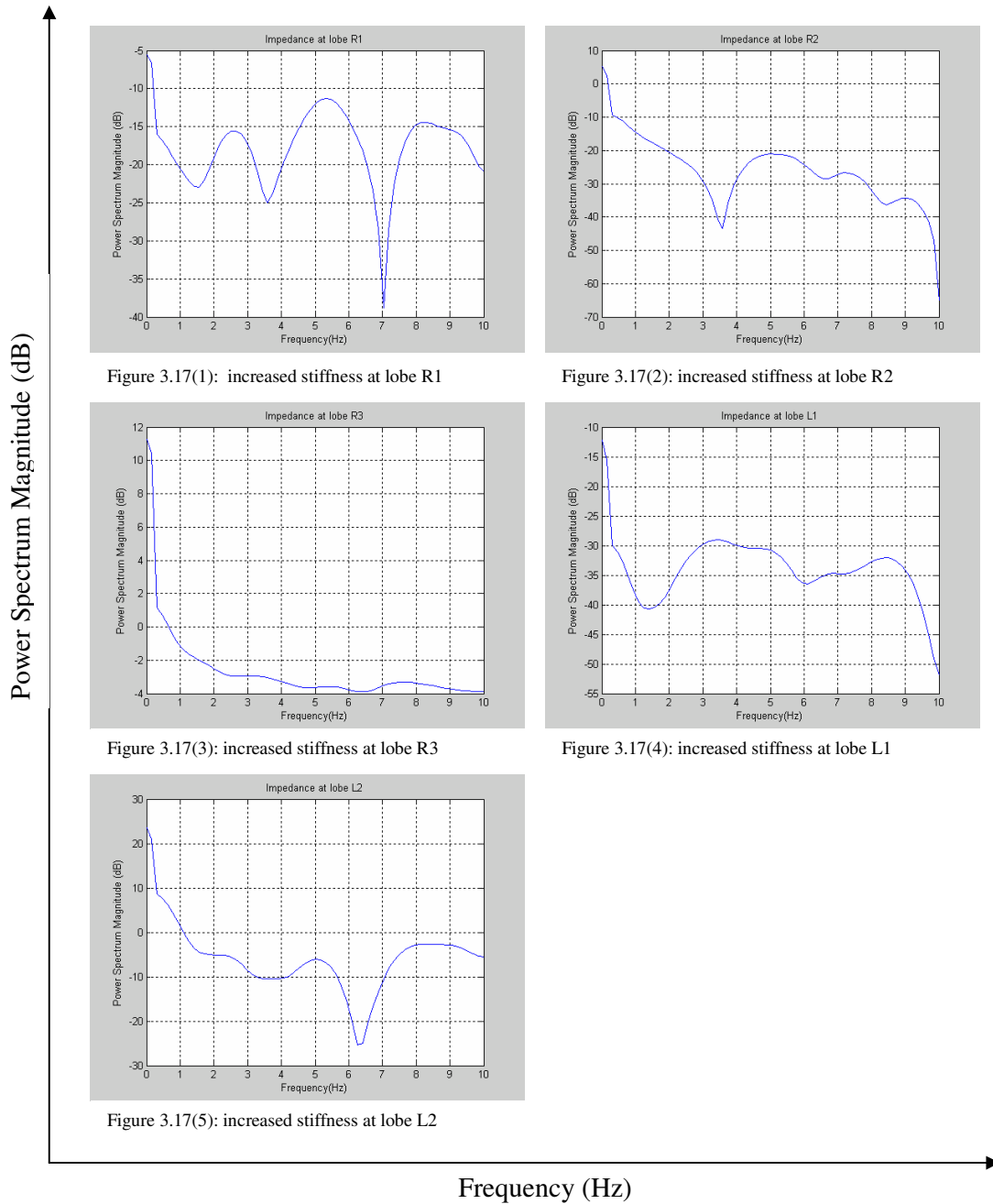


Figure 3.17: Power Spectrum of the experiment impedances of the lung simulator measured by increasing stiffness of each lobe respectively

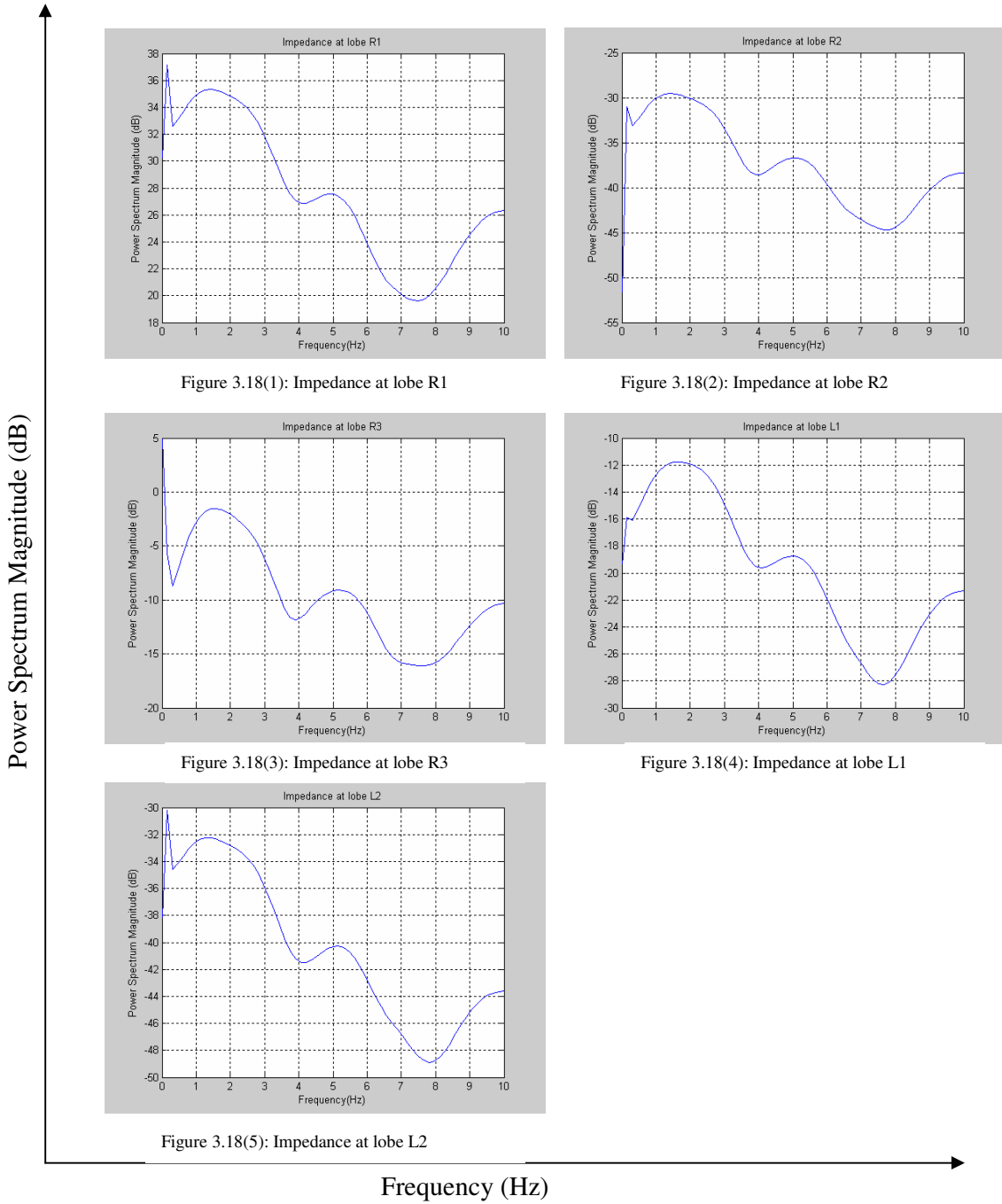


Figure 3.18: Power Spectrum of the Impedance of 5-lobe lung simulator when increasing stiffness at lobe R1 and R2

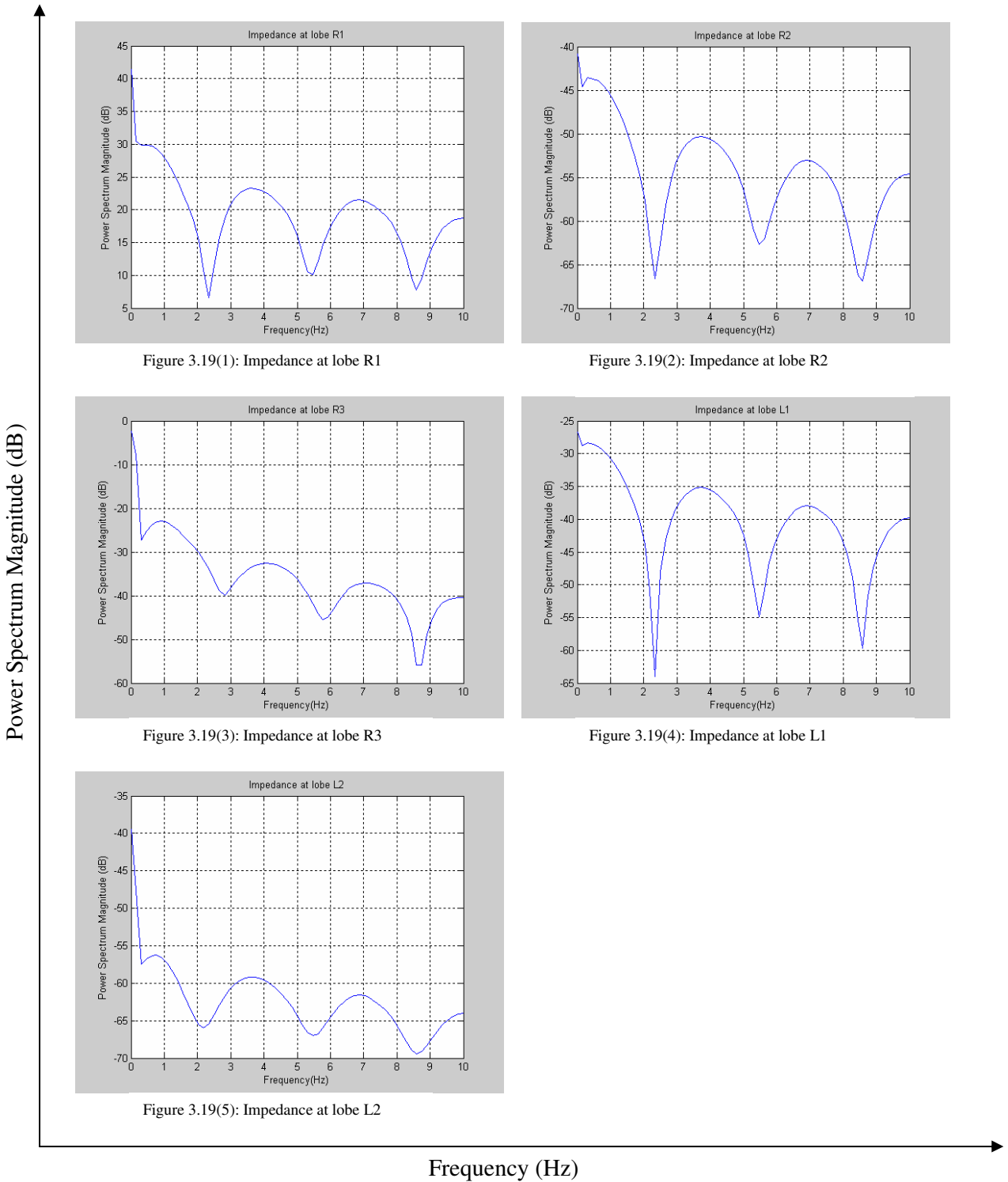


Figure 3.19: Power Spectrum of the Impedance of the 5-lobe lung simulator when increasing stiffness at lobe R1, R2 and R3.

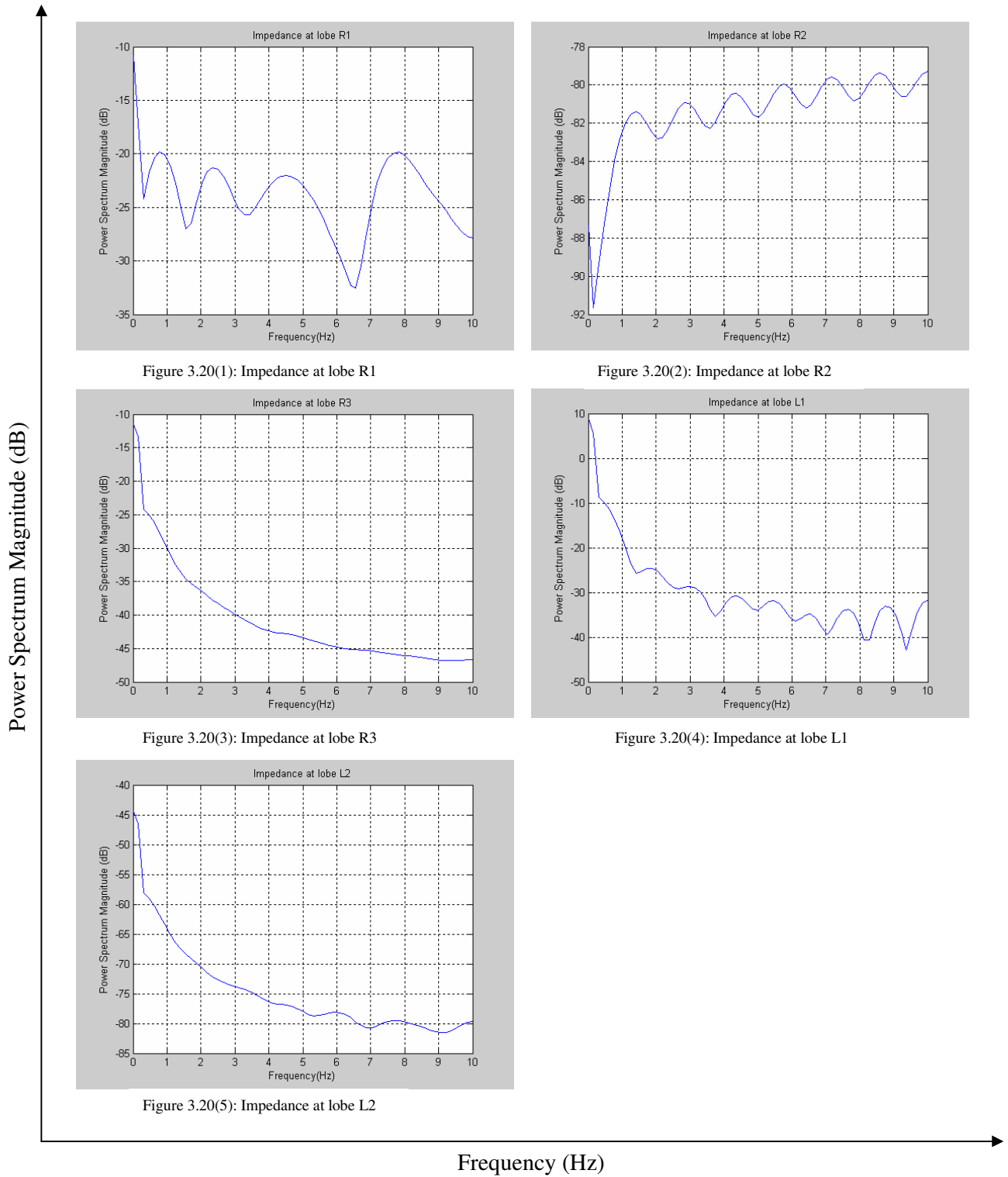


Figure 3.20: Power Spectrum of the Impedance of the 5-lobe lung simulator when increasing stiffness at lobe R1, R2, R3 and L1

3.7 Comments about Experimental Equipment

The lung simulator was used to determine the terminal impedance at the alveolar of the tested-lung in both normal and abnormal conditions. However, there were few difficulties encountered during the investigations on obstruction. This could explain the reason for the errors occurred in the measurement system. For example, leaks occurred at the connection points of the bronchial when high pressure is applied. This leads to the fact that the pressure dropped dramatically during operation. Another issue is that in-house custom design thermal flow meters did not provide solutions for the over heated to stabilize the reading of measurement system. This issue has caused DC offset occurred in the record files. Due to the complexity of the respiratory system, it is concluded that more specialised equipments are required for more accurate measurements. However, the experimental results obtained in this work give acceptable trend of variation for occlusion identification.

3.8 Summary

The experiment investigations were performed using the lung simulator to identify resonant frequencies that occurred during different operations at different conditions. However, in occlusion investigations, the effects of those conditions on terminal impedance, which is generated by the lung simulator, need to be analysed further. Nevertheless, the experiment results still give a good validation procedure.

CHAPTER 4

4. INPUT IMPEDANCE RESULTS

4.1 Introduction

This chapter describes the results of this work on conductive airway dynamics. Both theoretical modelling and experimental investigations are considered. These are described in Chapter 2 and Chapter 3 respectively. For the mathematical model, the results are obtained by applying the values of the terminal impedance calculated in the proposed model in Chapter 2. Variation of the stiffness values that causes airway contraction is also investigated in this model by considering the input impedance values. For the experimental investigations, the measured impedances are used to calculate the input impedance of the entire 5-Lobe Model using mathematical methods developed in Chapter 2.

Figures 4.1 to 4.8 show the frequency spectrum of the input impedance produced from the mathematical model and the experimental investigation including the occlusion scenario. Results are approached and discussed with regard to the frequency response. The results are first presented in their entity and thereafter discussed in Chapter 5 to identify the effects and relative power or strengths of the resonant frequencies generated in the 5-lobe model. The theoretical model is validated by comparing the results to the experimental investigations. This chapter presents the following:

1. The predicted input impedance of the mathematical 5-lobe model simulated at normal conditions;

2. The experimental input impedance of the lung simulator is obtained in both normal and abnormal conditions and then is used to compare with the mathematical results;
3. Predicted results on occlusion by changing the stiffness values of the five lobes model from healthy to unhealthy conditions in the mathematical modelling are presented and then used to compare with the experimental investigations;
4. A brief of summary of the results of both mathematical and experimental investigations is presented.

4.2 Input Impedance Results

In this section, the results of the input impedance calculation of both mathematical and experiment models are presented and compared. The models are simulated up to 256 Hz. In the mathematical model, the frequency spectrum of the 5-Lobe model is determined using the physical properties as described in Table 2.1, while the experiment investigations were done by using the mechanical lung simulator (Appendix E). Using the backward substitution for the model, a MatlabTM computer program (Appendix B) is developed to determine the frequency spectrum of the input impedance. Typical results of the power spectrum of the input impedance are presented in the following sections.

4.2.1 Mathematical Input Impedance at Normal Conditions

The results of input impedance simulation in Figure 4.1 show several dominant resonance frequencies of the input impedance occurred during the process. To further evaluate the predictive capabilities of the practical model, experiments are performed to alter the sampling rates while recording the pressure and volume flow rate using the lung simulator. The frequency spectrums of the input impedance are then simulated and determined at different sampling rates.

Simulation is made at the 10 Hz frequency range in Figure 4.1(1), resonant frequencies of the input impedance are found in the range of 0 Hz to 10 Hz. The first resonant frequency occurs at approximately 4 Hz and has the greatest amplitude. The second resonant frequency occurs in the range of 7 Hz to 8 Hz. This is the second largest in amplitude. Moreover, in the range of 8 Hz to 9 Hz, there are also several resonant frequencies but it can be clearly seen as they are smaller in amplitude.

For the sake of accuracy, the sampling rate is increased to investigate whether other resonances may occur. By increasing the sampling rate to 512 Hz in Figure 4.1 (2, 3, 4, 5 and 6), similar results of the resonant frequencies are also found within the range of 0 to 10 Hz. However, by comparing to Figure 4.1(1), magnitudes of these impedances are different as can be easily seen. Moreover, new resonant frequencies occur within the range of 15 to 20 Hz, this resonant frequency is regarded as the dominant frequency because it has the greatest peak compared to the other resonant frequencies.

Figure 4.1(2, 3, 4, 5 and 6) shows insignificant amplitude of the resonant frequencies within a range of 20 to 256 Hz. A new resonant frequency can be seen at 25 Hz although remains very small in amplitude.

4.2.2 Experimental Input Impedance at Normal Conditions

The frequency spectrum of the input impedance is performed by the Matlab™ computer program with the physical properties of the terminal impedance collected from experimental investigations using the lung simulator as it showed in Chapter 3. Figure 4.2 shows the spectrum of the resonant frequencies of the experimental input impedances up to 256 Hz. In comparison to the spectrums of input impedance in Figure 4.1, the results obtained in the experimental investigations show a good matching.

The first resonant frequency of the input impedance is found to be the same as the first resonant frequency in the mathematical model. However, by comparing with each other graph in Figure 4.2, the first resonant frequency of the experiment measured at 20 Hz sampling rate seems to be the dominant frequency because it has the greatest amplitude. Similar result is found in the first resonant frequency which is obtained in mathematical model in Figure 4.1(1).

By increasing sampling rate up to 512Hz, the magnitude of the input impedance over frequency is clearly reduced. The first resonant frequency is found at 4 Hz but has smaller magnitude compared to the first resonance at Figure 4.1(1). It can be clearly seen in Figure 4.2(2, 3, 4, 5 and 6). The second resonant frequency is found to be around 7Hz to 8Hz. The results of resonances also match the results that found in Figure 4.1(1). In the range of 7 Hz to 10 Hz, several resonant frequencies are found but remaining very small in amplitude. However, new

resonant frequencies are found within a range of 15 Hz to 20 Hz and can be regarded as the dominant frequency because they have the greatest amplitude.

4.2.3 Experimental Input Impedance at Different Exciting Frequencies

To be more precise with the results obtained in both mathematical model and experimental investigation as described in previous sections, the lung simulator is set to operate with different exciting frequencies as indicated in Chapter 3. The purpose of those experiments is to confirm that those resonant frequencies are attributed to the whole system and not just a conscience.

In this section, the experimental results are presented as obtained from the mechanical lung simulator. Experiments performed at several breath cycles from approximately 0.17 Hz to 1 Hz are shown in Figure 4.3. The trends of frequencies in Figure 4.3 show similar results to that obtained in the mathematical investigation. The first resonant frequency is found around 4 Hz. By contrast, there are some differences when the lung simulator is set to operate at a breath cycle of 2 seconds. Figure 4.3(2) shows the first resonant frequency shifts to the left and occurs around 3 Hz. The magnitudes of the other resonant frequencies around 7 Hz to 9 Hz are also different compared to the mathematical results [Figure 4.1(1)]. It shows clearly when the lung simulator is set to operate at 3 and 4 seconds per cycle. Nevertheless, based on the results obtained from these experiments, the first conclusion can be made is that the resonant frequencies obtained in the mathematical 5-Lobe lung model at the normal condition are accurately predicted. The use of this model can be expanded further to investigate occlusion that might occur in the unhealthy condition.

4.2.4 Summary

Agreements between the spectrum responses of the input impedance are found by comparing both mathematical and experimental results in Figure 4.1 and Figure 4.2 respectively. It is also confirmed by the results obtained in Figure 4.3. It indicates that the mathematical model is able to predict reasonably well the resonances of the input impedance of the five lobes lung model.

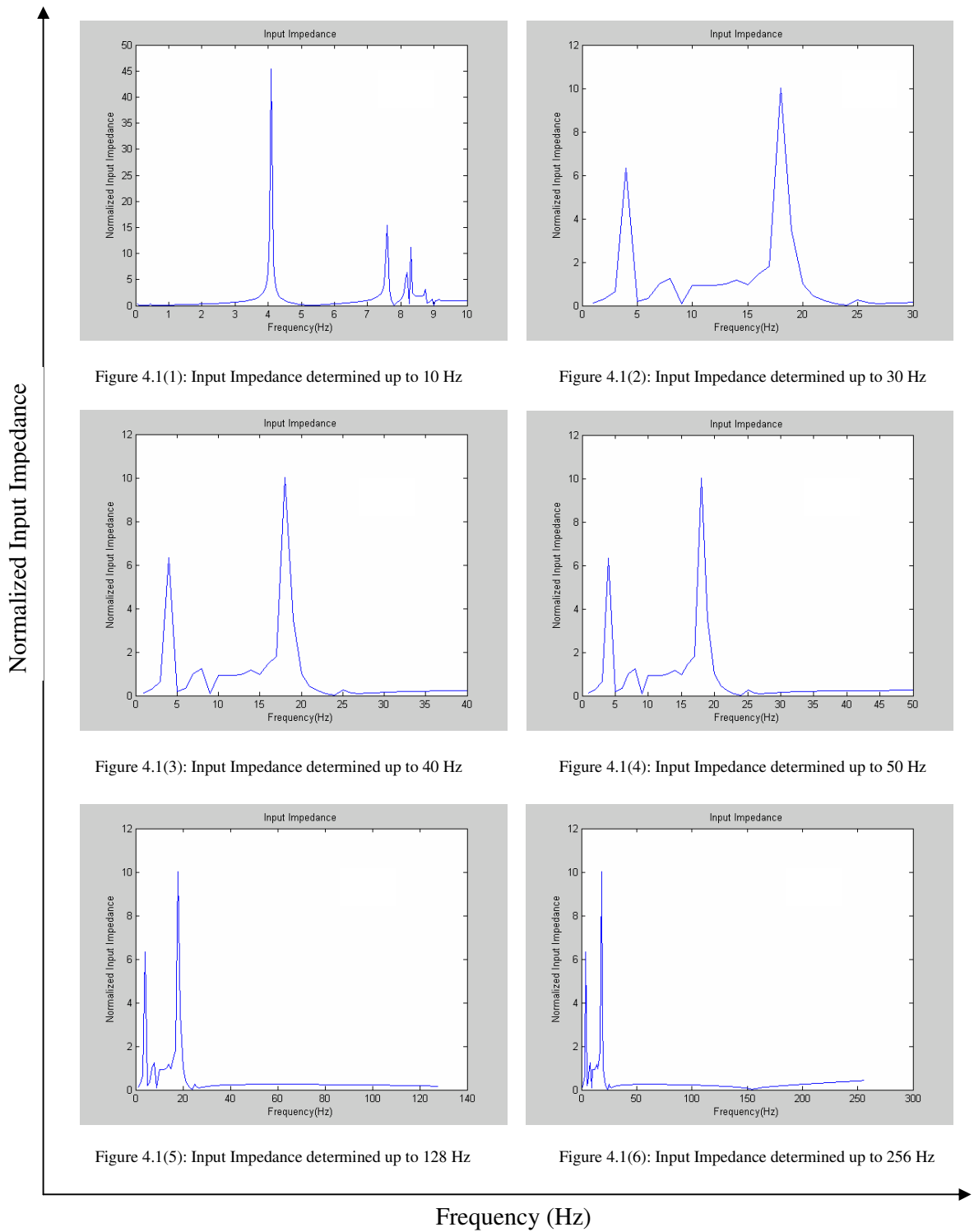


Figure 4.1: Normalized Input Impedance of the mathematical model determined for normal conditions

Normalized Input Impedance

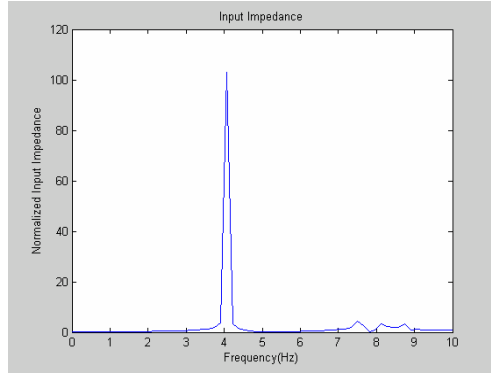


Figure 4.2(1): Input Impedance determined up to 10 Hz

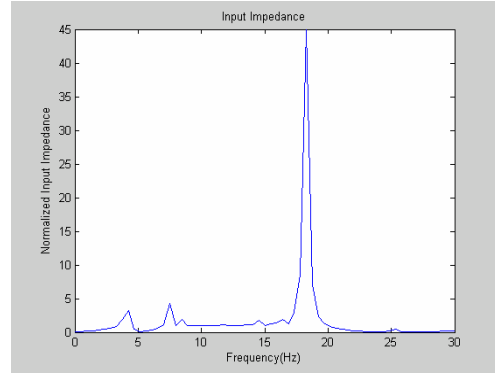


Figure 4.2(2): Input Impedance determined up to 30 Hz

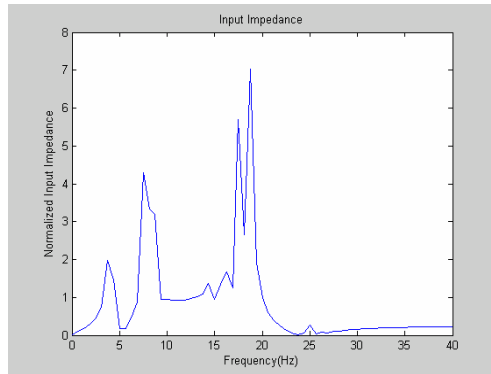


Figure 4.2(3): Input Impedance determined up to 40 Hz

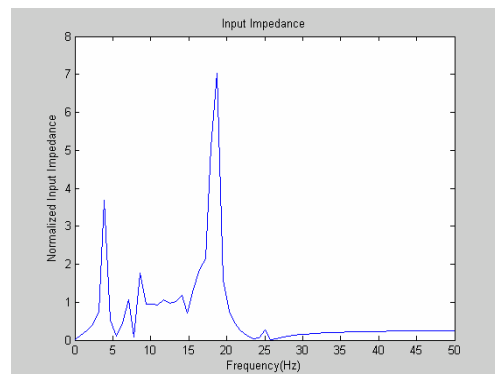


Figure 4.2(4): Input Impedance determined up to 50 Hz

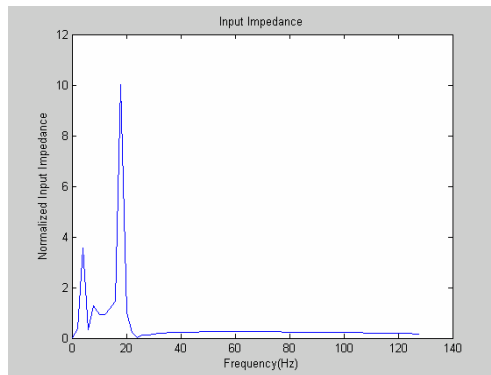


Figure 4.2(5): Input Impedance determined up to 128 Hz

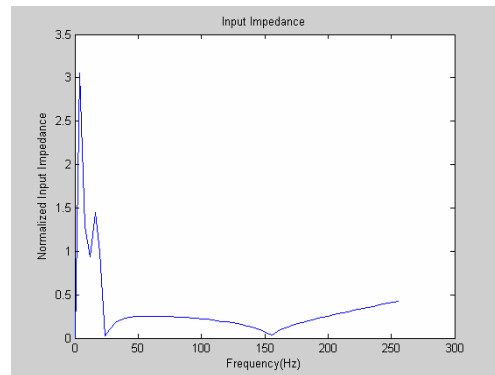


Figure 4.2(6): Input Impedance determined up to 256 Hz

Frequency (Hz)

Figure 4.2: Normalized Input Impedance of the experiment investigations determined for normal conditions

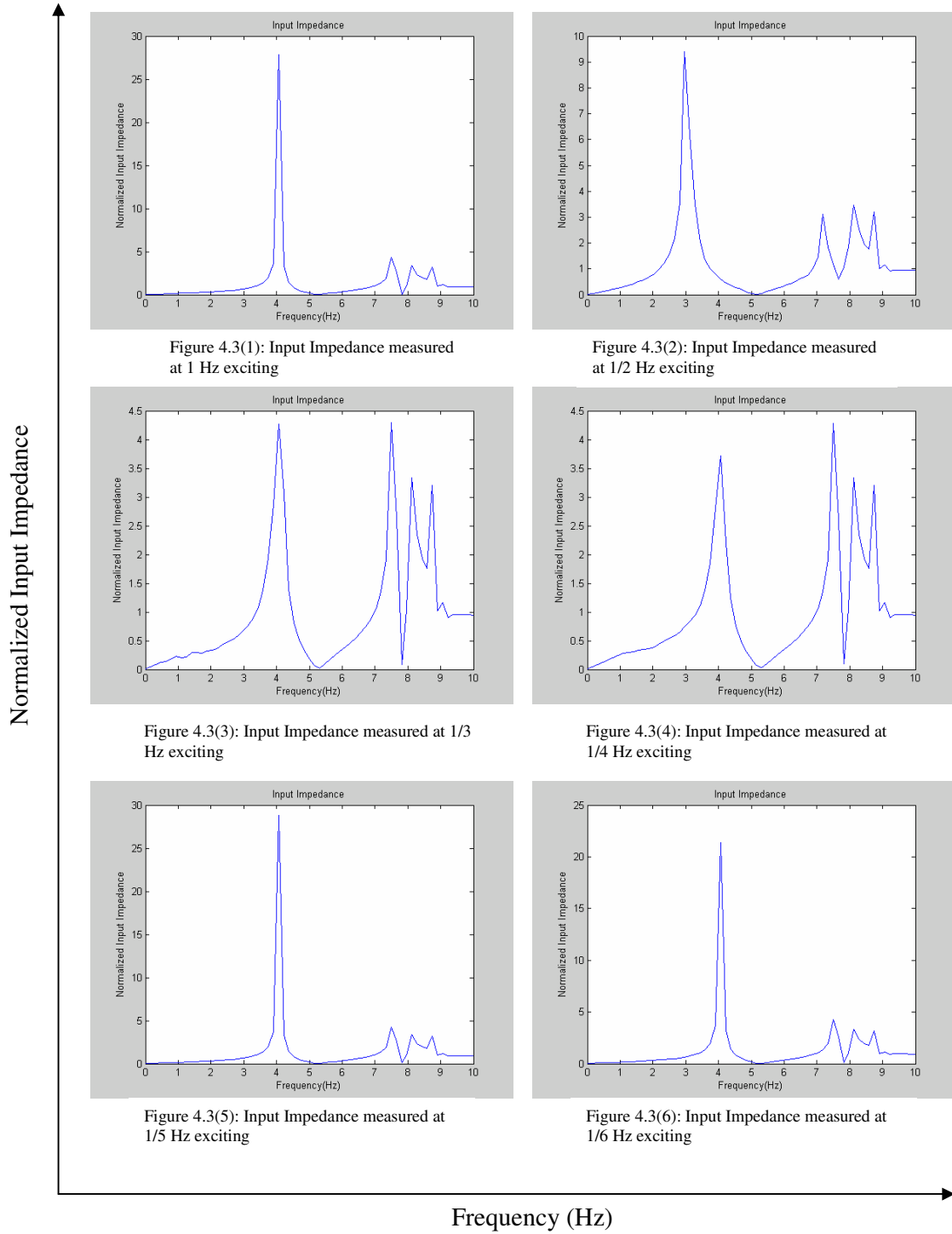


Figure 4.3: Normalized Input Impedance of the experiment investigations determined at varied exciting frequencies up to 1 Hz

4.3 Obstruction Investigations

The aim of this investigation is to study the effects of various stiffness values on the input impedance spectrum and to perform a closer study at the effect of obstruction at different locations in the lung system. The 5-Lobe mathematical model is modified by introducing an obstruction at each individual lobe and then run a series of simulations. The model is simulated up to 10 Hz in these investigations. The input impedance is simulated by increasing the stiffness at each lobe for every experiment. The stiffness of the healthy lung is around 30MPa and very unhealthy lung is up to 100MPa according to [49]. Taking into account these values, the results from Figures 4.4 to 4.8 show the first resonant frequency occurs between 3 to 4 Hz and there are also several resonant frequencies in the range of 7 Hz to 9 Hz. However, there are differences in magnitude as well as separation between resonant frequencies. It is a result of changing the stiffness of each lobe at each experiment and will be discussed in depth in Chapter 5.

4.3.1 One-Lobe Obstruction

Figure 4.4 shows how the input impedance is simulated by changing the stiffness values from healthy to unhealthy values at every lobe at each experiment respectively. To evaluate the model, a simulation is performed on the five-lobe model using the same mathematical model described in Chapter 2 where each lobe is considered to have increased stiffness values to unhealthy values. To excite the resonances, a sinusoidal frequency is varied from 0 to 10 Hz.

The first simulation is made by assuming an obstruction at lobe R1. Resonant frequencies are found in the range of 0 to 10 Hz. There are approximately three resonant frequencies that are dominant in Figure 4.4(1). The first resonance occurs around 3 Hz, while the second and third resonant frequencies are detected within the range of 7 Hz to 9 Hz. The third resonant frequency has the greatest amplitude. In comparison to the spectrum of the input impedance in Figure 4.1(1), magnitude of the first resonance is smaller. However, the magnitudes of the second and third resonances are increasing dramatically.

Separation between the first and the second resonances is getting larger as well as the separation between the second and the third resonances.

In Figure 4.4(2), simulation is made by changing stiffness of lobe R2. The resulted spectrum is then compared with the results in Figure 4.1(1). It can be seen that there is almost no effect when changing the stiffness of this lobe, except the magnitude of the first resonance is larger. By contrast, for lobe R3 obstruction in Figure 4.4(3), clearly different results can be seen by comparing with Figure 4.1(1). The first and the second resonances decrease their magnitudes while the third increases its magnitude in contrast. There is no change in separation between the first and the second resonances. However, there are small changes in distances between the second and the third resonances as well as the third and the fourth resonances.

The last two simulations are made by increasing stiffness at lobes L1 and L2 respectively. The results of obstruction on these lobes are similar as the results in Figure 4.1(1). The first resonant frequency shifts to the left. The second resonant frequency increases its magnitude as well as it moves closer to 7 Hz. The dominant frequency is the third resonant frequency with the greatest amplitude. There is also a fourth resonant frequency as it can be seen clearly, although it is in small amplitude.

4.3.2 Two- Lobe Obstruction

To evaluate the input impedance of this model, every two lobes are considered to be obstructed separately. Simulations are performed starting with the same mathematical model described in Chapter 2. The input impedance is calculated based on the geometry of the airways system using the formulas and constants from Chapter 2. The resulting spectrum is shown in Figure 4.5 and used to compare with resulting spectrum of the input impedance at normal condition in Figure 4.1(1).

The first simulation is to set lobes R1 and R2 to be obstructed. In Figure 4.5(1), all the resonant frequencies are shifted to the left. The separation

between the first resonant and the second resonant frequencies is larger, while the distance between the third and the fourth resonant frequencies is closer.

The second simulation is set for lobes R1 and R3 obstructed in Figure 4.5(2), only first resonant frequency is shifted further to the left and its magnitude increases dramatically. The second resonance reduces magnitude to very small as it is almost insignificant, while the separation between the third and the fourth resonant frequencies is larger.

The next simulation is then to change stiffness for lobes R1 and L1 in Figure 4.5(3). The first resonant frequency continues to shift to the left with very small amplitude. The separation between the second resonant and the third resonant frequencies is larger. However, in contrast the fourth resonant frequency is shifted to the right at around 9 Hz. Similarity in frequency distillation is found as lobes R1 and L2 are set to be obstructed in Figure 4.5(4).

In Figure 4.5(5), obstructions introduce in lobes R2 and R3. The first resonant frequency is shifted back to the right around 4 Hz. The separation between the second and third resonant frequencies is therefore closer, while the magnitude of the third resonance dramatically increases and remains as the dominant frequency. Also the distance between the third and fourth resonant frequencies is smaller.

Another simulation is introduced occlusion in lobes R2 and L1. The result is presented in Figure 4.5(6). The first resonant frequency again shifts back to the left leading to larger separation between the first and the second resonant frequency. In this case of the study, the second and third resonant frequencies increase their magnitude; however, the fourth resonant frequency decreases its amplitude to be very small and a new fifth resonant frequency appears at around 9 Hz. Similar behaviour in frequency distribution is found for lobe R2 and L1 obstruction in Figure 4.5(7).

Figure 4.5(8) shows the frequency spectrum when lobes R3 and L1 are obstructed. It is clearly shown that the first resonant frequency remains the

same as the one in Figure 4.5(5) but smaller in amplitude. The separation between the second and third resonant frequencies is smaller and their amplitudes are also smaller. The dominant frequency occurs at 9 Hz and had the greatest amplitude. The similarity in frequency distribution is also found for lobe R3 and L2 obstruction in Figure 4.5(9).

When lobe L1 and L2 are obstructed, Figure 4.5(10) shows that the first resonant frequency shifts further to the left within the range of 2 to 3 Hz. The separation between this frequency and the second resonant frequency is larger. A very small distance between the third and the fourth resonant frequency is also found as the fifth and the sixth decrease their magnitude to very small values.

4.3.3 Three -Lobe Obstruction

The stiffness of three lobes is increased to simulate unhealthy conditions. Six simulations are made by assuming obstruction occurs at every three lobes alternatively. Figure 4.6 shows the results of the spectrums of the input impedance which are simulated by changing stiffness values at every three lobes simultaneously.

For the first simulation, an obstruction of three lobes occurs on the right of the lung (R1, R2 and R3) as it shows in Figure 4.6(1). Dominant frequency returned to the first resonant frequency as it shifts to the left and has the greatest amplitude. The second resonant frequency also shifts to the left as well but then decreases its magnitude to very small value. The third resonant frequency is found at 8 Hz while the fourth, fifth and sixth are remained between 8 to 9 Hz with small amplitude almost insignificant especially for the sixth resonant frequency.

The second simulation is made for lobes R1, R2 and L1 obstruction, the first resonant frequency shifts further to the left and decreases its magnitude as it shows in Figure 4.6(2). The second resonant frequency is found around 7 Hz. A significant fourth resonant frequency is appeared to have very large amplitude while the rests are remained very small and could not clearly

observed. Similarities are found for lobes R1, R2 and L2 are set to be obstructed in Figure 4.6(3).

The next simulations in Figure 4.6(4 and 5) show similar results as lobes R1, R3, L1 and L2 are set to be obstructed respectively. Six resonant frequencies are found in the range of 0 to 10 Hz and can be clearly seen. The first resonant frequency is found within 3 to 4 Hz. The separation between the first and the second resonances is closer when compared to Figure 4.6(3). The sixth resonant frequency has the strongest magnitude while the others remain to be smaller especially for the fifth as it decreases to almost zero.

The last simulation is shown in Figure 4.6(6), the unhealthy condition at lobes R3, L1 and L2 are applied. Three resonant frequencies are found to be dominant in magnitude even though there are other existing resonant frequencies but stay to be very small of powers. The first resonant frequency shifts to the left again leading the larger separation between it and the second resonant frequency.

4.3.4 Four- Lobe Obstruction

By increasing the obstruction to four lobes at the same time, simulations are made similarly as previous section. Figure 4.7 shows the results of the input impedance when simulated at different constriction locations respectively.

For lobes R1, R2, R3 and L1 in constricted conditions, six resonant frequencies are clearly identified in the range of 0 to 10 Hz in Figure 4.7(1). The first resonant frequency occurs approximately at 2 Hz. The second resonant frequency is found in between 6 to 7 Hz. The third resonant frequency appears within 7 to 8 Hz while the fourth , fifth and sixth are found in the range of 8 to 9 Hz. Similar results are found as the constriction applied to lobes R1, R2, R3 and L2 as it shows in Figure 4.7 (2) for the second simulation.

In Figure 4.7 (3), however, the results of constriction that applied to lobes R1, R2, L1 and L2 are clearly different. The first resonant frequency shifts to the left while the second resonant frequency stays the same but increases in

amplitude. No resonant frequency can be found in the range of 7 to 8 Hz as the third resonant frequency shifts to the right in the range of 8 to 9 Hz. The fourth resonant frequency seems to be a dominant frequency in magnitude as it has the strongest power.

The next simulation is made that lobes R1, R3, L1 and L2 are set to be in constricted conditions, the separation between the first and second resonant frequencies is very large as the first resonant frequency is shifted to the left almost to 0 Hz as it shows in Figure 4.7(4). The second resonant frequency is also moved further to the left around 6 Hz while the third is stayed the same when compared to Figure 4.7(1). The dominant frequency in this case is the fourth resonant frequency with the greatest amplitude.

Three resonant frequencies with the largest scale are found in Figure 4.7 (5) as obstruction occurred in lobes R2, R3, L1 and L2. In this simulation, the first resonant frequency occurs within 2 to 3 Hz, while the second resonant frequency with the largest amplitude occurs in the range of 6 to 7 Hz. The third one is in the range of 7 to 8 Hz but remains very small in amplitude. The fourth and fifth resonances are found in the range of 8 to 9 Hz.

4.3.5 Five- Lobe Obstruction

Figure 4.8 shows the result of the input impedance which is simulated as all of five lobes were set to be obstructed. The result shows that the first resonant frequency is shifted to the left as it is closer to 0 Hz. The second resonant is found around 6 Hz. The third resonant frequency is within 7 to 8 Hz while the fourth resonant frequency has the strongest power and stays within the range of 8 to 9 Hz. At 9 Hz, there also are insignificant resonant frequencies.

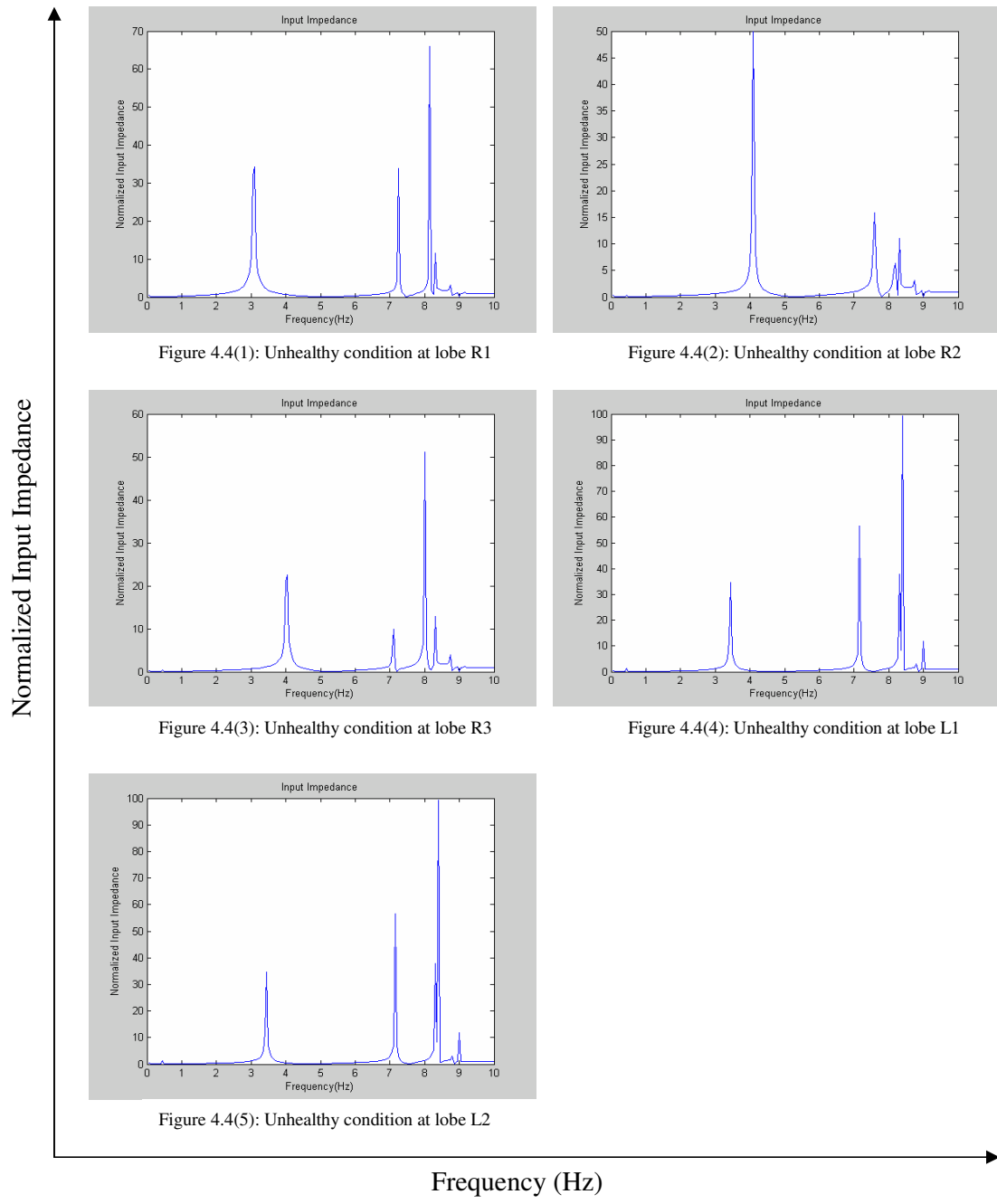


Figure 4.4: Normalized Input Impedance determined by increasing stiffness to unhealthy condition at each lobe respectively

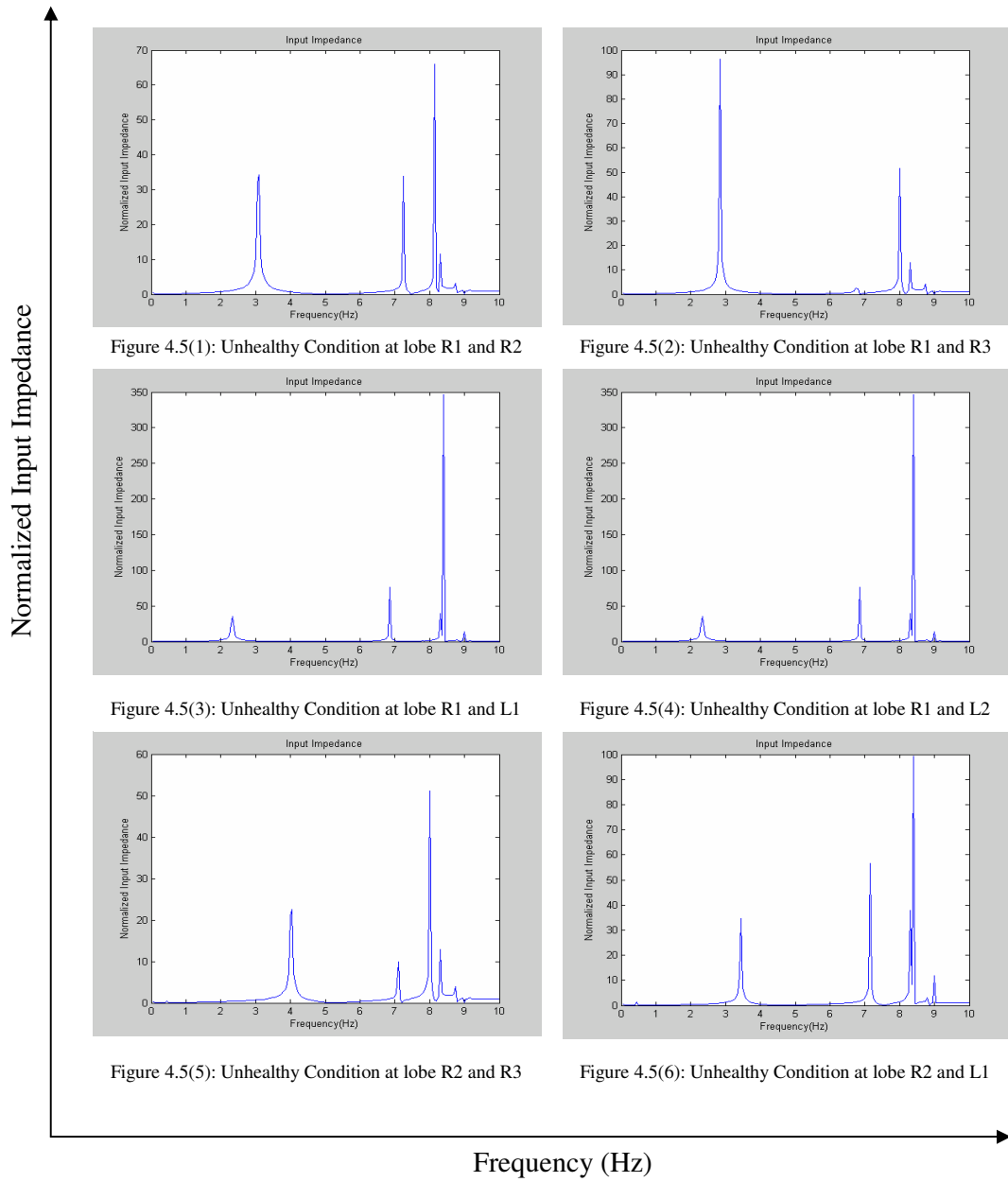


Figure 4.5: Normalized Input Impedance determined by increasing stiffness to unhealthy condition at every two lobes respectively

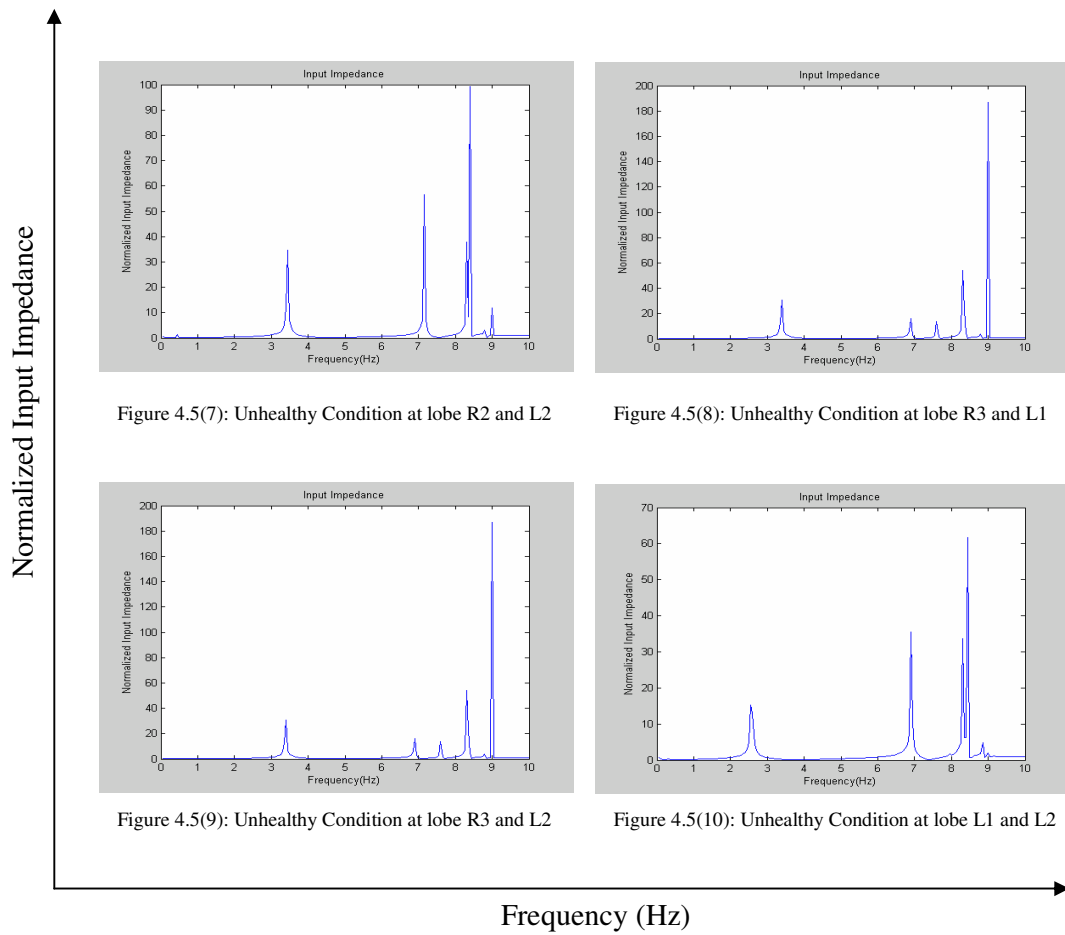


Figure 4.5 (Continues): Normalized Input Impedance determined by increasing stiffness to unhealthy condition at every two lobes respectively

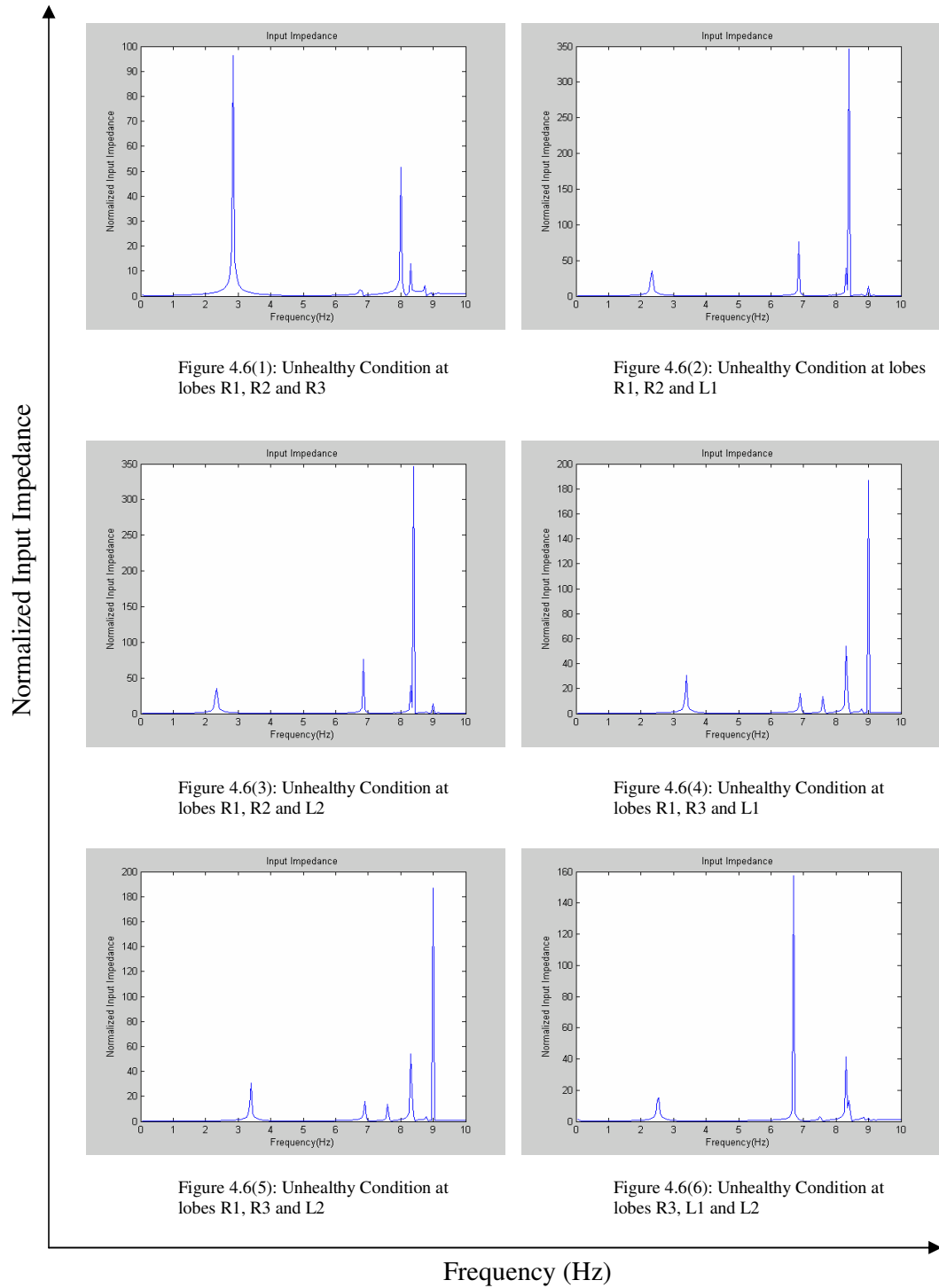


Figure 4.6: Normalized Input Impedance determined by increasing stiffness to unhealthy condition at every three lobes respectively

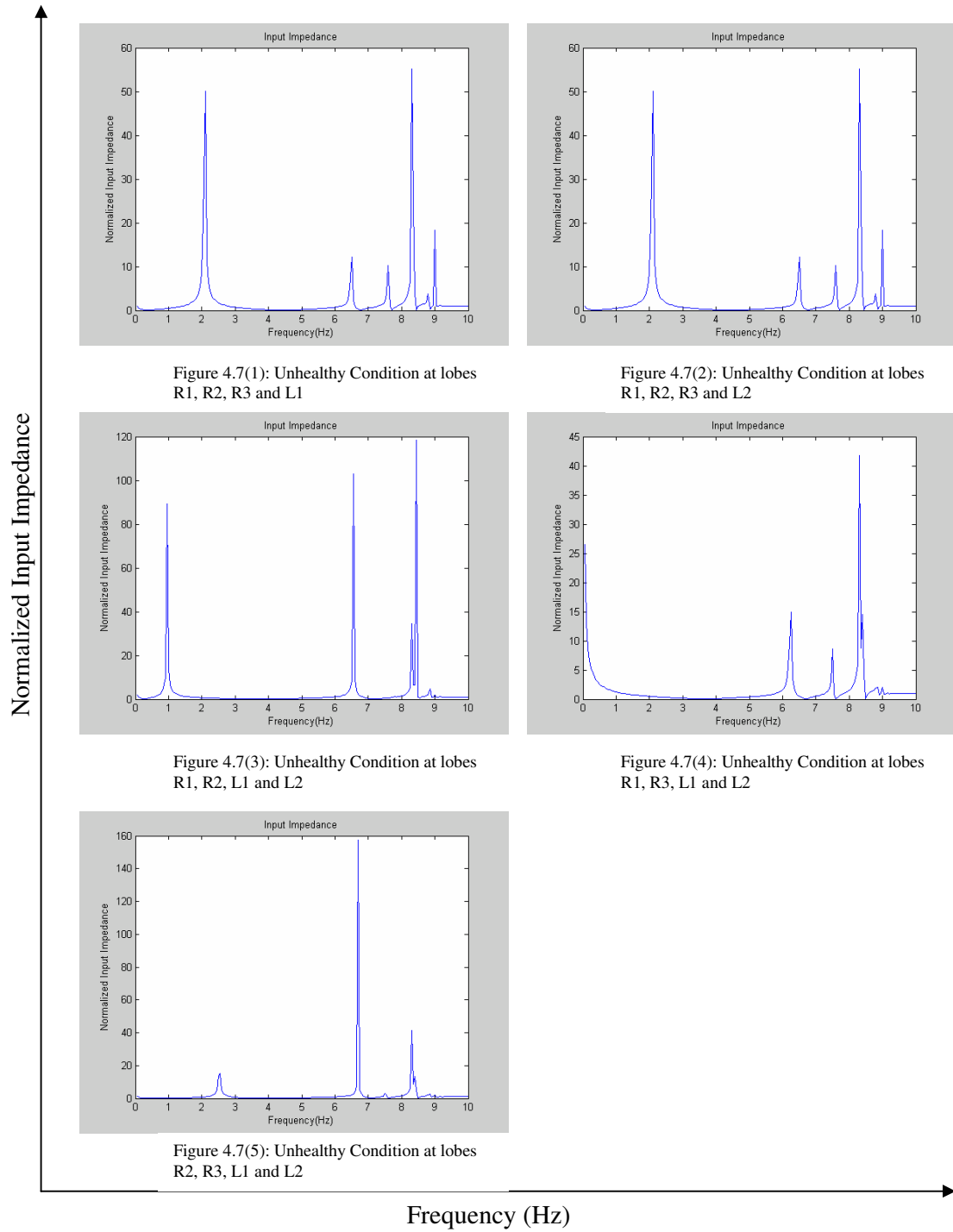


Figure 4.7: Normalized Input Impedance determined by increasing stiffness to unhealthy condition at every four lobes respectively

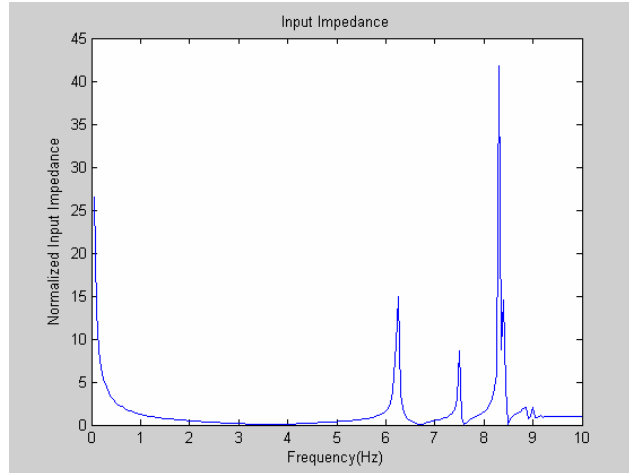


Figure 4.8: Normalized Input Impedance determined by increasing stiffness to unhealthy condition at all five lobes.

4.4 Experiments on Obstruction Investigation

The stiffness of each one of the lobes was increased by adding some rubber band stiffness to the outer surfaces of the lobe. The data results presented in Chapter 3 are used to calculate the input impedance of the 5-Lobe lung model. The graphs show that when increasing stiffness by adding more stiffness into each lobe at each experiment, dominant resonant frequency occurs approximately at 4 Hz. There are also some harmonic frequencies at a range of 7 Hz to 9 Hz but by comparing to the input impedance in Figure 4.7, their magnitudes are very small. However, in comparison to the predicted results on obstruction in Figure 4.4(1), the trends can not show any similarity as the first resonant frequency is found at around 4 Hz. Insignificant resonant frequencies are also found in between 7 to 9 Hz but can not be seen clearly. It might be assumed that the change of stiffness in experiment investigation can not have or may have a little effect when the system operates. Therefore, the results show in Figure 4.9 can not be used to validate the predict obstruction in the mathematical model, but further improvement of the lung simulator is necessary for more accurate validation.

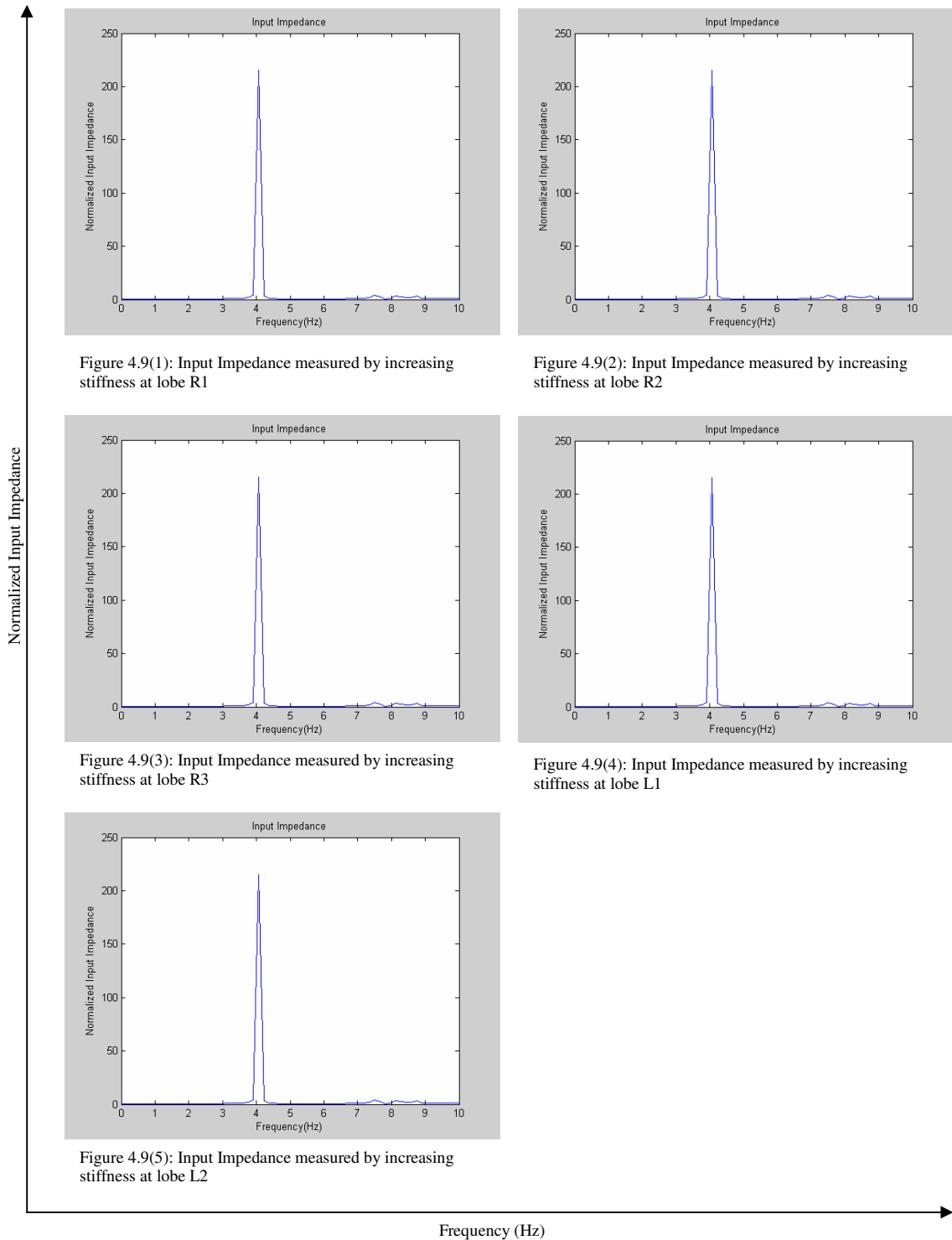


Figure 4.9: Normalized Input Impedance of the experiment investigations determined by increasing stiffness at each lobe respectively

4.5 Summary

The mathematical model is validated by comparing its results with experiment investigation results. Interestingly, the comparison has shown a very good matching between mathematical and experiment investigations results. However, due to mechanical problems that occurred in the lung simulator, the verdict of obstruction in five-lobe model can not be validated as expected. The future investigation will continue to complete this research. Nevertheless, the detailed discussions will be made in the next Chapter based on the results presented so far.

CHAPTER 5

5. OVERALL DISCUSSION

5.1 Introduction

Study of the dynamic behaviour of the respiratory system is not an easy task. The respiratory system is considered as a very complex system [4, 5]. However, many researchers have concluded that it is possible to model the lung system by using appropriate mathematical methods [4, 5, 7, 8, and 9]. To the best of our knowledge, no five-lobe lung model identical to the current one has been found in the present literature. This study investigates the frequency response of the input impedance and the basic dynamic characteristics of the five lobes lung model. The mathematical model is developed with five-lobes representing to the lung in this thesis as well as the practical model. Since the exact solutions are not available, experimental investigations are used to confirm and validate the mathematical model under certain conditions. Although the investigations may not give exact answers, it is believed that the mathematical methods can be used to predict or model the complex lung system in practice. This study is considered to have potential contribution to modelling dynamic respiratory system in the future.

This chapter provides detailed discussions for the mathematical results and experimental results presented in Chapter 4. The results documented in Tables 5.1 to 5.9 are summarised. Comparisons are also made to provide a better insight in the effects of obstruction on the input impedance of the five lobes model. Explanations of why there are some differences between the predicted model and practical model are proposed.

5.2 Comparison at healthy condition

Comparison between the spectrums of the input impedance in mathematical 5-Lobe lung model and experiment investigation in Figure 4.1 and Figure 4.2 has shown accurately results as many similarities can be observed. Tables 5.1 and 5.2 summarise the resonances found during simulation in both mathematical and experimental models, respectively. Six identical resonant frequencies have been found within the range of interest from 0 to 10 Hz. Similar results have been found by simulating the models up to 256 Hz. However, due to the setup in practical lung simulator, oscillating force signals were varied from 1/6 Hz up to 1 Hz; therefore, this thesis focuses on the frequency range up to 10 Hz and overlooks the resonant frequencies found in the range of 10 to 20 Hz. Overall, the model is consistent with the measured data, except the slight decrease in measured input impedance in the range of 7 to 9 Hz. Presumably, it might be a result of volume flow distortions or shunt effects in the airway system, or even the different equipment resistance that led to the systematic calculation errors. Although, the compared results between the mathematical and the experimental investigations have shown good agreement, there are still essential differences between these models. For instance, the difference between the magnitudes of the mathematical and experiment spectrum can be clearly seen in Figure 4.1 and Figure 4.2. This may be corresponded to the equipment resistance's differences or a lack of agreement between physical parameters used on this study.

In tables 5.1 to 5.2, six identical resonant frequencies are comparable in the frequency range of 0 to 10 Hz. It is observed that all of the experimental variables are correlated with the mathematical empirical equations. However, by comparing the normalised input impedance as shown in Figures 4.1 to 4.3, the results indicate there are some differences in magnitudes and separations. It indicates that physical parameters that used in both mathematical and experimental models need to be considered in this study such as elasticity of the airways in this case. There are several possible explanations for the differences that might be considered in this case. Firstly, it may be possible that there are differences between the damping ratio and stiffness of the balloon over the damping ratio and stiffness values that used in terminal impedance calculation, but due to the experimental setup we can not detect this possible difference. Secondly, there may be some measurement errors in the lung simulator elements which affect the correlations between pressure and volume flow rate due to the handling of the practical lung simulator when assembling them together. Thirdly, it may indicate that the

magnitude of the exciting force applied do not play an active role in this simulation, rather there are other more dominant factors influence the simulation process such as tension, tissue damping and tissue elastance. By contrast, most of the resonances seem to be highly correlated with the parameter properties variables of the lung tissues and airway smooth muscles, which may suggest that these factors have more dominant influences in these models. However, a more likely explanation for the lack of expected relationships may be that the practical lung simulator cannot deliver expectations due to some problems found during experimental trials. For example, a DC offset was found in experiment records of air velocity of five lobes, a possible reason may be explained that the heat produced from heating wire circuits has caused to this problem. Another problem is that there were some leaks inside the chamber of the lung simulator that may explain the reason why the pressure measurements were unstable during operations. Those errors may be the factors that lead to errors in calculation.

Table 5.1: Comparison between the predicted resonances for the mathematical model simulated by different range of frequencies

Range of Frequency	0 - 10 Hz	0-30 Hz	0-40 Hz	0-50 Hz	0-128 Hz	0-256 Hz
Resonance Number	Resonance					
1	4 Hz	4.8 Hz	4 Hz	4 Hz	4 Hz	4 Hz
2	7.5 Hz	7.1 Hz	7 Hz	7 Hz	7 Hz	7 Hz
3	8.3 Hz	8 Hz	8 Hz	8 Hz	8 Hz	8 Hz
4	8.4 Hz	14 Hz	14 Hz	14 Hz	14 Hz	14 Hz
5	8.8 Hz	18 Hz	18 Hz	18 Hz	18 Hz	18 Hz
6	9 Hz	25 Hz	25 Hz	25 Hz	25 Hz	25 Hz

Table 5.2: Comparison between measured resonances for the experiment five-lobe model recorded by different sampling rates

Sampling Rate	20 Hz	60 Hz	80 Hz	100 Hz	256 Hz	512 Hz
Resonance Number	Resonance					
1	4 Hz	4.25 Hz	3.8 Hz	4 Hz	4 Hz	4 Hz
2	7.5 Hz	7.5 Hz	7.5 Hz	7 Hz	7 Hz	7 Hz
3	8.3 Hz	8.5 Hz	9 Hz	8 Hz	8 Hz	8 Hz
4	-	14.5 Hz	14.5 Hz	14 Hz	14 Hz	14 Hz
5	8.8 Hz	18.2 Hz	19 Hz	18 Hz	18 Hz	18 Hz
6	9.2 Hz	25.2 Hz	25 Hz	25 Hz	25 Hz	25 Hz

Furthermore, experiment investigations on the lung simulator are performed at different exciting frequencies to validate the results of the mathematical investigation. Interestingly, the spectrums of the input impedance in Figure 4.3 of Chapter 4 still show very good agreement in comparison to the spectrum of mathematical investigations, except there is a difference when the lung simulator is set to simulate at 0.5 Hz as the whole spectrum shifts to the left. Differences are found in the range of 7 to 10 Hz as the measured data seems to oscillate in larger scale when the lung simulator is set to operate at 3 and 4 seconds per breath cycle. Summary of the resonances of the experiment investigation with different exciting frequencies is shown in Table 5.3.

Table 5.3: Comparison between resonances of the lung simulator measured at different exciting frequency.

Exciting Frequency	1/6 Hz	1/5 Hz	1/4 Hz	1/3 Hz	1/2 Hz	1 Hz
Resonance Number	Resonance					
1	4.1 Hz	4.2 Hz	4 Hz	4.1 Hz	3 Hz	4 Hz
2	7.5 Hz	7.5 Hz	7.5 Hz	7.5 Hz	7.3 Hz	7.5 Hz
3	8.2 Hz	8.2 Hz	8.2 Hz	8.2 Hz	8.3 Hz	8.2 Hz
4	8.8 Hz	8.8 Hz	8.9 Hz	8.8 Hz	8.8 Hz	8.8 Hz
5	9.2 Hz	9.2 Hz	9 Hz	9.1 Hz	9.2 Hz	9.2 Hz
6	-	-	-	-	-	-

Due to the interesting feature of low frequency up to 10 Hz as indicated previously, analysis only focuses on all the simulation and experiments within this range. Tables 5.4 and 5.5 are summaries of the results resonances observed from data collected in Chapter 4. It shows a good agreement between resonances of predicted and measured models even though there are still slight differences due to the errors in calculations.

Table 5.4: Comparison between predicted and measured resonances of the five-lobe models as measured at normal breath cycle.

Range of Determine Frequency	0-10 Hz	
Resonance Number	Predicted Model	Measured Model
1	4 Hz	4.1 Hz
2	7.5 Hz	7.5 Hz
3	8.3 Hz	8.2 Hz
4	8.4 Hz	8.8 Hz
5	8.8 Hz	9.2 Hz
6	9 Hz	-

Table 5.5: Comparison between predicted and measured resonances of the 5-Lobe models as measured at different exciting frequencies

Exciting Frequency		1/6 Hz	1/5 Hz	1/4 Hz	1/3 Hz	1/2 Hz	1 Hz
Resonance Number	Predicted Model	Experiment Model					
		1	4 Hz				
2	7.5 Hz	7.4 Hz	7.5 Hz	7.8 Hz	7.5 Hz	7.3 Hz	7.5 Hz
3	8.3 Hz	8.2 Hz	8.2 Hz	8.3 Hz	8.3 Hz	8.3 Hz	8.3 Hz
4	8.4 Hz	8.8 Hz	8.7 Hz	8.8 Hz	8.9 Hz	8.8 Hz	8.8 Hz
5	8.8 Hz	-	-	-	-	-	-
6	9 Hz	9 Hz	9.1 Hz	9.1 Hz	9.2 Hz	9.1 Hz	9.1 Hz

Overall, the similar spectrum of the input impedance obtained in both mathematical and experiment investigations have proven that the characteristics of the five-lobe model can be predicted in the low frequency range up to 10 Hz. By comparing between Tables 5.1 to 5.4, the six resonant frequencies have shown a good matching. It may be concluded that the mathematical model can be used for the future investigation in modelling the dynamic airway system.

5.3 Obstruction Investigation

Inspired by the results obtained in both mathematical and experiment investigations in normal conditions, the research is expanded to investigate the effect of various stiffness values on input impedance determination. Due to difficult experiences in mechanical lung simulator as described in Chapter 3, experimental investigations on obstruction are not fully achieved. Therefore, validation is based on qualitative rather than quantitative measurement. Theoretically, with the encouraging of the results obtained in previous section, predictably the experiment five-lobe model should behave as the mathematical model. The results produced a qualitative trend of variation rather than quantitative. This indicates that further work has to be made on the lung simulator to improve it for the future investigation.

Figure 4.4 in Chapter 4 shows the results that are obtained by varying the stiffness values of the proposed lung model from healthy to unhealthy condition at each lobe respectively. Overall, the first resonant frequency changes in the range of 3 to 4 Hz while the others remained within the range of 7 to 10 Hz. Specifically, the change in stiffness parameter has an impact in the results of resonant frequencies, mostly in the first three resonant frequencies. Figure 4.4 indicates that the second and third resonant

frequencies are affected the most by the change of stiffness as they dramatically increased their magnitudes.

Table 5.6 summarized and compared the resonances for this model and predicted model. The results show that the resonances are slightly affected when constrictions occurs in each lobe respectively. This is attributed to the fact that not only stiffness but also other factors such as tension, tissue damping have an impact in the results of spectrum of the input impedance.

Table 5.6: Summary and Comparison between the resonances for One-Lobe Obstruction and predicted models

Resonance Number	Predicted Model	Number of Simulation				
		1	2	3	4	5
1	4 Hz	3 Hz	4 Hz	4 Hz	3.5 Hz	3.5 Hz
2	7.5 Hz	7.2 Hz	7.5 Hz	7.1 Hz	7.1 Hz	7.2 Hz
3	8.3 Hz	8.2 Hz	8.3 Hz	8 Hz	8.3 Hz	8.3 Hz
4	8.4 Hz	8.4 Hz	8.4 Hz	8.3 Hz	8.5 Hz	8.4 Hz
5	8.8 Hz	8.7 Hz	8.8 Hz	8.7 Hz	8.8 Hz	8.8 Hz
6	9 Hz	-	9 Hz	-	9 Hz	9 Hz

For Two-Lobe obstruction, ten simulations are made to investigate the effects of changing stiffness values on the mathematical model. Figure 4.5 in Chapter 4 shows all of resonant frequencies are varied by increasing either their magnitude or the distance between them. For example, the separation between the first and the second resonant frequency is larger as the first frequency shifted to the left. This indicates that the impact on the entire system is significant, when increased stiffness at every two lobes. Table 5.7 shows the results.

Table 5.7 clearly indicate that the frequencies affected the most in this simulation are the first and the second resonances. The results show that the constriction in every two lobes did affect the value of the first resonant frequency. It suggests there are relationships between the first resonance and tissue elasticity.

Table 5.7: Summary and Comparison between the resonances for the Two-Lobe Obstruction and predicted simulations

Resonance Number	1	2	3	4	5	6	
Predicted Model	4Hz	7.5 Hz	8.3 Hz	8.4 Hz	8.8 Hz	9 Hz	
Number of Simulation	1	3 Hz	7.2 Hz	8.2 Hz	8.3 Hz	8.8 Hz	-
	2	2.9 Hz	6.8 Hz	8 Hz	8.3 Hz	8.8 Hz	-
	3	2.4 Hz	6.8 Hz	8.3 Hz	8.4 Hz	9 Hz	9.2 Hz
	4	2.4 Hz	6.8 Hz	8.3 Hz	8.4 Hz	9 Hz	9.2 Hz
	5	4 Hz	7.2 Hz	8 Hz	8.3 Hz	8.8 Hz	8.9 Hz
	6	3.5 Hz	7.2 Hz	8.3 Hz	8.5 Hz	8.8 Hz	9 Hz
	7	3.4 Hz	7.1 Hz	8.2 Hz	8.4 Hz	8.8 Hz	9 Hz
	8	3.4 Hz	6.8 Hz	7.6 Hz	8.4 Hz	8.8 Hz	9 Hz
	9	3.4 Hz	6.9 Hz	7.5 Hz	8.3 Hz	8.8 Hz	9 Hz
	10	2.6 Hz	6.9 Hz	8.3 Hz	8.5 Hz	8.8 Hz	9 Hz

For three-lobe obstruction, Figure 4.6 in Chapter 4 shows the entire spectrum affected. It is clear that higher resonant frequencies are affected by changing stiffness variables. However, the first resonant frequency is also influenced by shifting to the left, it results in the separation between it and the second is larger. Table 5.8 shows the summary for comparison.

Table 5.8: Summary and Comparison between the resonances for Three-Lobe Obstruction and predicted simulations

Resonance Number	1	2	*3	*4	*5	6	
Predicted Model	4 Hz	7.5 Hz	8.3 Hz	8.4 Hz	8.8 Hz	9 Hz	
Number of Simulation	1	3 Hz	6.8 Hz	8 Hz	8.3 Hz	8.8 Hz	-
	2	2.4 Hz	6.8 Hz	8.3 Hz	8.5 Hz	-	9 Hz
	3	2.4 Hz	6.8 Hz	8.3 Hz	8.5 Hz	-	9 Hz
	4	3.4 Hz	6.9 Hz	7.5 Hz	8.4 Hz	8.8 Hz	9 Hz
	5	3.4 Hz	6.9 Hz	7.5 Hz	8.4 Hz	8.8 Hz	9 Hz
	6	2.5 Hz	6.8 Hz	7.5 Hz	8.4 Hz	8.6 Hz	8.9 Hz

* Very close that could be attributed to the same resonance

Figure 4.7 in Chapter 4, varied stiffness was applied to four lobes at the same time. The results show that by increasing the number of obstruction location, the impact has strong influence on the whole spectrum in their magnitudes and separations. Especially the first and second resonances shift to the left, separation between them and the others becomes larger. Table 5.9 shows the result of summary for comparison.

Table 5.9: Summary and Comparison between the resonances for Four-Lobe Obstruction and predicted models

Resonance Number	1	2	3	4	5	6	
Predicted Model	4 Hz	7.5 Hz	8.3 Hz	8.4 Hz	8.8 Hz	9 Hz	
Number of Simulation	1	2 Hz	6.5 Hz	7.5 Hz	8.3 Hz	8.8 Hz	9 Hz
	2	2 Hz	6.5 Hz	7.5 Hz	8.4 Hz	8.8 Hz	9 Hz
	3	1 Hz	6.5 Hz	8.4 Hz	8.5 Hz	8.8 Hz	-
	4	0.2 Hz	6.2 Hz	7.5 Hz	8.4 Hz	8.5 Hz	9 Hz
	5	2.5 Hz	6.8 Hz	7.5 Hz	8.4 Hz	8.5 Hz	-

In Table 5.10, the results of resonances of the input impedance when five-lobe model is obstructed. It shows that the first resonance shifts almost to zero. The second and the third resonant frequencies also shift further to the left. The other resonances stay the same but change their magnitudes as well as their separations.

Table 5.10: Summary and Comparison between the resonances for Five-Lobe Obstruction and predicted models

Resonance Number	Predicted Results	Simulation
1	4 Hz	0.2 Hz
2	7.5 Hz	6.3 Hz
3	8.3 Hz	7.5 Hz
4	8.4 Hz	8.4 Hz
5	8.8 Hz	8.5 Hz
6	9 Hz	9 Hz

5.4 Summary

The mathematical and experimental models have been simulated. The discussions have shown that the impact of changing stiffness value of the lung parameters on the spectrum of the input impedance. Even though the study needs further improvement of the experimental side on the effect of occlusion on the input impedance determination, however, the major finding of this present study is that strong contribution of stiffness parameter on the resonant frequencies of the input impedance. More importantly, the mathematical methods used in this research have proved to be appropriate in modelling dynamic airway system.

Another observation in this study of obstruction is that large stiffness significantly affects the impedance magnitude of the spectrum of the resonances occurs during simulations.

CHAPTER 6

6. CONCLUSIONS AND FUTURE WORK

6.1 Conclusion

The objective of this thesis is to develop and investigate five lobes lung simulation model in both mathematical and experimental aspects in order to study the characteristics of the input impedance of the lung system. This study represents the first use of a dynamic and distributed-parameter acoustic model of the respiratory system to predict the characteristics of the 5-Lobe lung model. Despite the fact that the study is unable to perform some of the work due to the practical difficulties mentioned previously, mathematical model is consistent with a number of trends observed from measurements performed on normal conditions. The initial research aims set out in Chapter 1 have been achieved as the following.

Mathematical model of the dynamic acoustic five-lobe model representing to the actual lung system developed. This model extends previous research on conductive tubes [9] and includes two important components which are built as the airway dynamic component and the lung component. Mathematical equations of the dynamic of the airways component include complex parameters such as elastance, resistance and inertance of the airway properties. The lung component is proposed by a simple idealized lobe model that allows the terminal impedance at each lobe of the tested-lung is determined. In general, this model enables the input impedance of the actual lung to be simulated in different conditions such as healthy and unhealthy scenarios by changing its parameter properties.

Measurements of five terminal impedances at the five lobes model are performed using the existing lung simulator. Terminal impedances are measured at different pressure exciting frequencies as well as different sampling rates to determine resonant

frequencies occur during its operations. The results conclude that measured impedances are dependant on exciting frequencies.

The experiment input impedance of the five lobes model is determined using the measured results of the terminal impedances. This result is then compared with the result of the mathematical input impedance. Comparison allows us to conclude that the mathematical model can be used to predict the characteristics of the input impedance of the lung system. It also concludes that parameter properties used in the model are correlated. Therefore, validation of the mathematical model is gained.

Cases of study include numbers of obstruction on the mathematical model are investigated. The results identified numbers of resonant frequencies and are dependant on the change of stiffness of the lung's properties.

Despite encouraging results of this study, however, there are numbers of limitation identified in this research. First, the experiment terminal impedances are found to contain a DC offset. This problem can not be prevented but can be removed computationally. Second, pressure distortions are found due to the leaks of the pleural compartment and the tested-airways. As the results, the lung simulator can not produce some of experiment obstructions. Therefore, validation of obstructions needs further research.

6.2 Future Work

In the future, it is necessary to produce both a mechanical lung simulator and a computer lung simulation with a complex control system that is capable of accurately measuring the input impedance at different conditions. A more complex and accurate model, validated by experimental investigations on animals or humans would be useful for further studies. Also, an improvement in the electronics might enable to observe correctly measured data.

In the long term, the models might be developed into both a diagnostic aid model for researchers and a learning tool where the model is used to generate input impedance associated with specific diseases and/or obstructions.

REFERENCES

1. Dekker, E., *The transition between laminar and turbulent flow in the trachea*. J Appl Physiol, 1961. **16**: p. 1060-1064.
2. Rohrer, F., *Der Stromungswiderstand in den menschlichen Atemwegen*, Pflugers Arch. Ges. Physiol, 1915. Vol. 162, pp.255-259.
3. Jaffin, M.Y. and P. Kesic, *Airway resistance: a fluid mechanics approach*, Journal of Applied Physiology, 1974. Vol. 36, No. 3, pp.354-361.
4. Al-Jumaily, A. M. and P. Mithraratne. *Simulation of respiratory system for identifying airway occlusion*. Journal of Nonlinear Sciences and Numerical Simulation, 2000. **2**(1): 21-28.
5. Al-Jumaily, A.M. and Al-Saffar, A.M. *Dynamic Response Characteristics of Upper Respiratory System*, 1999. The Journal of the Acoustical Society of America, Vol. 106: 4, pt 2, 2172.
6. Fredberg, J.J. and J.A. Moore, *The distributed response of complex branching duct networks*. Journal of Acoustic Society of America, 1978. **63**: p. 954 - 961.
7. Al-Jumaily, A. M. and Y. Al-Fakhri. *Occlusion identification in respiratory system using asymmetric model*, 2003. Communications in Nonlinear Science and Numerical Simulation **8**(1): 37-47.
8. Al-Jumaily, A. M. and Y. Al-Fakhri. *Asymmetrically respiratory system simulation to identify airway occlusion*, 2001. ASME, International Mechanical Engineering Congress and Exposition, New York.
9. Al-Jumaily, A. M. and Y. Du. *Obstruction identification in a compliant tube with application to airway passages*, 2002. Journal of Vibration and Control **8**(5): 643-657.
10. Fredberg, J.J., and A. Hoenig. *Mechanical response of the lungs at high frequencies*. Journal of Biomedical Engineering, 1978. Vol: 100, pp: 57-66.
11. Fedberg, J.J., R.S, Sidell, M.E. Wohl and R.G. DeJong. *Canine pulmonary input-impedance measured by transient forced oscillations*. Journal of Biomedical Engineering, 1978. Vol: 100, pp: 67-71.
12. Fredberg, J.J, K.A. Jones, S. Nathan, S. Raboudi, Y.S. Prakash, S.A. Shore, J.P. Buther, and G.C. Sieck. *Friction in airway smooth muscle: mechanism, latch and implications in asthma*. Journal of Applied Physiology, 1996. Vol: 83, No3, pp: 731-738.
13. Fredberg, J.J. *A modal perspective of lung response*. Journal of Acoustic Society of America. 1978. Vol: 63, No 3, pp: 962-966.
14. Fredberg, JJ, Inouye D, Miller B, Nathan M, Jafari S, Raboudi SH, Butler JP, and Shore SA. *Airway smooth muscle, tidal stretches, and dynamically*

- determined contractile states.* Am J Respir Crit Care Med 156: 1752-1759, 1997
15. Fry, D.L. *A Preliminary Lung Model for Simulating the Aerodynamics of the Bronchial Tree.* Computers and Biomedical Research, 1968; Vol 2, pp: 111-134.
 16. Heather, L.G. and K.R. Lutchen. *Airway remodelling in asthma heterogeneities in smooth muscle shortening causing hyperresponsiveness.* Journal of Applied Physiology, 1999. Vol 86, No 6, pp: 2001-2012.
 17. Schmid-Schoenbein, G.W. and Y.C. Fung. *Force perturbation of respiratory system: (A) The traditional model.* Journal of Applied Physiology, 1978. Vol 63, pp: 194-204.
 18. Schmid-Schoenbein, G.W. and Y.C. Fung. *Force perturbation of respiratory system: (B) A continuum mechanics analysis.* Journal of Applied Physiology, 1978. Vol: 63, pp: 367-398.
 19. Reisch, S., Steltner, H., Timmer, J., Renotte, C. and Guttman, J. *Early Detection of Upper Airway Obstructions by Analysis of Acoustical Respiratory Input Impedance.* Biological Cybernetics, 1999; Vol. 81, pp. 25-37.
 20. Jackson, A.C., et al., *Branching airway network models for analyzing high-frequency lung input impedance.* Journal of Applied Physiology, 1993; Vol: 75(1): pp: 217-227
 21. Weibel, E.R., *Morphometry of the Human Lung.* 1963, New York: Academic Press.
 22. Au, P. and A. Al-Jumaily, *Asthma Relief and Airway Mechanics "A Literature Review".* to appear in Transworld Research Network, Advances in Vibration, 2002. TRN/SV/3.
 23. Au, P. *Vibration of Branched Circular Cylindrical Shells as Applied to the Airway Walls.* PhD Thesis, Auckland University of Technology, New Zealand. 2004.
 24. Ritz T, Dahme B, DuBois B.A, Folgering H, Fritz, G.K, Harver A, Kotses H, Lehrer P.M, Ring C, Steptoe A and Woestijne K. *Special Report: Guidelines for mechanical lung function measurements in psychophysiology.* Psychophysiology, 2002; Vol: 39, pp: 546-567.
 25. John. B. West. *Respiratory Physiology: The Essentials.* Lippincott Williams & Wilkins, U.S.A.
 26. J.P. Dalmont. *Acoustic Impedance Measurement, Part I: A Review.* Journal of Sound and Vibration, 2001, 243(3): 427-439.
 27. Oostveen E, MacLeod D, Lorino H, Farré R, Hantos Z, Desager K and Marchal F on behalf of the ERS Task Force on Respiratory Impedance Measurements. *The force oscillation technique in clinical practice:*

- methodology, recommendations and future developments.* European Respiratory Journal, 2003; Vol: 22, pp: 1026-1041.
28. Van de Woestijne, K. *The forced oscillation technique in intubated, mechanically-ventilated patients* [editorial]. European Respiratory Journal, 1993; Vol: 6, pp: 767-769.
 29. DuBois AB, Brody AW, Lewis DH, Burgess BF. *Oscillation mechanics of lungs and chest in man.* Journal Applied Physiology, 1956; Vol:8, pp: 587–594.
 30. Otis D. R., Petak F., Hantos Z., Fredberg J. J. and Kamm R. D. *Airway Closure and Reopening Assessed by the Alveolar Capsule Oscillation Technique.* Journal of Applied Physiology, 1996. Vol: 80, pp 2077-2084.
 31. Louis B, Glass G, Kresen B, Fredberg J. *Airway area by acoustic reflection: The two-microphone method.* J.Biomech.Eng, 1993. Vol: 115, pp 278-285.
 32. Louis B, Glass G and Fredberg J.J. *Pulmonary airway area by the two-microphone acoustic reflection method.* Journal of Applied Physiology, 1994. 76(5): 2234-2240.
 33. Louis B, Fodil R, Jaber S, Pigeot J, Jarreau P, Lofaso F, and Isabey D. *Dual assessment of airway area profile and respiratory input impedance from a single transient wave.* Journal Applied Physiology, 2001. Vol: 90 (2), pp630-637.
 34. Hoffstein V, Fredberg JJ. *The acoustic reflection technique for non-invasive assessment of upper airway area.* European Respiratory Journal, 1991. Vol: 4, pp: 602–611.
 35. Raphael D, Benbassat M, Arnaudov D, Bohorquez A, Nasser B (2002) *Validation study of two microphone acoustic reflectometry for determination of breathing tube placement in 200 adult patients.* Anesthesiology, 2002. Vol: 97, pp: 1371–1377.
 36. Jackson, A.C., J.P. Butler, E.J. Millet, F.G. Hoppin and S.V. Dawson. *Airway geometry by analysis of acoustic pulse response measurements.* Journal of Applied Physiology, 1977. Vol: 43, pp: 523-536.
 37. Fredberg, J.J, M.E. Wohl, G.M Glass and H.L. Dorkin. *Airway area by acoustic reflections measured at the mouth.* Journal of Applied Physiology, 1980. Vol: 48, pp: 748-758.
 38. Tang, D., Anderson, D., Biz, S. and Ku, D. N. *Steady Viscous Flow in Constricted Elastic Tubes Subjected to a Uniform External Pressure.* International Journal for Numerical Methods in Engineering, 1998; Vol. 41, pp. 1391-1415.
 39. Elad, D., Kamm, R. D. and Shapir, A. H. *Tube Law for the Intrapulmonary Airway.* Journal of Applied Physiology, 1988; Vol. 65, pp. 7-13.
 40. Halpern D., Grotberg J.B. *Fluid-elastic instabilities of liquid-lined flexible tubes.* Journal of Fluid Mechanics, 1992; Vol: 244, pp: 615-632.

41. Halpern D., Grotberg J.B. *Surfactant effects on fluid-elastic instabilities of liquid-lined flexible tubes: a model of airway closure.* Journal of Biomechanical Engineering, 1993; Vol: 115, pp: 271-277.
42. Margolis, D.L., M. Tabrisi. *Acoustic modelling of lung dynamics using bond graphs.* Journal of Biomechanical Engineering, 1983. Vol: 105, No 1, pp: 84-91.
43. Harper V. P. *Respiratory Tract Acoustical Modelling and Measurements.* PhD Thesis, Purdue University. U.S.A, 2000.
44. Nucci G, Tessarin S and Cobelli C. *A morphometric model of lung mechanics for time-domain analysis of alveolar pressures during mechanical ventilation.* Annals of Biomedical Engineering, 2002; Vol: 30, pp: 537-545.
45. Horsfield K, Dart G, Olson F.G, Cumming G. *Model of the human bronchial tree.* Journal Applied Physiology; 1971.
46. Bates J.H.T, Rossi A. and Milic-Emili J. *Analysis of the behaviour of the respiratory system with constant inspiratory flow.* Journal of Applied Physiology, 1985; Vol 58, pp: 1840-1848.
47. Otis A, McKerrow C, Bartlett R, Mead J, McIlroy M, Selverstone N and Radford E. *Mechanical factors in distribution of pulmonary ventilation.* Journal of Applied Physiology, 1956; Vol 8, pp: 427-443.
48. Wanner A, Zarzecki S, Atkins N, Zapata A and Sackner M.A. *Relationship between Frequency Dependence of Lung Compliance and Distribution of Ventilation.* The Journal of Clinical Investigation, 1974; Vol 54, pp: 1200-1213.
49. Prasika M. *The effect of pressure oscillations on neonatal breathing.* Master Thesis, Auckland University of Technology, New Zealand. 2004.
50. Gijs I. *Breathing Simulator.* Thesis, Auckland University of Technology, New Zealand. 2003.

APPENDICES

Appendix A	Mathematical Equations
Appendix B	Matlab Programs for Calculating Input Impedance of the Mathematical Model and Experiment Model
Appendix C	Matlab File of FFT function for calculating terminal impedance
Appendix D	Experiment Investigation Results
Appendix E	Experiment Input Impedance Results

Al-Jumaily and Du [9] developed these equations by studying a distributed-parameter of a hydraulic tube. They used Newton's second law of motion, which consider wall inertance and elastance. Further mathematical manipulation and linearized methods applied, results obtained as:

$$\frac{1}{\rho_0} \cdot \frac{\partial p_p}{\partial x} + \frac{\partial v_p}{\partial t} = 0 \quad (A1)$$

$$\frac{1}{K_c} \cdot \frac{\partial v_p}{\partial x} + \frac{\partial p_p}{\partial t} = 0 \quad (A2)$$

Where: p_p is perturbation of fluid pressure, v_p is perturbation of fluid velocity, ρ_0 is initial steady-state fluid mass density, K_c is tube total compliance.

Total compliance is given by:

$$K_c = \frac{1}{M_B} + \frac{1}{K_w \left(\frac{D^2}{\omega_n^2} + 1 \right)} \quad (A3)$$

Where: K_w is tube wall elastance and is given by:

$$K_w = \frac{r_0}{2K} = \frac{E \cdot t_w - p_0 \cdot r_0}{2r_0} \quad (A4)$$

Using Laplace transform with zero initial condition, equations (A1) and (A2) reduce to:

$$\frac{1}{\rho_0} \cdot \frac{dP_p(x,s)}{dx} + s \cdot V_p(x,s) = 0 \quad (A5)$$

$$\frac{1}{\frac{1}{M_B} + \frac{1}{K_w \left(\frac{s^2}{\omega_n^2} + 1 \right)}} \cdot \frac{dV_p(x,s)}{dx} + s \cdot P_p(x,s) = 0 \quad (A6)$$

Equation (A4) can be differentiated with x to be:

$$\frac{1}{M_B} + \frac{1}{K_w \left(\frac{s^2}{\omega_n^2} + 1 \right)} \cdot \frac{d^2 V_p(x,s)}{dx^2} + s \cdot \frac{dP_p(x,s)}{dx} = 0 \quad (\text{A7})$$

Rearranged this equation to be:

$$\frac{dP_p(x,s)}{dx} = -\frac{1}{s} \cdot \frac{1}{\frac{1}{M_B} + \frac{1}{K_w \left(\frac{s^2}{\omega_n^2} + 1 \right)}} \cdot \frac{d^2 V_p(x,s)}{dx^2} \quad (\text{A8})$$

Substituting equation (A6) into equation A1 resulted in:

$$-\frac{1}{\rho_0 s} \cdot \frac{1}{\frac{1}{M_B} + \frac{1}{K_w \left(\frac{s^2}{\omega_n^2} + 1 \right)}} \cdot \frac{d^2 V_p(x,s)}{dx^2} + s \cdot V_p(x,s) = 0 \quad (\text{A9})$$

Equation A7 can be rewritten as:

$$\frac{d^2 V_p(x,s)}{dx^2} - \frac{\rho_0 \cdot [K_w s^2 + (K_w + M_B) \cdot \omega_n^2] \cdot s^2}{K_w M_B (s^2 + \omega_n^2)} \cdot V_p(x,s) = 0 \quad (\text{A10})$$

Let:

$$M = \frac{\rho_0 \cdot [K_w s^2 + (K_w + M_B) \cdot \omega_n^2]}{K_w M_B (s^2 + \omega_n^2)} : \text{is parameter} \quad (\text{A11})$$

In equation A10, solution for $V_p(x,s)$ is given:

$$V_p(x,s) = C_1 \cdot e^{s \cdot \sqrt{M} \cdot x} + C_2 \cdot e^{-s \cdot \sqrt{M} \cdot x} \quad (\text{A12})$$

If considering the boundary conditions $V_p(0,s)$ and $V_p(L,s)$, respectively for $x=0$ and $x=L$, to obtain for the constants C_1 and C_2 , this gives:

$$V_p(0,s) = C_1 + C_2 \quad (\text{A13})$$

$$V_p(L,s) = C_1 \cdot e^{s \cdot \sqrt{M} \cdot L} + C_2 \cdot e^{-s \cdot \sqrt{M} \cdot L} \quad (\text{A14})$$

$$C_1 = \frac{-V_p(0,s) \cdot e^{-s \cdot \sqrt{M} \cdot L} + V_p(L,s)}{2 \cdot \sinh(s \cdot \sqrt{M} \cdot L)} \quad (\text{A15})$$

$$C_2 = \frac{V_p(0,s) \cdot e^{s \cdot \sqrt{M} \cdot L} - V_p(L,s)}{2 \cdot \sinh(s \cdot \sqrt{M} \cdot L)} \quad (\text{A16})$$

Manipulating and implementing the boundary condition at $x=0$ and $x=L$. Relationships between inlet pressure and volume flowrate with outlet pressure and volume flowrate can be written as:

$$\cosh(s \cdot \sqrt{M} \cdot L) \cdot V_p(0, s) - \frac{\sqrt{M}}{\rho_0} \sinh(s \cdot \sqrt{M} \cdot L) \cdot P_p(0, s) = V_p(L, s) \quad (\text{A17})$$

and

$$-\frac{\rho_0}{\sqrt{M}} \cdot \sinh(s \cdot \sqrt{M} \cdot L) \cdot V_p(0, s) + \cosh(s \cdot \sqrt{M} \cdot L) \cdot P_p(0, s) = P_p(L, s) \quad (\text{A18})$$

Using matrix notation, equation A15 and A16 may be written as:

$$\begin{bmatrix} V_p(L, s) \\ P_p(L, s) \end{bmatrix} = \begin{bmatrix} \cosh(s \cdot \sqrt{M} \cdot L) & -\frac{\sqrt{M}}{\rho_0} \sinh(s \cdot \sqrt{M} \cdot L) \\ -\frac{\rho_0}{\sqrt{M}} \cdot \sinh(s \cdot \sqrt{M} \cdot L) & + \cosh(s \cdot \sqrt{M} \cdot L) \end{bmatrix} \begin{bmatrix} V_p(0, s) \\ P_p(0, s) \end{bmatrix} \quad (\text{A19})$$

Matlab computer program for calculating input impedance of the mathematical 5-lobe model

System Geometry

MB=142355.2900;	air bulk modulus kg/(m.s ²)
pa=1.21;	air mass density kg/m ³
p0=980;	10 cmH ₂ O, initial steady-state pressure pa
m=0.005;	mass of lobe material (kg);
f=0:1/20:10;	exciting frequency (Hz)

Airway inside radius (m)

r0=1e-2;	main tube inside radius in initial steady-state m
r11=8e-3;	right primary tube inside radius in initial steady-state m
r12=6e-3;	left primary tube inside radius in initial steady-state m
r1=5e-3;	secondary branch number 1 tube inside radius in initial steady-state m
r2=3e-3;	secondary branch number 2 tube inside radius in initial steady-state m
r3=3e-3;	second branch 3 tube inside radius in initial steady-state m
r4=3e-3;	second branch 4 tube inside radius in initial steady-state m
r5=2e-3;	first and second branches

Cross-Sectional Area:

A0=pi*r0 ² ;	main tube area in initial steady-state m ²
A11=pi*r11 ² ;	first branch 1 tube area in initial steady-state m ²
A12=pi*r12 ² ;	first branch 2 tube area in initial steady-state m ²
A1=pi*r1 ² ;	second branch 1 tube area in initial steady-state m ²
A2=pi*r2 ² ;	second branch 2 tube area in initial steady-state m ²
A3=pi*r3 ² ;	second branch 3 tube area in initial steady-state m ²
A4=pi*r4 ² ;	second branch 4 tube area in initial steady-state m ²
A5=pi*r5 ² ;	

Airway length(m)

L0=12e-2;	total length of main tube
-----------	---------------------------

L1=10e-2; total length of first branch tube
 l=8e-2; total length of second branch tube
 l1=7e-2;

Airway wall thickness (m)

tw=3e-3; main tube wall thickness m
 tw1=1e-3; first branch tube wall thickness m
 tw2=5e-4; second branch tube wall thickness m
 tw3=4e-4; third branch tube wall thickness (m)

Linear density of material (kg/m)

pw=1000; kg/m3

Elastance of material wall

E=6e3; Elastance of the airway wall material N/m2

.....
PROGRAMING

Inertance of the tube wall equations

Kn0=2*r0/(E*tw-p0*r0);
 Kn11=2*r11/(E*tw1-p0*r11);
 Kn12=2*r12/(E*tw1-p0*r12);
 Kn1=2*r1/(E*tw2-p0*r1);
 Kn2=2*r2/(E*tw2-p0*r2);
 Kn3=2*r3/(E*tw2-p0*r3);
 Kn4=2*r4/(E*tw2-p0*r4);
 Kn31=2*r5/(E*tw3-p0*r5);
 Kn32=2*r5/(E*tw3-p0*r5);

%-----

% **Parameters Calculation**

%-----

% **....Calculation of natural frequency of the airways:**

%-----

wn0=sqrt((E*tw-p0*r0)/(r0^2*pw*tw));
 wn11=sqrt((E*tw1-p0*r11)/(r11^2*pw*tw1));
 wn12=sqrt((E*tw1-p0*r12)/(r12^2*pw*tw1));
 wn1=sqrt((E*tw2-p0*r1)/(r1^2*pw*tw2));
 wn2=sqrt((E*tw2-p0*r2)/(r2^2*pw*tw2));
 wn3=sqrt((E*tw2-p0*r3)/(r3^2*pw*tw2));
 wn4=sqrt((E*tw2-p0*r4)/(r4^2*pw*tw2));
 wn31=sqrt((E*tw3-p0*r5)/(r5^2*pw*tw3));
 wn32=sqrt((E*tw3-p0*r5)/(r5^2*pw*tw3));

%-----

% **.....Calulation M parameter:Equation**

%-----

M0=(pa*((1+Kn0*MB)*wn0^2-(2*pi*f).^2))/(MB*(wn0^2-(2*pi*f).^2));
 M11=(pa*((1+Kn11*MB)*wn11^2-(2*pi*f).^2))/(MB*(wn11^2-(2*pi*f).^2));

```

M12=(pa*((1+Kn12*MB)*wn12^2-(2*pi*f).^2))./(MB*(wn12^2-(2*pi*f).^2));
M1=(pa*((1+Kn1*MB)*wn1^2-(2*pi*f).^2))./(MB*(wn1^2-(2*pi*f).^2));
M2=(pa*((1+Kn2*MB)*wn2^2-(2*pi*f).^2))./(MB*(wn2^2-(2*pi*f).^2));
M3=(pa*((1+Kn3*MB)*wn3^2-(2*pi*f).^2))./(MB*(wn3^2-(2*pi*f).^2));
M4=(pa*((1+Kn4*MB)*wn4^2-(2*pi*f).^2))./(MB*(wn4^2-(2*pi*f).^2));
M31=(pa*((1+Kn31*MB)*wn31^2-(2*pi*f).^2))./(MB*(wn31^2-(2*pi*f).^2));
M32=(pa*((1+Kn32*MB)*wn32^2-(2*pi*f).^2))./(MB*(wn32^2-(2*pi*f).^2));

```

```

%-----
%
% termination Impedance Calculation
%-----

```

```

k=6e3; % lung stiffness at normal conditions
k1=10e9; % Lung stiffness at abnormal conditions
B=20; % lung damping coefficient
B1=20; % Lung damping coefficient at abnormal
A=0.5; % lung cross-sectionnal area
wn=(1/2*pi)*sqrt(k/m); % lung natural frequency
w=2*pi*f; % frequency exciting
s=j*w; % Laplace transform s
Ze=(m.*s.^2+B.*s+k)./(A.^2*s); % Terminal Impedance calculated at normal
conditions
Ze1=(m.*s.^2+B.*s+k1)./(A.^2*s); % Terminal Impedance calculated at abnormal
conditons
ZL31=Ze1; % terminal Impedance at lobe R2
ZL32=Ze1; % terminal impedance at lobe R3
ZL1=Ze1; % terminal impedance at lobe R1
ZL3=Ze1; % terminal impedance at lobe L1
ZL4=Ze1; % terminal impedance at lobe L2

```

```

%-----
% Calculation of Input Impedance at 5- lobe model
%-----

```

```

%Zo31=((pa./sqrt(M31)).*sinh(i*2*pi*11*sqrt(M31).*f))./(A5*(cosh(i*2*pi*11*sqrt(M
31).*f)));

```

```

Zo31=((pa./sqrt(M31)).*sinh(i*2*pi*11*sqrt(M31).*f)+A5*ZL31.*cosh(i*2*pi*11...
.*sqrt(M31).*f))./(A5*(cosh(i*2*pi*11*sqrt(M31).*f)+A5*ZL31.*(sqrt(M31)/pa).*...
sinh(i*2*pi*11*sqrt(M31).*f)));

```

```

%Zo32=((pa./sqrt(M32)).*sinh(i*2*pi*11*sqrt(M32).*f))./(A5*(cosh(i*2*pi*11*sqrt(M
32).*f)));

```

```

Zo32=((pa./sqrt(M32)).*sinh(i*2*pi*11*sqrt(M32).*f)+A5*ZL32.*cosh(i*2*pi*11...
.*sqrt(M32).*f))./(A5*(cosh(i*2*pi*11*sqrt(M32).*f)+A5*ZL32.*(sqrt(M32)/pa).*...
sinh(i*2*pi*11*sqrt(M32).*f)));

```

```

ZL2=Zo31.*Zo32./Zo31+Zo32;

```

```

%Z1=((pa./sqrt(M1)).*sinh(i*2*pi*1*sqrt(M1).*f))./(A1*(cosh(i*2*pi*1*sqrt(M1).*f)));

```

```

Z1=((pa./sqrt(M1)).*sinh(i*2*pi*1*sqrt(M1).*f)+A1*ZL1.*cosh(i*2*pi*1...
.*sqrt(M1).*f))./(A1*(cosh(i*2*pi*1*sqrt(M1).*f)+A1*ZL1.*(sqrt(M1)/pa).*...
sinh(i*2*pi*1*sqrt(M1).*f)));

```

```

%Z2=((pa./sqrt(M2)).*sinh(i*2*pi*1*sqrt(M2).*f))./(A2*(cosh(i*2*pi*1*sqrt(M2).*f)));

Z2=((pa./sqrt(M2)).*sinh(i*2*pi*1*sqrt(M2).*f)+A2*ZL2.*cosh(i*2*pi*1...
.*sqrt(M2).*f))./(A2*(cosh(i*2*pi*1*sqrt(M2).*f)+A2*ZL2.*(sqrt(M2)/pa).*...
sinh(i*2*pi*1*sqrt(M2).*f)));

%Z3=((pa./sqrt(M3)).*sinh(i*2*pi*1*sqrt(M3).*f))./(A3*(cosh(i*2*pi*1*sqrt(M3).*f)));

Z3=((pa./sqrt(M3)).*sinh(i*2*pi*1*sqrt(M3).*f)+A3*ZL3.*cosh(i*2*pi*1...
.*sqrt(M3).*f))./(A3*(cosh(i*2*pi*1*sqrt(M3).*f)+A3*ZL3.*(sqrt(M3)/pa).*...
sinh(i*2*pi*1*sqrt(M3).*f)));

%Z4=((pa./sqrt(M4)).*sinh(i*2*pi*1*sqrt(M4).*f))./(A4*(cosh(i*2*pi*1*sqrt(M4).*f)));

Z4=((pa./sqrt(M4)).*sinh(i*2*pi*1*sqrt(M4).*f)+A4*ZL4.*cosh(i*2*pi*1...
.*sqrt(M4).*f))./(A4*(cosh(i*2*pi*1*sqrt(M4).*f)+A4*ZL4.*(sqrt(M4)/pa).*...
sinh(i*2*pi*1*sqrt(M4).*f)));

%Zo31=((pa./sqrt(M31)).*sinh(i*2*pi*11*sqrt(M31).*f))./(A5*(cosh(i*2*pi*11*sqrt(M
31).*f)));

Z11=(Z1.*Z2)/(Z1+Z2);
Z12=(Z3.*Z4)/(Z3+Z4);
Z110=((pa./sqrt(M11)).*sinh(i*2*pi*L1*sqrt(M11).*f)+A11*Z11.*cosh(i*2*pi*L1...
.*sqrt(M11).*f))./(A11*(cosh(i*2*pi*L1*sqrt(M11).*f)+A11*Z11.*(sqrt(M11)/pa).*...
sinh(i*2*pi*L1*sqrt(M11).*f)));
Z120=((pa./sqrt(M12)).*sinh(i*2*pi*L1*sqrt(M12).*f)+A12*Z12.*cosh(i*2*pi*L1...
.*sqrt(M12).*f))./(A12*(cosh(i*2*pi*L1*sqrt(M12).*f)+A12*Z12.*(sqrt(M12)/pa).*...
sinh(i*2*pi*L1*sqrt(M12).*f)));
ZL=(Z110.*Z120)/(Z110+Z120);
Z0=((pa./sqrt(M0)).*sinh(i*2*pi*L0*sqrt(M0).*f)+A0*ZL.*cosh(i*2*pi*L0...
.*sqrt(M0).*f))./(A0*(cosh(i*2*pi*L0*sqrt(M0).*f)+A0*ZL.*(sqrt(M0)/pa).*...
sinh(i*2*pi*L0*sqrt(M0).*f)));
z=abs(Z0);
% Normalized Input Impedance:
Mw=0.1508;
Kw0=(E*tw-p0*r0)/(2*r0);
w0=sqrt(Kw0/Mw);
w1=sqrt((Kw0+MB)/Mw);
H=(w1^2-(2*pi*f).^2)/(w0^2-(2*pi*f).^2);
Zs=(1/A0)*sqrt((MB*pa)/abs(H)); % Characteristic Impedance
NII=abs(Z0)/abs(Zs);
figure(1);
plot(f,NII);
xlabel('Frequency(Hz)');
ylabel('Normalized Input Impedance');
title('Input Impedance');

```

Matlab Computer program for calculating the experiment input impedance of the 5-lobe model

```

% *****
% SYSTEM GEOMETRY

MB=142355.2900;           % air bulk modulus kg/ (m*s2)
Pa=1.21;                 % air mass density kg/m3
p0=980;                  % 10 cmH20, initial steady-state pressure pa
[a1, b1]=xlsread('Z1');
[a2, b2]=xlsread('Z2');
[a3, b3]=xlsread('Z3');
[a4, b4]=xlsread('Z4');
[a5, b5]=xlsread('Z5');
[f, f1]=xlsread('frequency');
Z1=a1(:,1);
Z2=a2(:,1);
Z3=a3(:,1);
Z4=a4(:,1);
Z5=a5(:,1);
f=f(:,1);

% Airway inside radius (m)

r0=1e-2;                 % main tube inside radius in initial steady-state m
r11=8e-3;                % right primary tube inside radius in initial
                        % steady-state m
r12=6e-3;                % left primary tube inside radius in initial steady-
                        % state m
r1=5e-3;                 % secondary branch number 1 tube inside radius
                        % in initial steady-state m
r2=3e-3;                 % secondary branch number 2 tube inside radius
                        % in initial steady-state m
r3=3e-3;                 % second branch 3 tube inside radius in initial
                        % steady-state m
r4=3e-3;                 % second branch 4 tube inside radius in initial
                        % steady-state m
r5=2e-3;                 % first and second branches

% Cross-Sectional Area:

A0=pi*r0^2;              % main tube area in initial steady-state m2
A11=pi*r11^2;            % first branch 1 tube area in initial steady-state m2
A12=pi*r12^2;            % first branch 2 tube area in initial steady-state m2
A1=pi*r1^2;              % second branch 1 tube area in initial steady-state
                        % m2
A2=pi*r2^2;              % second branch 2 tube area in initial steady-state
                        % m2
A3=pi*r3^2;              % second branch 3 tube area in initial steady-state
                        % m2

```

A4=pi*r4^2; % second branch 4 tube area in initial steady-state
m2
A5=pi*r5^2;

% Airway length (m)

L0=12e-2; % total length of main tube
L1=10e-2; % total length of first branch tube
l=8e-2; % total length of second branch tube
l1=7e-2;

% Airway wall thickness (m)

tw=3e-3; % main tube wall thickness m
tw1=1e-3; % first branch tube wall thickness m
tw2=5e-4; % second branch tube wall thickness m
tw3=4e-4; % third branch tube wall thickness (m)

% Linear density of material (kg/m)

pw=1000; % kg/m3

% Elastance of material wall

E=6e3; % Elastance of the airway wall N/m2

% Inertance of the tube wall equations

%-----
Kn0=2*r0/(E*tw-p0*r0);
Kn11=2*r11/(E*tw1-p0*r11);
Kn12=2*r12/(E*tw1-p0*r12);
Kn1=2*r1/(E*tw2-p0*r1);
Kn2=2*r2/(E*tw2-p0*r2);
Kn3=2*r3/(E*tw2-p0*r3);
Kn4=2*r4/(E*tw2-p0*r4);
Kn31=2*r5/(E*tw3-p0*r5);
Kn32=2*r5/(E*tw3-p0*r5);

%-----
% Parameters Calculation

%-----
% Calculation of natural frequency of the airways:

%-----
wn0=sqrt((E*tw-p0*r0)/(r0^2*pw*tw));
wn11=sqrt((E*tw1-p0*r11)/(r11^2*pw*tw1));
wn12=sqrt((E*tw1-p0*r12)/(r12^2*pw*tw1));
wn1=sqrt((E*tw2-p0*r1)/(r1^2*pw*tw2));
wn2=sqrt((E*tw2-p0*r2)/(r2^2*pw*tw2));
wn3=sqrt((E*tw2-p0*r3)/(r3^2*pw*tw2));
wn4=sqrt((E*tw2-p0*r4)/(r4^2*pw*tw2));

```

wn31=sqrt((E*tw3-p0*r5)/(r5^2*pw*tw3));
wn32=sqrt((E*tw3-p0*r5)/(r5^2*pw*tw3));
%-----
% Calculation M parameter:Equation: M=rho*[(1+Kn*MB)*wn^2-w^2]/MB*(wn^2-
w^2)
%-----
M0=(pa*((1+Kn0*MB)*wn0^2-(2*pi*f).^2))/(MB*(wn0^2-(2*pi*f).^2));
M11=(pa*((1+Kn11*MB)*wn11^2-(2*pi*f).^2))/(MB*(wn11^2-(2*pi*f).^2));
M12=(pa*((1+Kn12*MB)*wn12^2-(2*pi*f).^2))/(MB*(wn12^2-(2*pi*f).^2));
M1=(pa*((1+Kn1*MB)*wn1^2-(2*pi*f).^2))/(MB*(wn1^2-(2*pi*f).^2));
M2=(pa*((1+Kn2*MB)*wn2^2-(2*pi*f).^2))/(MB*(wn2^2-(2*pi*f).^2));
M3=(pa*((1+Kn3*MB)*wn3^2-(2*pi*f).^2))/(MB*(wn3^2-(2*pi*f).^2));
M4=(pa*((1+Kn4*MB)*wn4^2-(2*pi*f).^2))/(MB*(wn4^2-(2*pi*f).^2));
M31=(pa*((1+Kn31*MB)*wn31^2-(2*pi*f).^2))/(MB*(wn31^2-(2*pi*f).^2));
M32=(pa*((1+Kn32*MB)*wn32^2-(2*pi*f).^2))/(MB*(wn32^2-(2*pi*f).^2));
%-----
%          termination Impedance Calculation
%-----

ZL31=Z2;          % Terminal impedance at R2
ZL32=Z3;          % Terminal Impedance at R3
ZL1=Z1;          % Terminal Impedance at R1
ZL3=Z4;          % Terminal Impedance at L1
ZL4=Z5;          % Terminal Impedance at L2
%-----
%          Calculation of Impedance at 5 lobes
%-----
%Zo31=((pa./sqrt(M31)).*sinh(i*2*pi*11*sqrt(M31).*f))/(A5*(cosh(i*2*pi*11*sqrt(M
31).*f)));

Zo31=((pa./sqrt(M31)).*sinh(i*2*pi*11*sqrt(M31).*f)+A5*ZL31.*cosh(i*2*pi*11...
.*sqrt(M31).*f))/(A5*(cosh(i*2*pi*11*sqrt(M31).*f)+A5*ZL31.*(sqrt(M31)/pa).*...
sinh(i*2*pi*11*sqrt(M31).*f)));

%Zo32=((pa./sqrt(M32)).*sinh(i*2*pi*11*sqrt(M32).*f))/(A5*(cosh(i*2*pi*11*sqrt(M
32).*f)));

Zo32=((pa./sqrt(M32)).*sinh(i*2*pi*11*sqrt(M32).*f)+A5*ZL32.*cosh(i*2*pi*11...
.*sqrt(M32).*f))/(A5*(cosh(i*2*pi*11*sqrt(M32).*f)+A5*ZL32.*(sqrt(M32)/pa).*...
sinh(i*2*pi*11*sqrt(M32).*f)));

ZL2=Zo31.*Zo32./Zo31+Zo32;

%Z1=((pa./sqrt(M1)).*sinh(i*2*pi*1*sqrt(M1).*f))/(A1*(cosh(i*2*pi*1*sqrt(M1).*f)));

Z1=((pa./sqrt(M1)).*sinh(i*2*pi*1*sqrt(M1).*f)+A1*ZL1.*cosh(i*2*pi*1...
.*sqrt(M1).*f))/(A1*(cosh(i*2*pi*1*sqrt(M1).*f)+A1*ZL1.*(sqrt(M1)/pa).*...
sinh(i*2*pi*1*sqrt(M1).*f)));

%Z2=((pa./sqrt(M2)).*sinh(i*2*pi*1*sqrt(M2).*f))/(A2*(cosh(i*2*pi*1*sqrt(M2).*f)));

Z2=((pa./sqrt(M2)).*sinh(i*2*pi*1*sqrt(M2).*f)+A2*ZL2.*cosh(i*2*pi*1...

```

```

*sqrt(M2).*f))./(A2*(cosh(i*2*pi*1*sqrt(M2).*f)+A2*ZL2.*(sqrt(M2)/pa).*...
sinh(i*2*pi*1*sqrt(M2).*f)));

%Z3=((pa./sqrt(M3)).*sinh(i*2*pi*1*sqrt(M3).*f))./(A3*(cosh(i*2*pi*1*sqrt(M3).*f)));

Z3=((pa./sqrt(M3)).*sinh(i*2*pi*1*sqrt(M3).*f)+A3*ZL3.*cosh(i*2*pi*1...
*sqrt(M3).*f))./(A3*(cosh(i*2*pi*1*sqrt(M3).*f)+A3*ZL3.*(sqrt(M3)/pa).*...
sinh(i*2*pi*1*sqrt(M3).*f)));

%Z4=((pa./sqrt(M4)).*sinh(i*2*pi*1*sqrt(M4).*f))./(A4*(cosh(i*2*pi*1*sqrt(M4).*f)));

Z4=((pa./sqrt(M4)).*sinh(i*2*pi*1*sqrt(M4).*f)+A4*ZL4.*cosh(i*2*pi*1...
*sqrt(M4).*f))./(A4*(cosh(i*2*pi*1*sqrt(M4).*f)+A4*ZL4.*(sqrt(M4)/pa).*...
sinh(i*2*pi*1*sqrt(M4).*f)));

%Zo31=((pa./sqrt(M31)).*sinh(i*2*pi*11*sqrt(M31).*f))./(A5*(cosh(i*2*pi*11*sqrt(M
31).*f)));

Z11=(Z1.*Z2)./(Z1+Z2);
Z12=(Z3.*Z4)./(Z3+Z4);
Z110=((pa./sqrt(M11)).*sinh(i*2*pi*L1*sqrt(M11).*f)+A11*Z11.*cosh(i*2*pi*L1...
*sqrt(M11).*f))./(A11*(cosh(i*2*pi*L1*sqrt(M11).*f)+A11*Z11.*(sqrt(M11)/pa).*...
sinh(i*2*pi*L1*sqrt(M11).*f)));
Z120=((pa./sqrt(M12)).*sinh(i*2*pi*L1*sqrt(M12).*f)+A12*Z12.*cosh(i*2*pi*L1...
*sqrt(M12).*f))./(A12*(cosh(i*2*pi*L1*sqrt(M12).*f)+A12*Z12.*(sqrt(M12)/pa).*...
sinh(i*2*pi*L1*sqrt(M12).*f)));
ZL=(Z110.*Z120)./(Z110+Z120);
Z0=((pa./sqrt(M0)).*sinh(i*2*pi*L0*sqrt(M0).*f)+A0*ZL.*cosh(i*2*pi*L0...
*sqrt(M0).*f))./(A0*(cosh(i*2*pi*L0*sqrt(M0).*f)+A0*ZL.*(sqrt(M0)/pa).*...
sinh(i*2*pi*L0*sqrt(M0).*f)));
z=abs(Z0);
% Normalized Input Impedance:
Mw=0.1508;
Kw0=(E*tw-p0*r0)/(2*r0);
w0=sqrt(Kw0/Mw);
w1=sqrt((Kw0+MB)/Mw);
H=(w1^2-(2*pi*f).^2)./(w0^2-(2*pi*f).^2);
Zs=(1/A0)*sqrt((MB*pa)./abs(H)); % Characteristic Impedance
NII=abs(Z0)./abs(Zs);
figure(1);
plot(f,NII);
xlabel('Frequency(Hz)');
ylabel('Normalized Input Impedance');
title('Input Impedance');

```

APPENDIX C

FFT TRANSFORM

Matlab File of FFT Transform and Terminal Impedance Calculation

```
-----  
clear all;  
[A, B]=xlsread('Breathingcycle1seconds');  
n=1:21;  
Vcontrol=A(n,1);  
Pchamp=A(n,2);  
Position=A(n,3);  
Flowrate=A(n,4)-0.05;  
VR1=(A(n,5)+1.98)*pi*0.02^2; % time domain  
VR2=A(n,6)+4.322*pi*0.02^2;  
VR3=A(n,7)+0.338*pi*0.02^2;  
VL1=A(n,8)+3.48*pi*0.02^2;  
VL2=A(n,9)-6.13*pi*0.02^2;  
PR1=A(n,10)-2.26;  
PR2=A(n,11)-2.27;  
PR3=A(n,12)-2.25;  
PL1=A(n,13)-2.26;  
PL2=A(n,14)-2.221;  
SP=20; % Sampling Rate  
nfft=128;  
window=hanning(nfft);  
figure(1);  
[Z1,f]=psd(PR1./VR1,nfft,SP>window,'mean'); % Impedance calculation at lobe R1  
psd(PR1./VR1,nfft,SP>window,'mean');  
title('Impedance at lobe R1');  
xlabel('Frequency(Hz)');  
dlmwrite('Z1.xls',Z1,'\t ');  
saveas(gcf,'Z1.fig')  
%PSD(X,NFFT,Fs,WINDOW);  
figure(2);  
[Z2,f]=psd(PR2./VR2,nfft,SP>window,'mean'); % Impedance calculation at lobe R2  
psd(PR2./VR2,nfft,SP>window,'mean');  
title('Impedance at lobe R2');  
xlabel('Frequency(Hz)');  
dlmwrite('Z2.xls',Z2,'\t ');  
saveas(gcf,'Z2.fig')  
figure(3);  
[Z3,f]=psd(PR3./VR3,nfft,SP>window,'mean'); % Impedance calculation at lobe R3  
psd(PR3./VR3,nfft,SP>window,'mean');  
title('Impedance at lobe R3');  
xlabel('Frequency(Hz)');  
dlmwrite('Z3.xls',Z3,'\t ');  
saveas(gcf,'Z3.fig')  
figure(4);  
[Z4,f]=psd(PL1./VL1,nfft,SP>window,'mean'); % Impedance calculation at lobe L1  
psd(PL1./VL1,nfft,SP>window,'mean');  
title('Impedance at lobe L1');
```

```
xlabel('Frequency(Hz)');
dlmwrite('Z4.xls',Z4,' \t');
saveas(gcf,'Z4.fig')
figure(5);
[Z5,f]=psd(PL2./VL2,nfft,SP>window,'mean'); % Impedance calculation at lobe L2
psd(PL2./VL2,nfft,SP>window,'mean'); % Power Spectrum
title('Impedance at lobe L2');
xlabel('Frequency(Hz)');
dlmwrite('Z5.xls',Z5,' \t ');
saveas(gcf,'Z5.fig')
dlmwrite('frequency.xls',f,' ');
```

The results of all experiment investigation for the lung simulator are presented. Data recorded and divided into 10 short recordings to analyse as discussed in Chapter 3. Measured impedance at each lobe is presented as the lung simulator operates in different frequencies.

- Part 1: Results of Terminal Impedance at lobe R2, R3, L1 and L2 recorded at different sampling rate (Figures D1 –D 4).
- Part 2: Results of Terminal Impedance recorded at different exciting frequencies (Figures D5-D34)

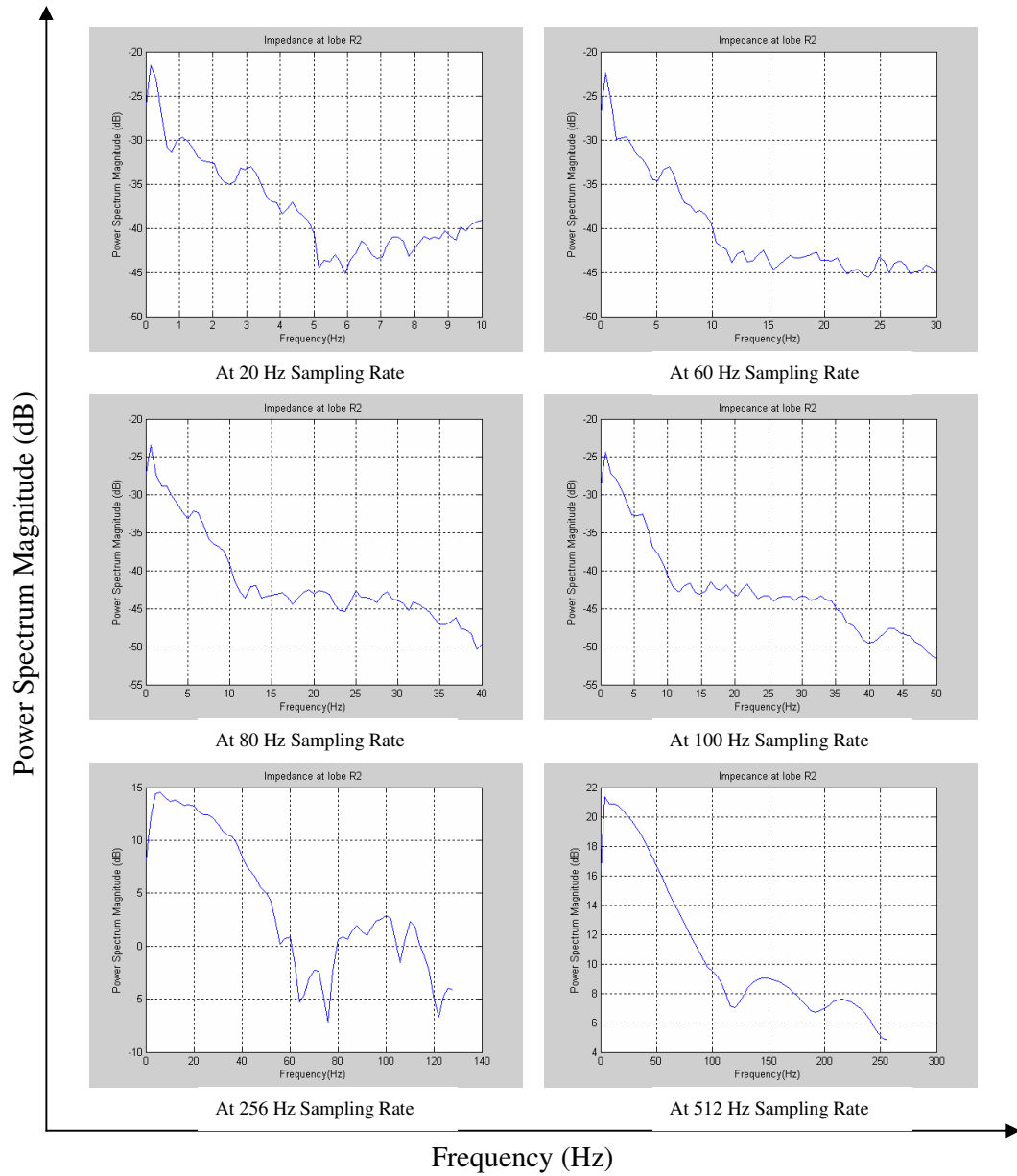


Figure D1: Power Spectrum of Impedance at lobe R2 recorded at different sampling rates

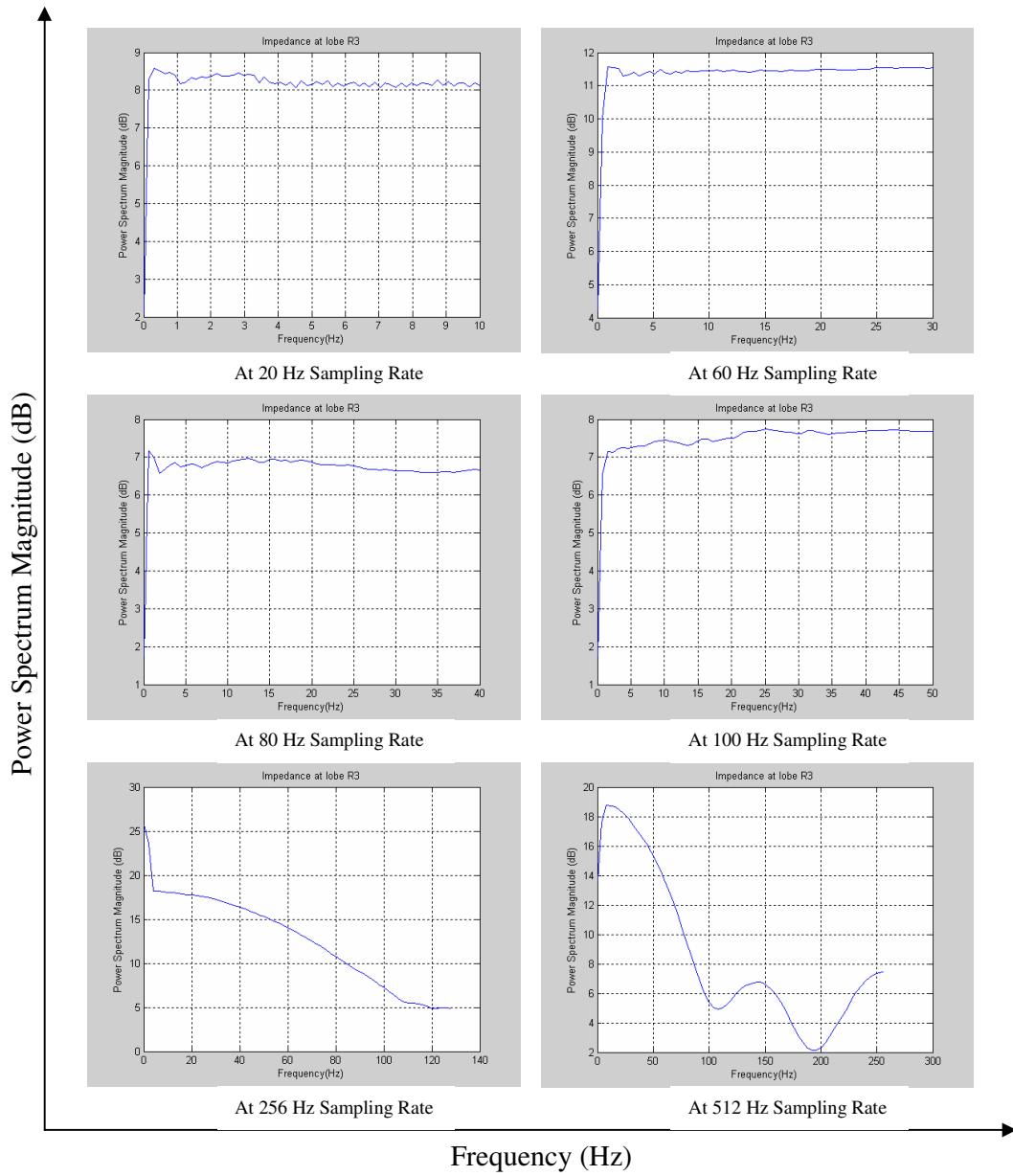


Figure D 2: Power Spectrum of Impedance at lobe R3 recorded at different sampling rates

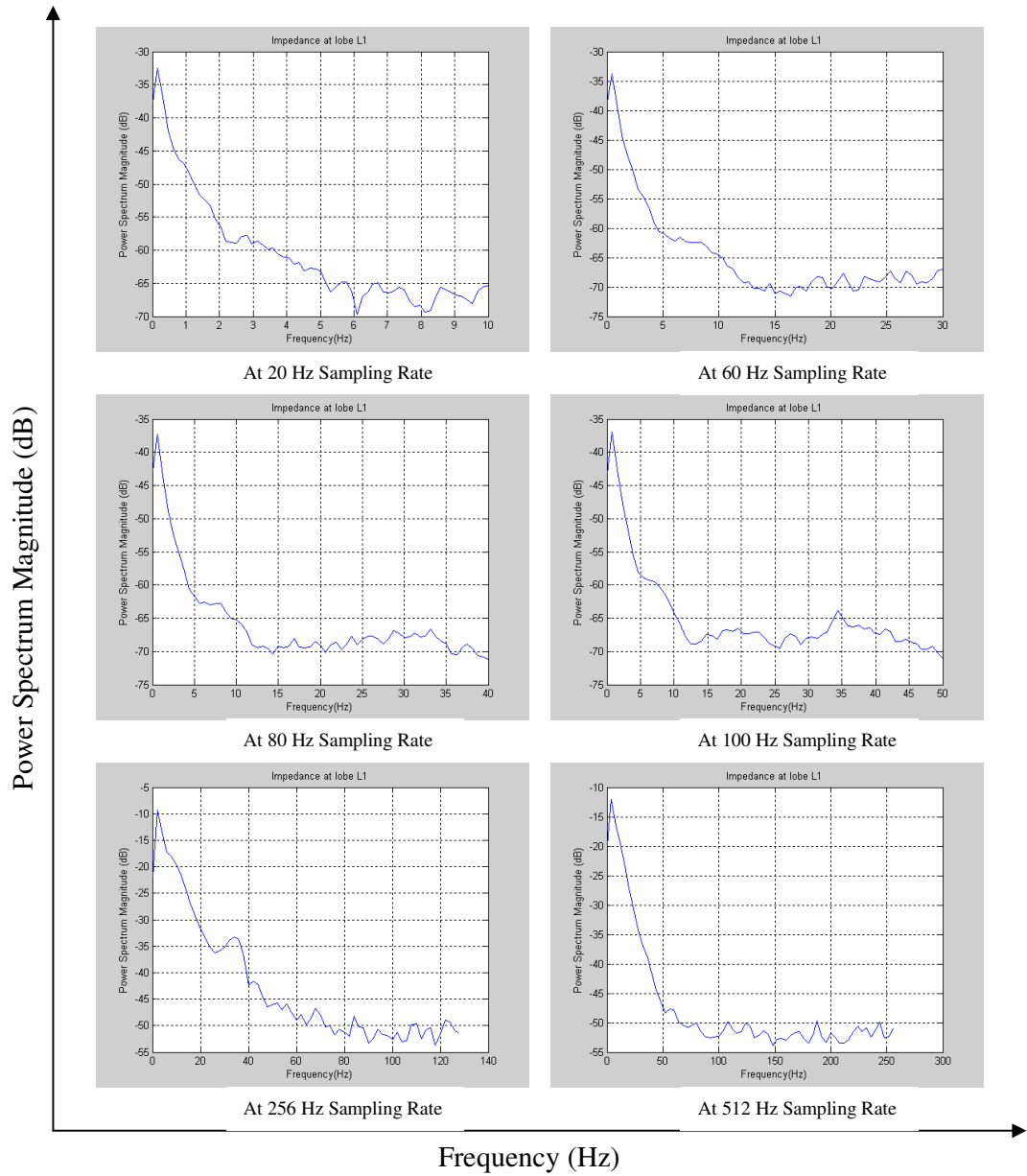


Figure D 3: Power Spectrum of Impedance at lobe L1 recorded at different sampling rates

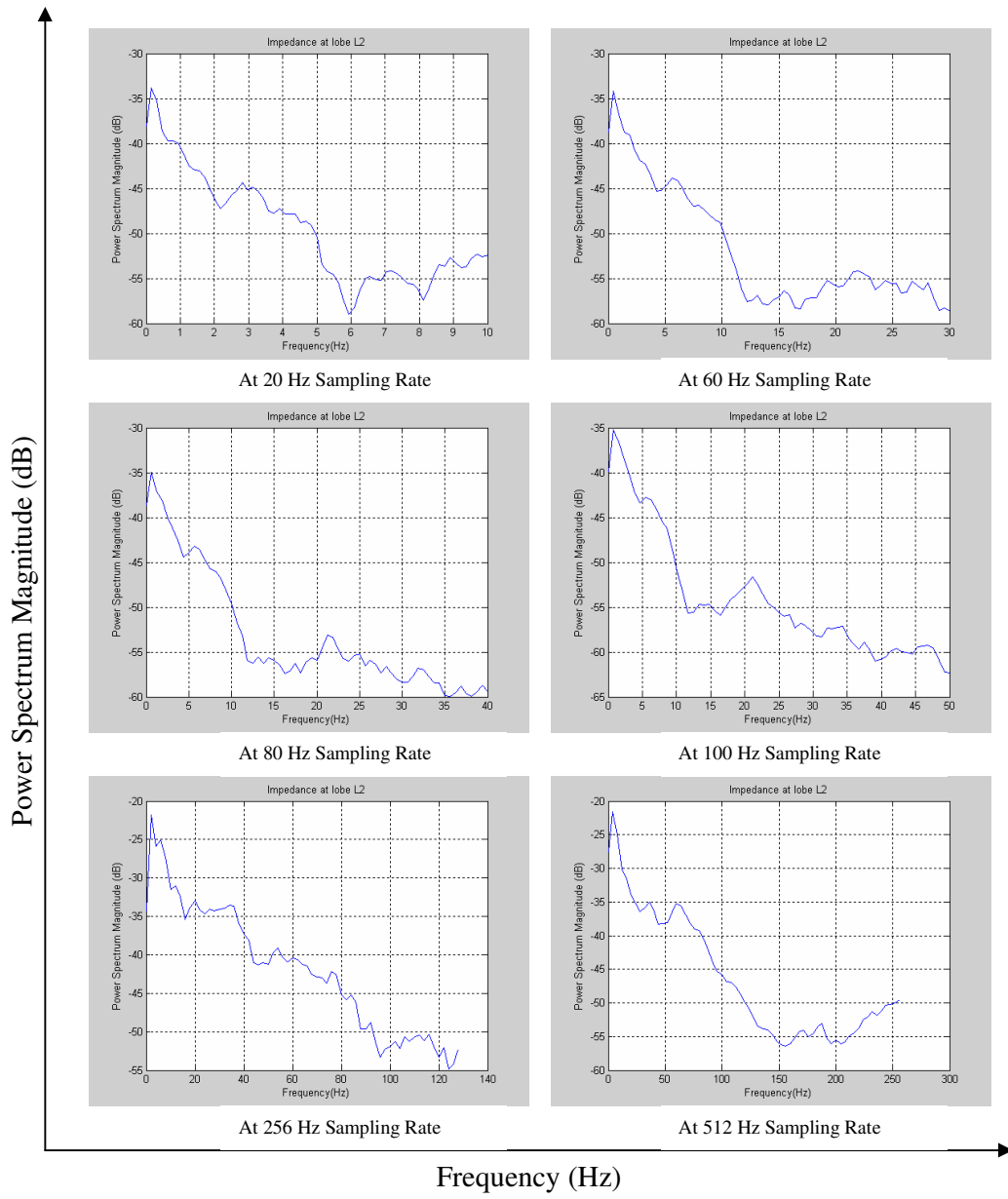


Figure D 4: Power Spectrum of Impedance at lobe L2 recorded at different sampling rates

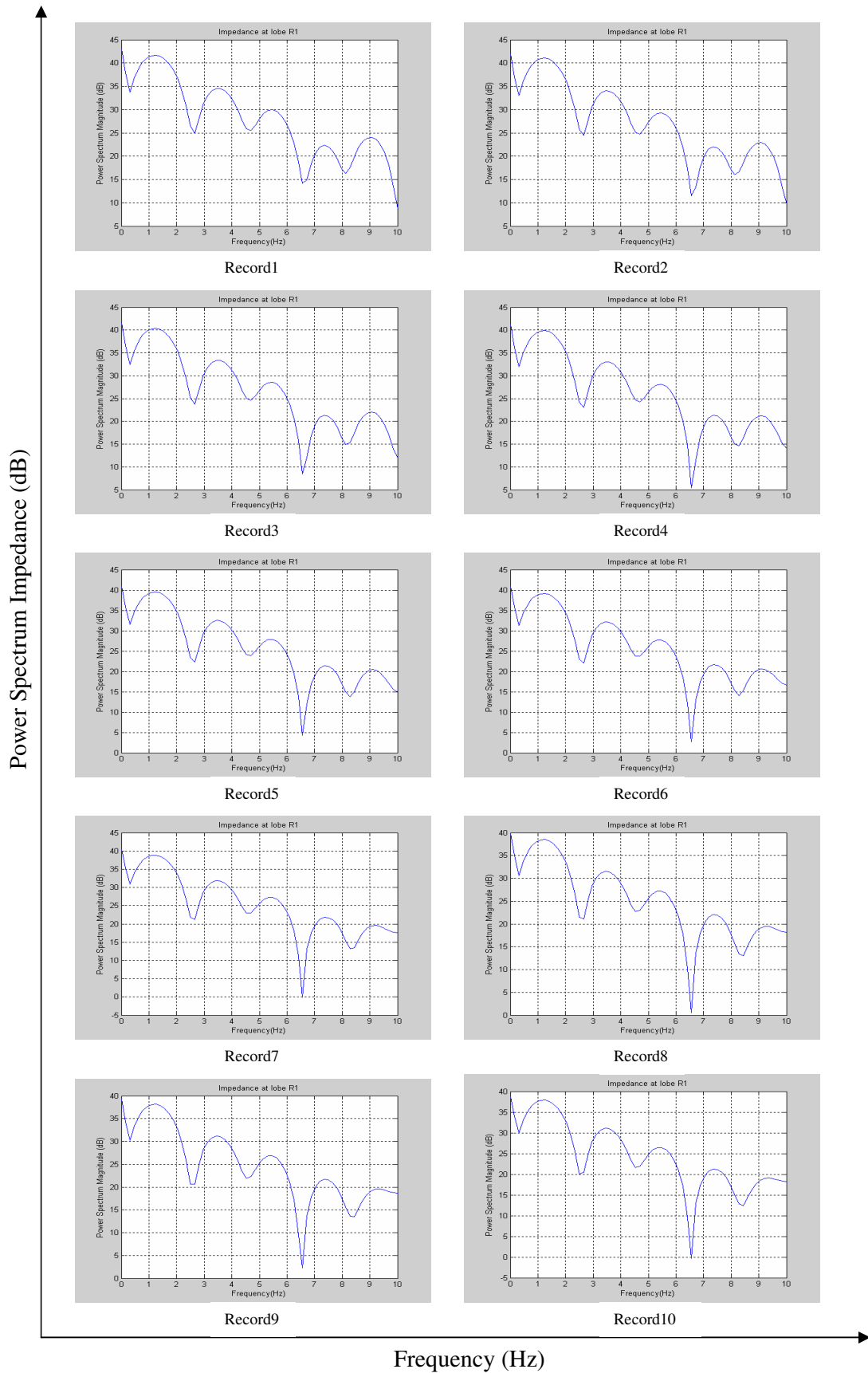


Figure D 5: Power Spectrum of Impedance at lobe R1 when the lung simulator operates at 1 second per cycle

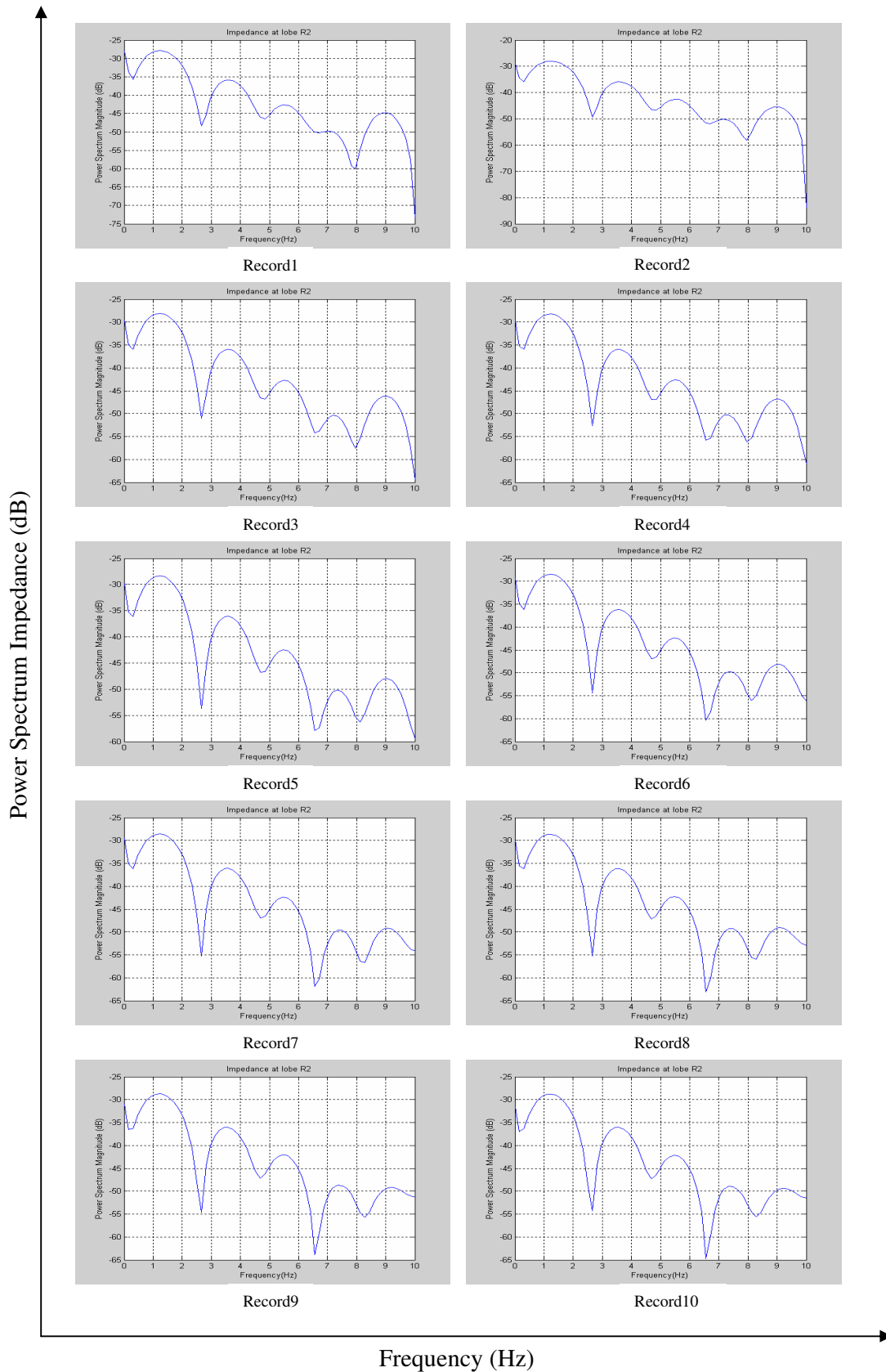


Figure D 6: Power Spectrum of Impedance at lobe R2 when the lung simulator operates at 1 second per cycle

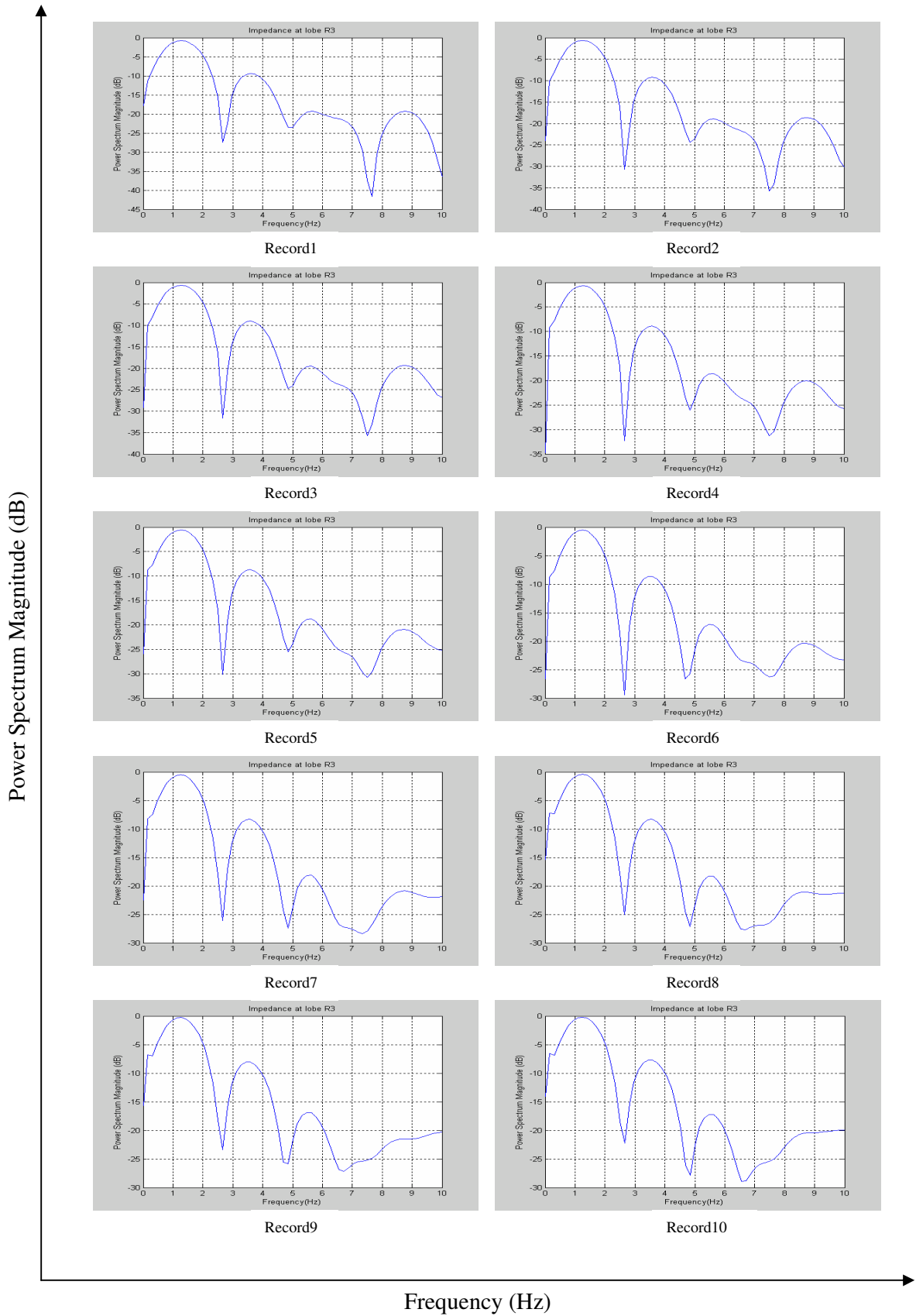


Figure D 7: Power Spectrum of Impedance at lobe R3 when the lung simulator operates at 1 second per cycle

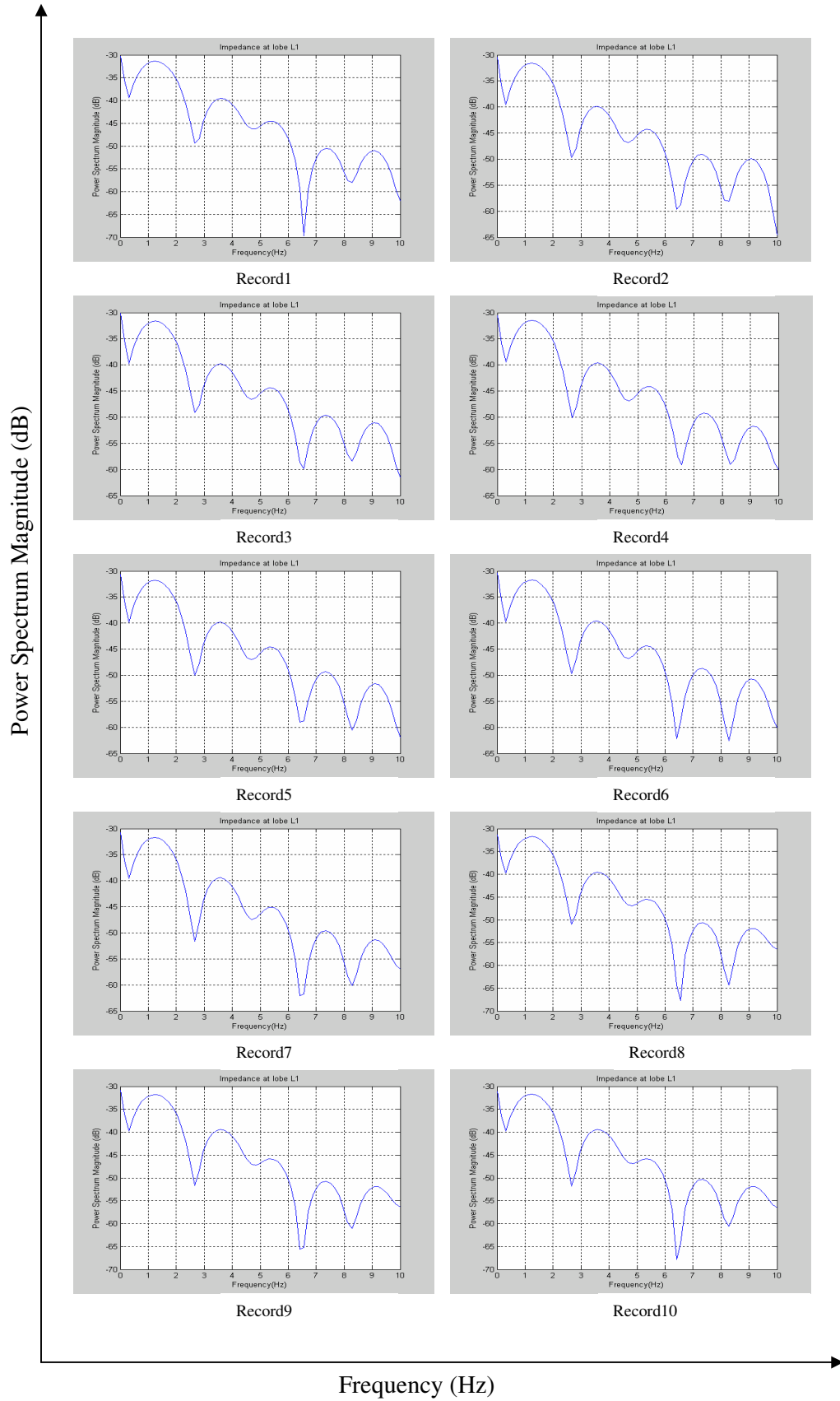


Figure D 8: Power Spectrum of Impedance at lobe L1 when the lung simulator operates at 1 second per cycle

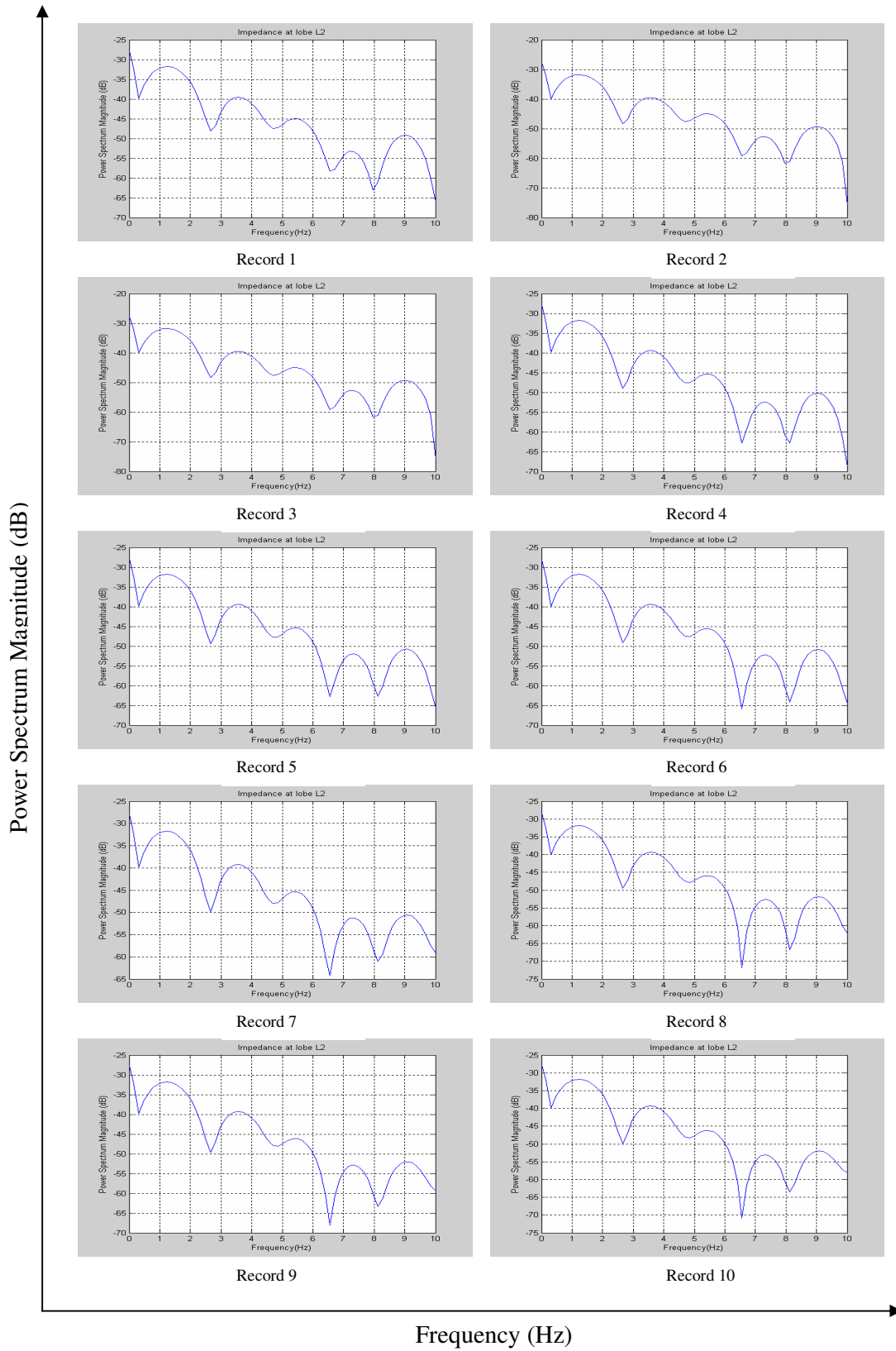


Figure D 9: Power Spectrum of Impedance at lobe L2 when the lung simulator operates at 1 second per cycle

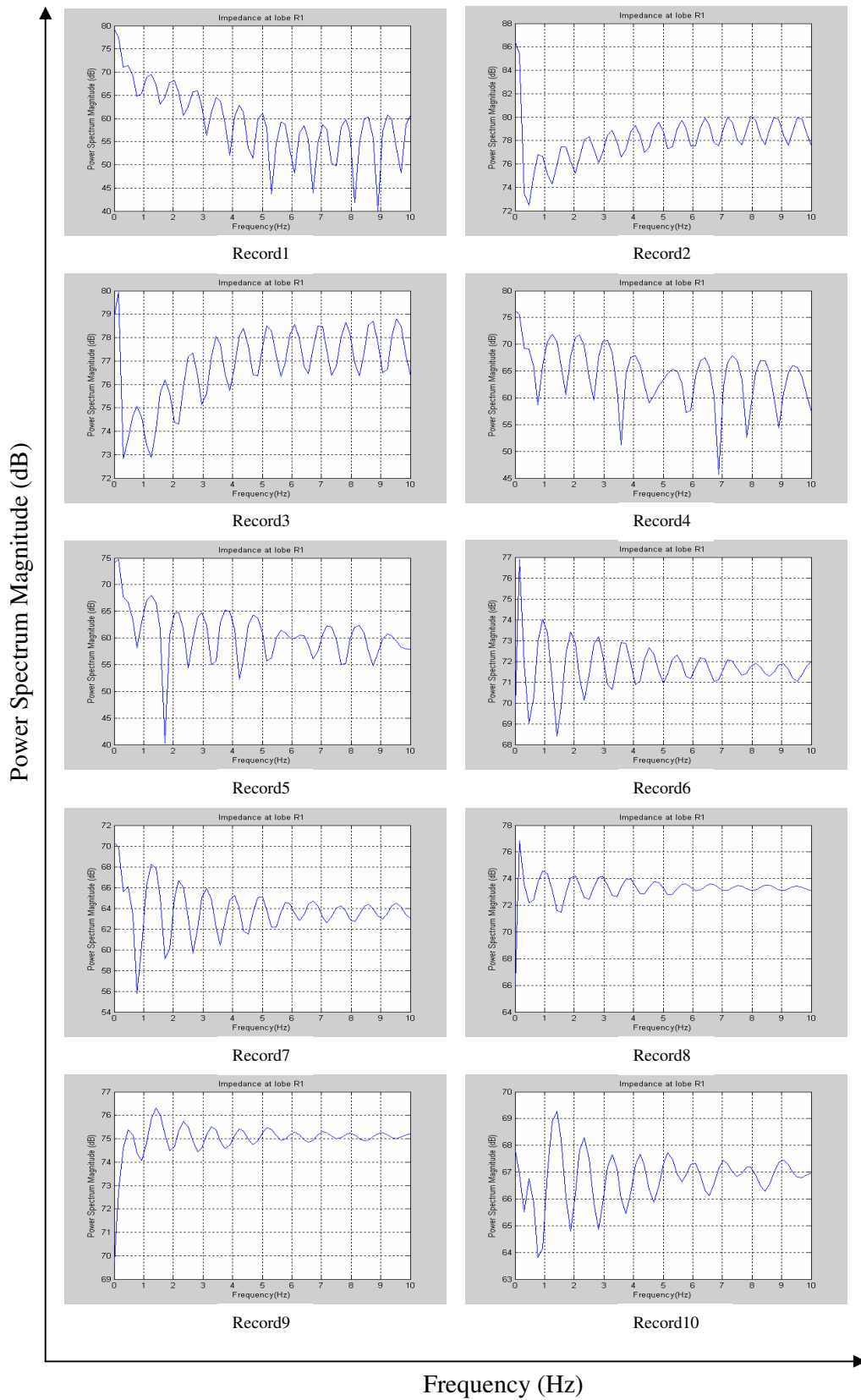


Figure D 10: Power Spectrum of Impedance at lobe R1 when lung simulator operates at 2 seconds per cycle

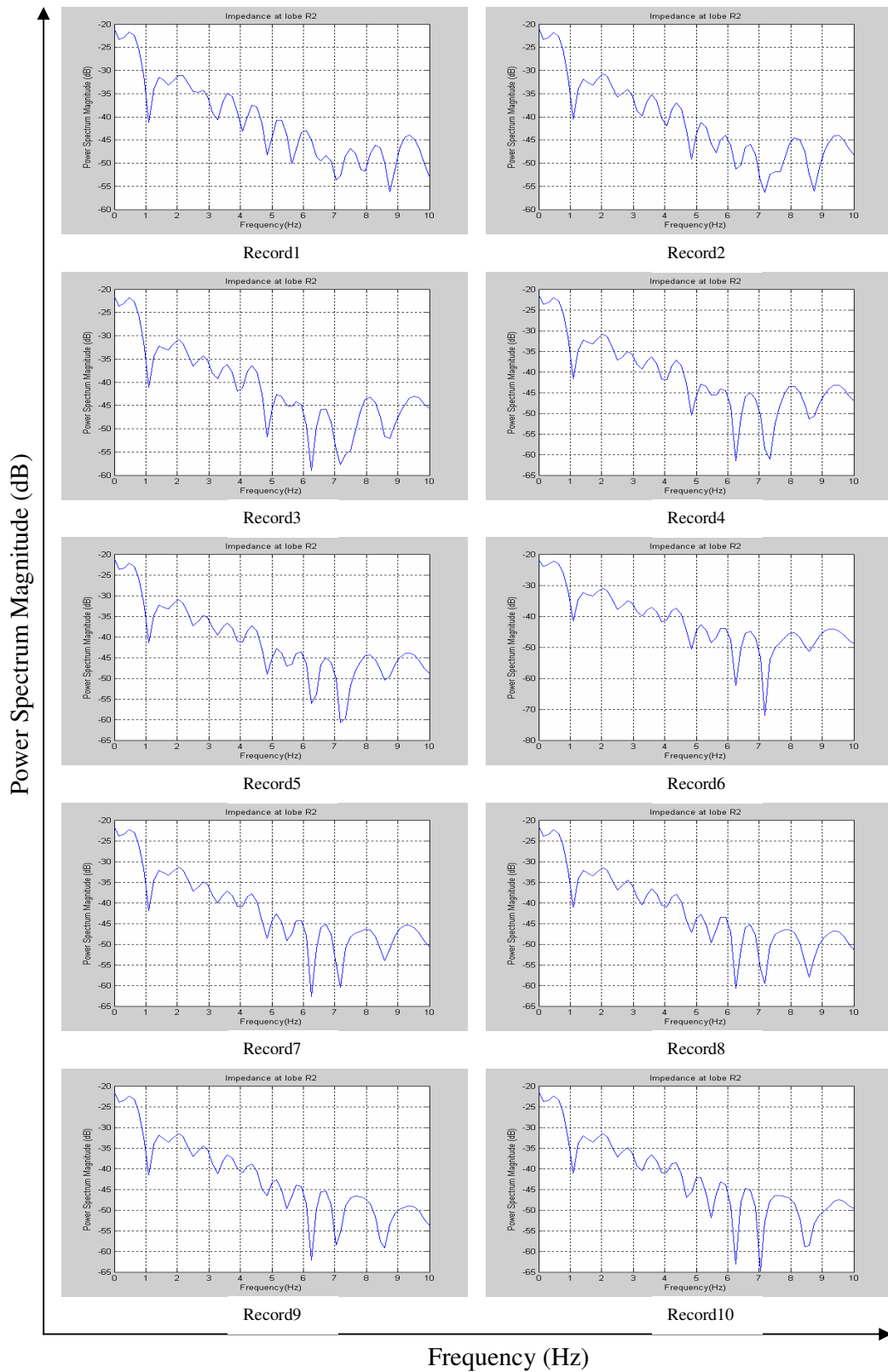


Figure D 11: Power Spectrum of Impedance at lobe R2 when the lung simulator operates at 2 seconds per cycle

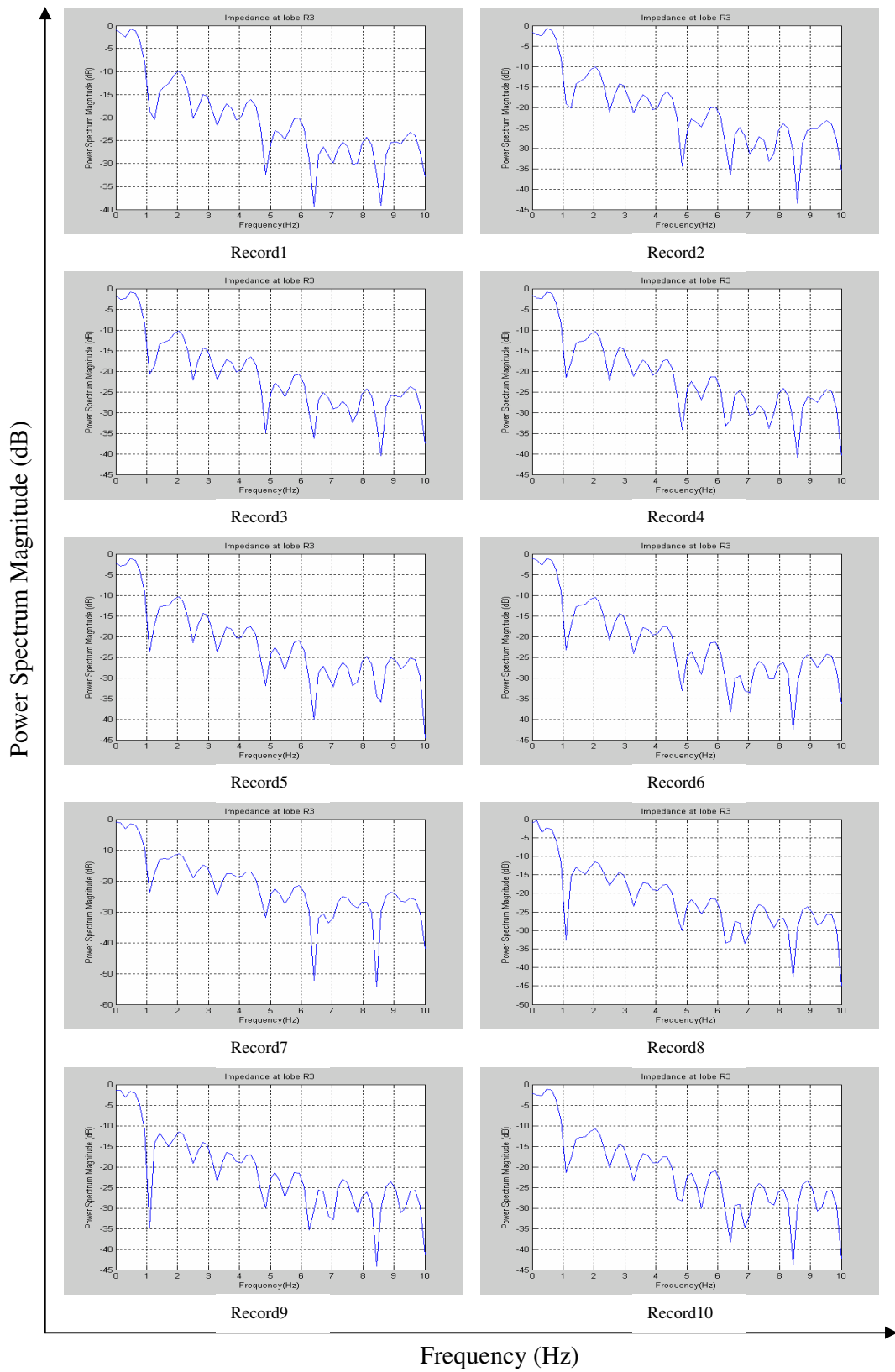


Figure D 12: Power Spectrum of Impedance at lobe R3 when the lung simulator operates at 2 seconds per cycle

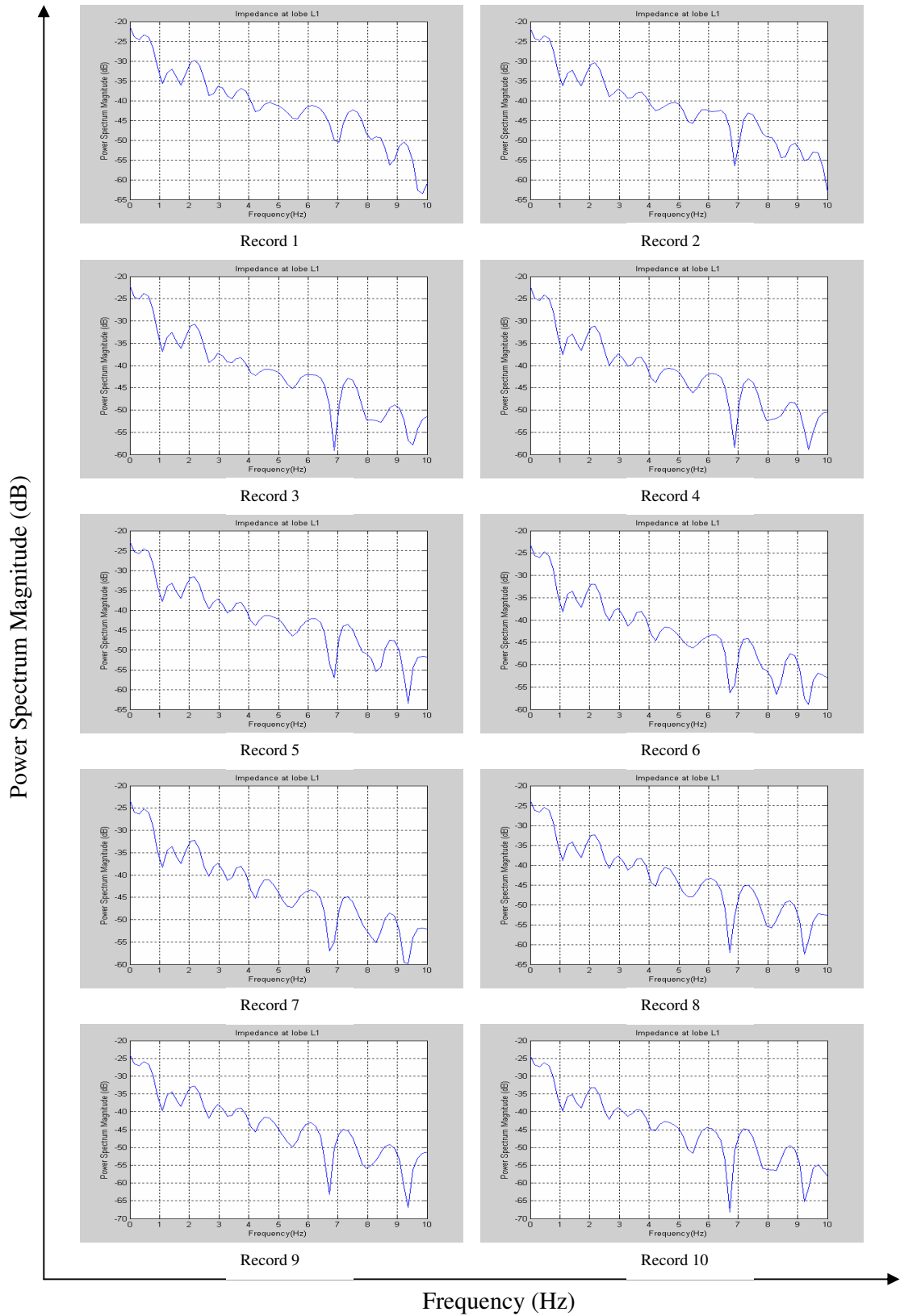


Figure D 13: Power Spectrum of Impedance at lobe L1 when the lung simulator operates at 2 seconds per cycles

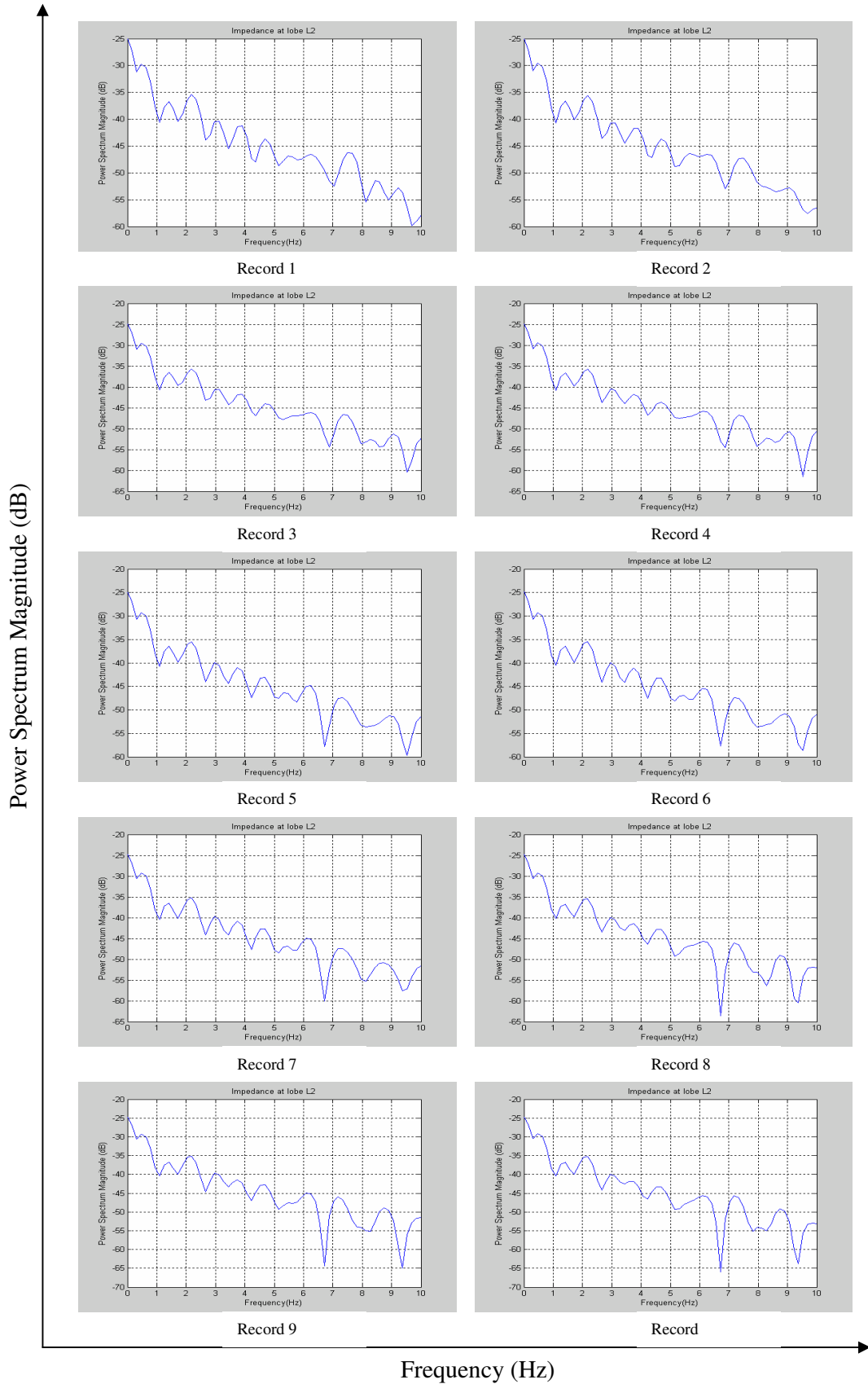


Figure D 14: Power Spectrum of Impedance at lobe L2 when the lung simulator operates at 2 seconds per cycle

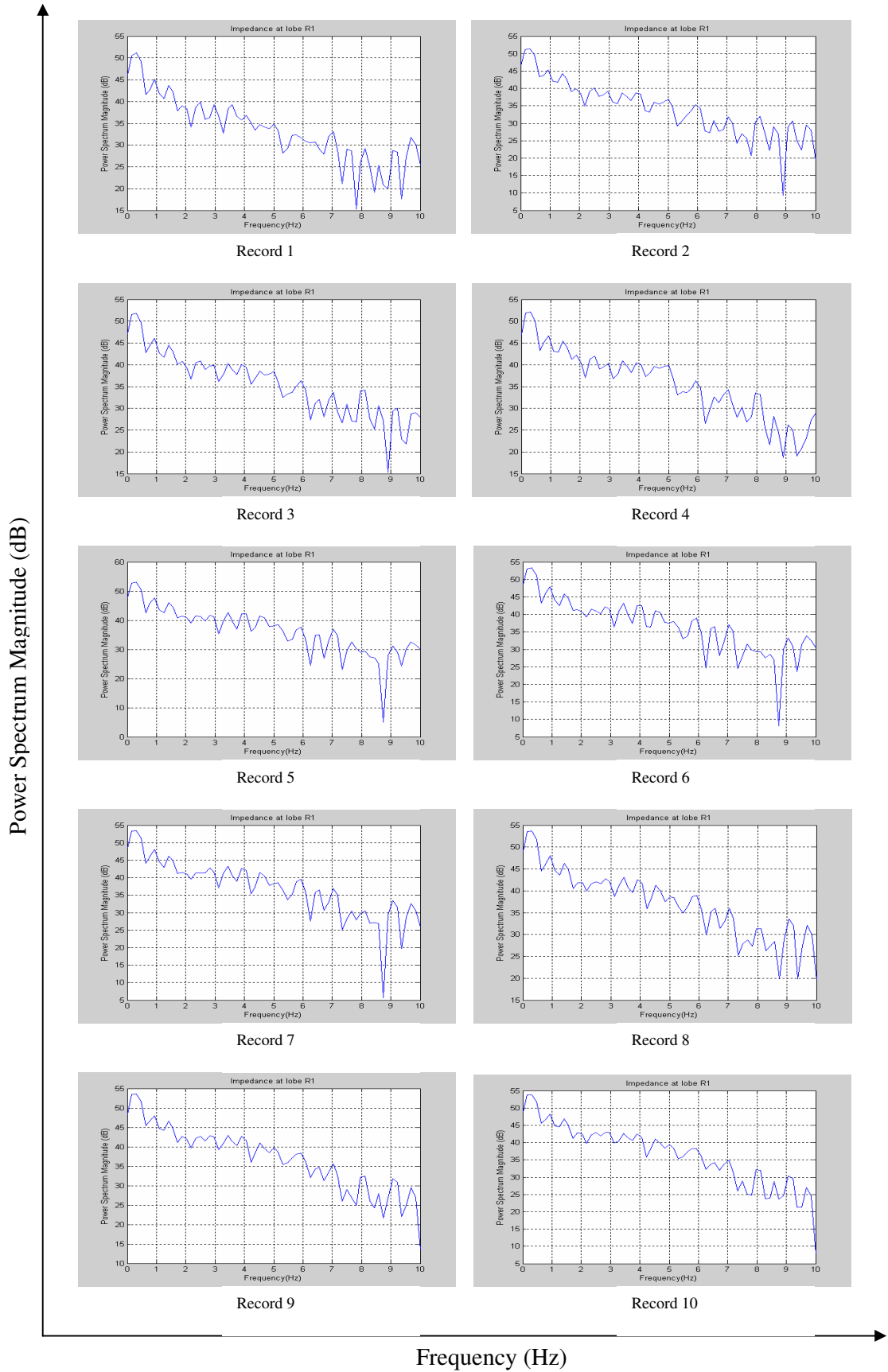


Figure D 15: Power Spectrum of Impedance at lobe R1 when the lung simulator operates at 3 seconds per cycle

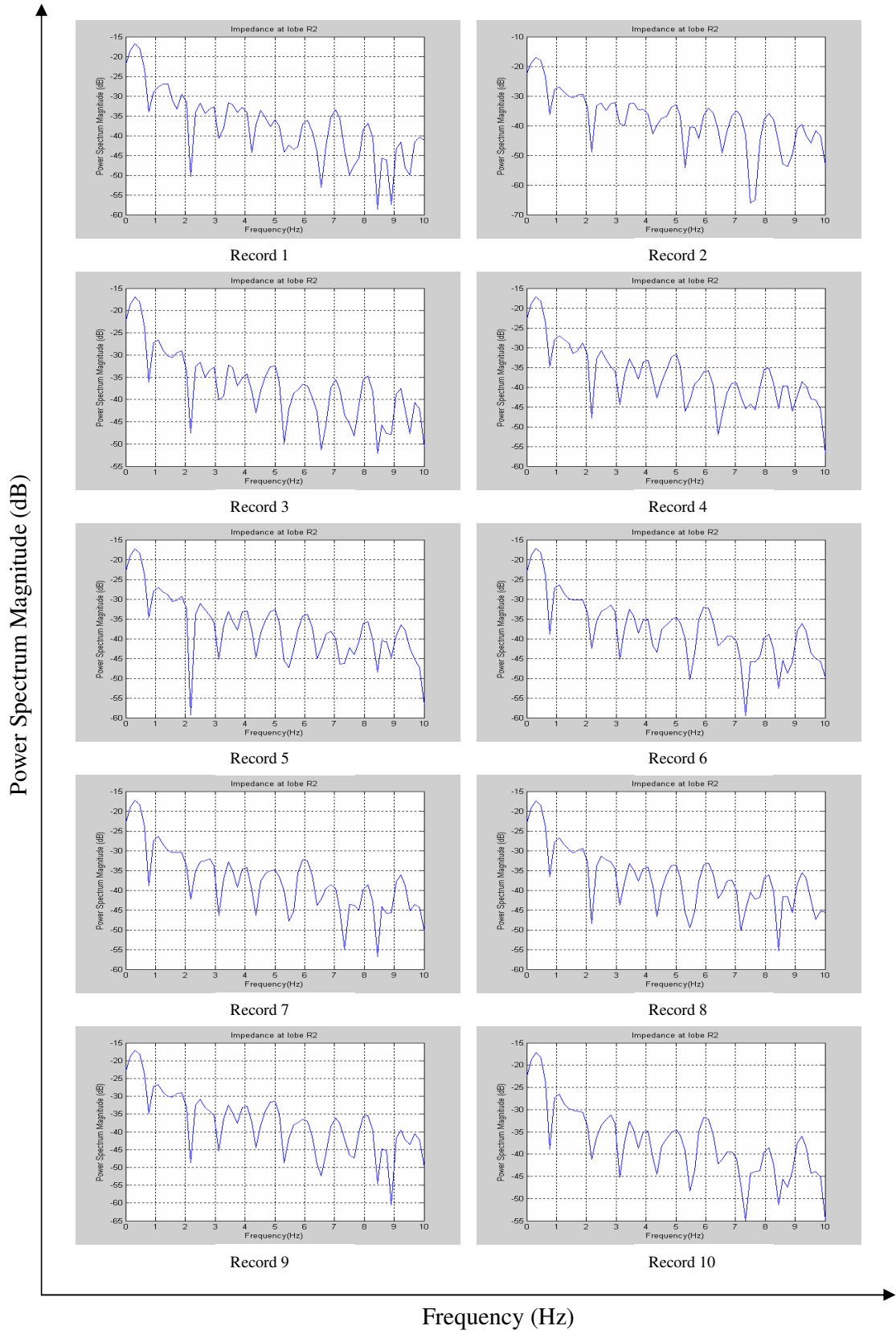


Figure D 16: Power Spectrum of Impedance at lobe R2 when the lung simulator operates at 3 seconds per cycle

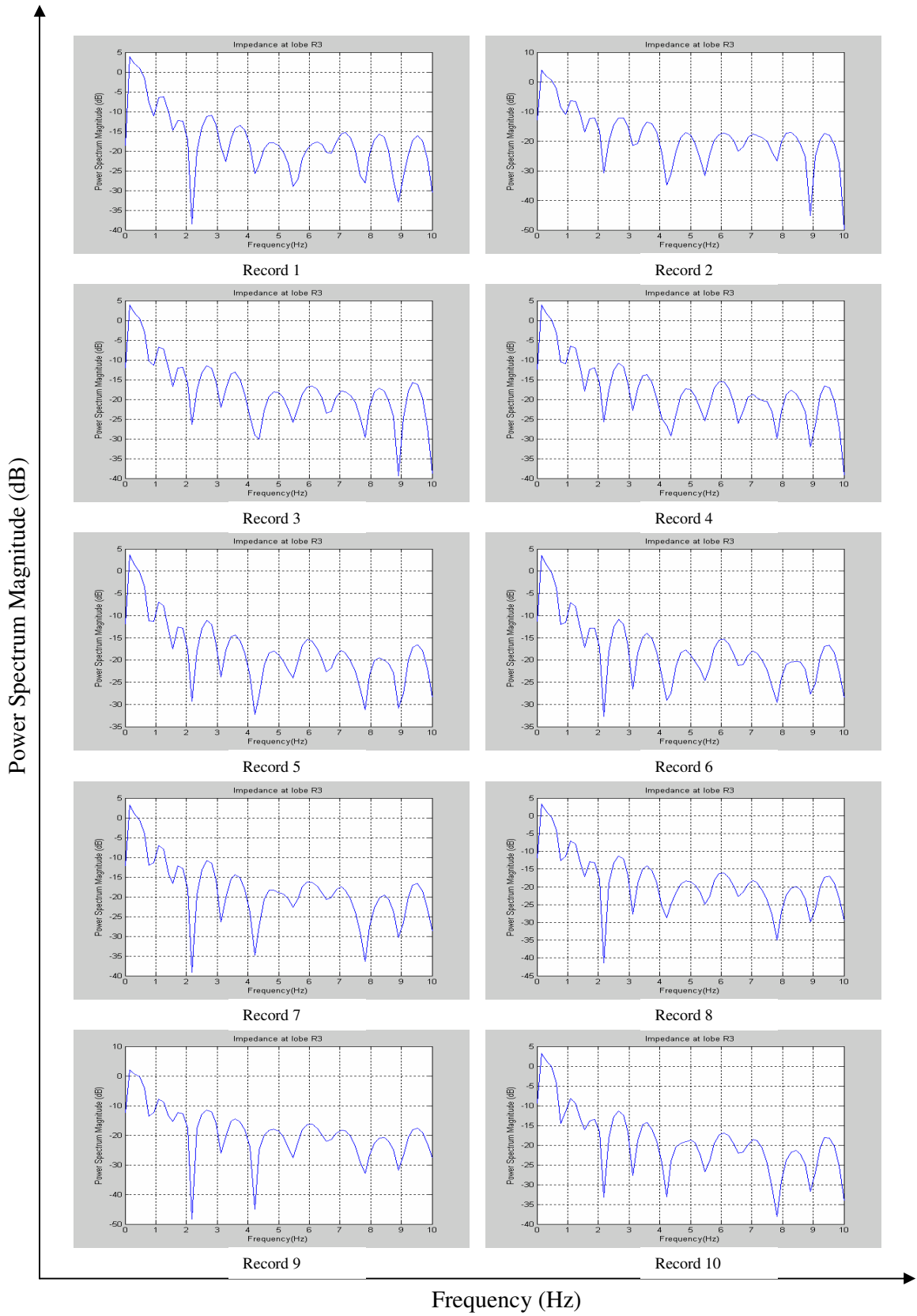


Figure D 17: Power Spectrum of Impedance at lobe R3 when the lung simulator operates at 3 seconds per cycle

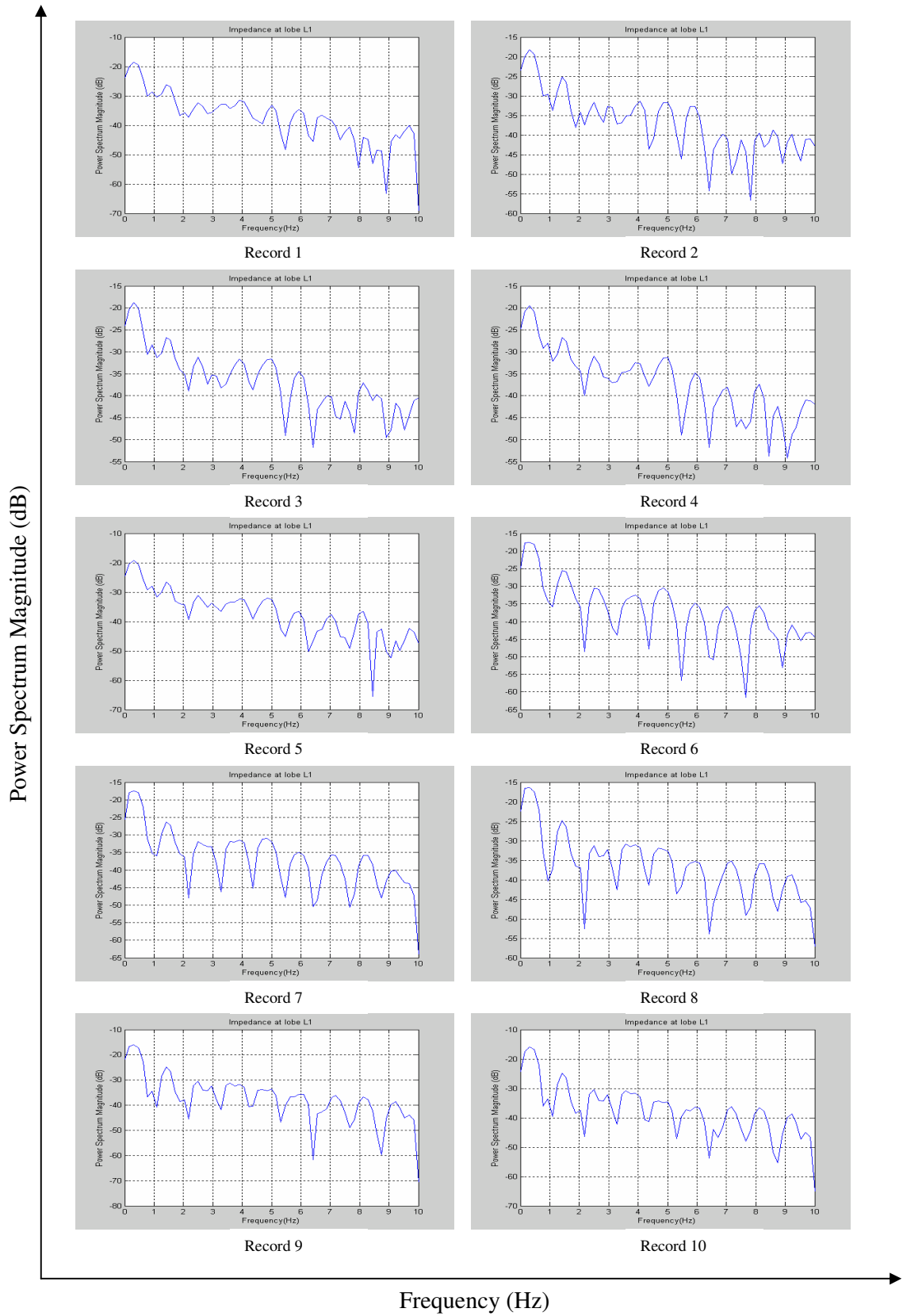


Figure D 18: Power Spectrum of Impedance at lobe L1 when the lung simulator operates at 3 seconds per cycle

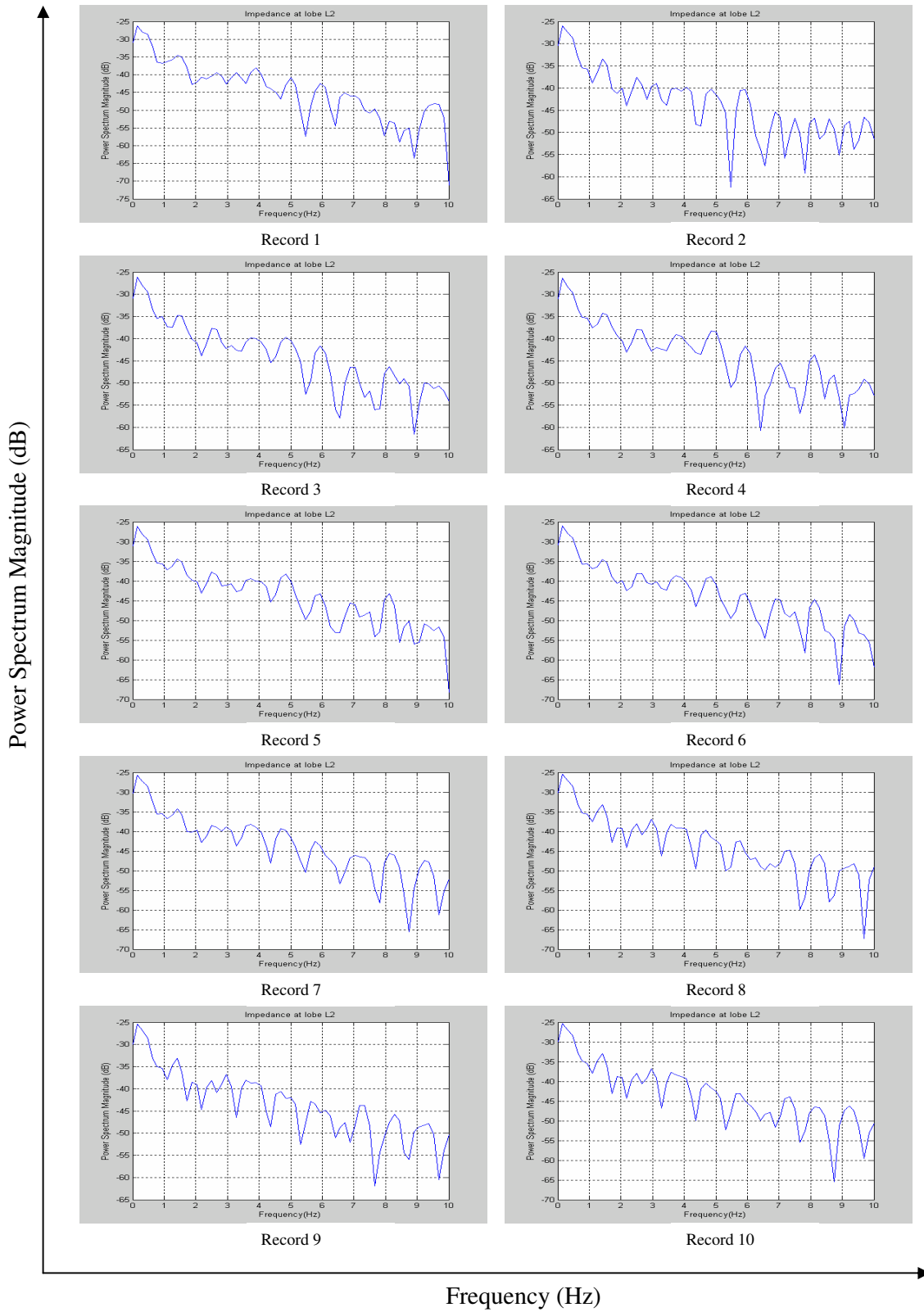


Figure D 19: Power Spectrum of Impedance at lobe L2 when the lung simulator operates at 3 seconds per cycle

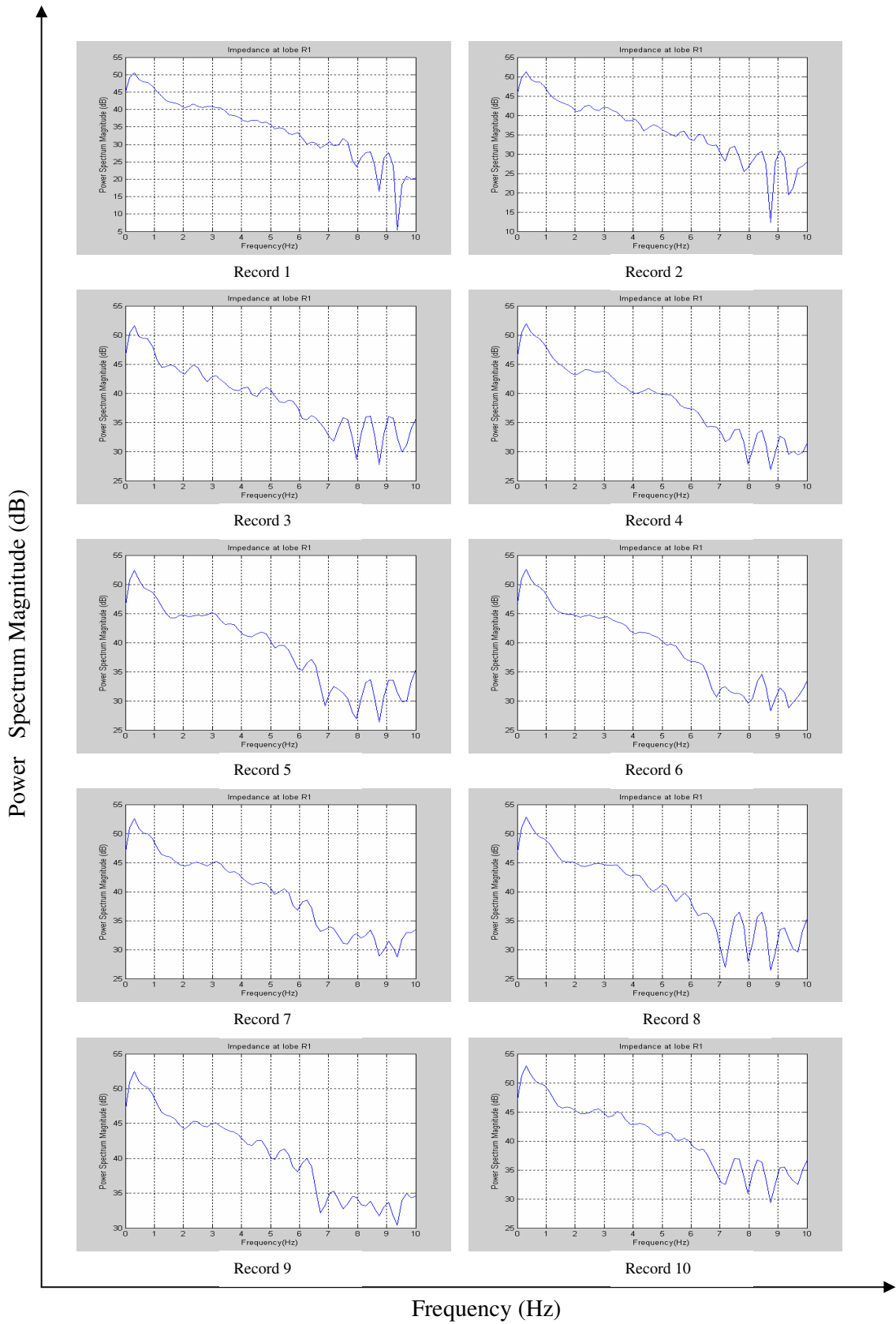


Figure D 20: Power Spectrum of Impedance at lobe R1 when the lung simulator operates at 4 seconds per cycle

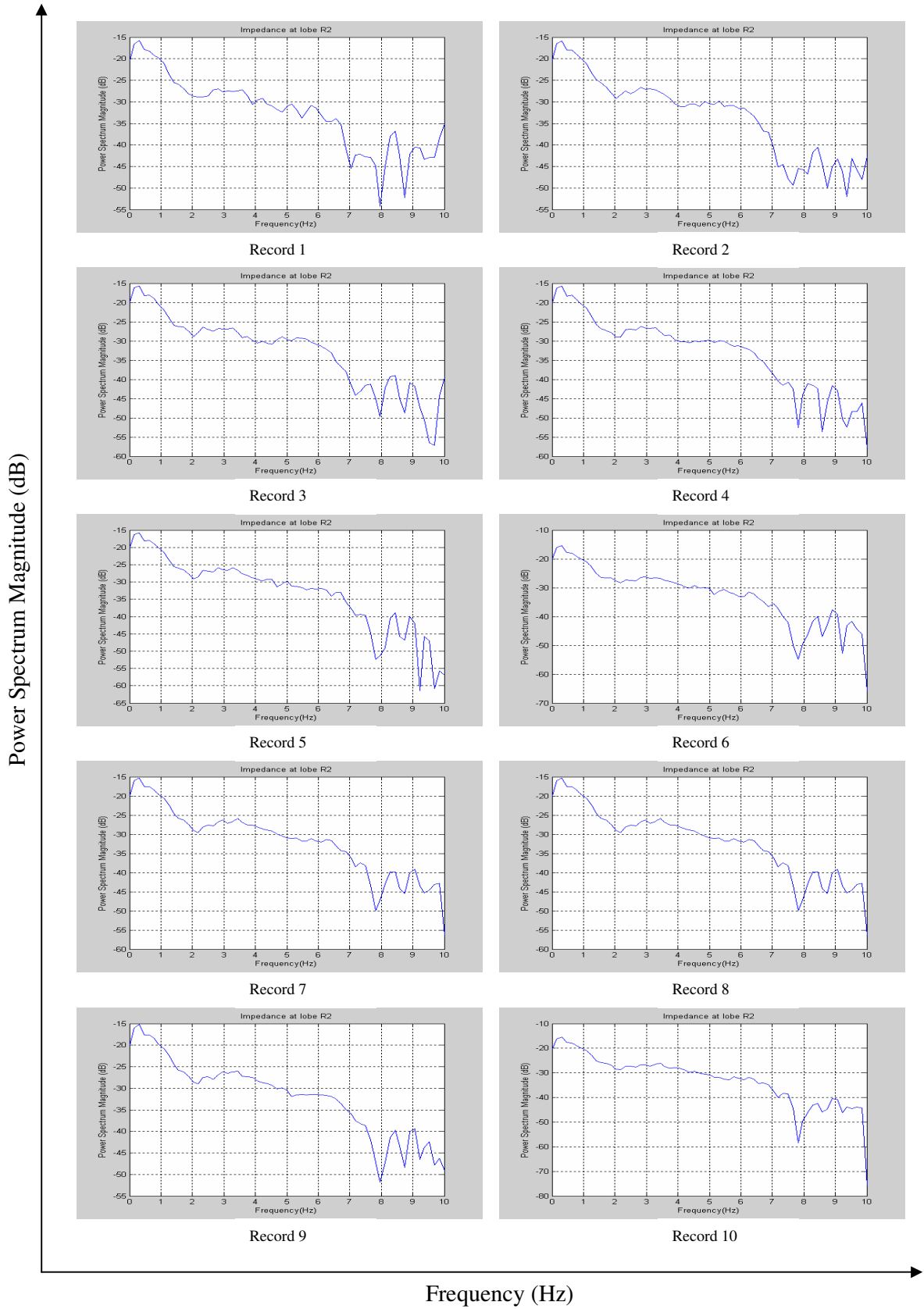


Figure D 21: Power Spectrum of Impedance at lobe R2 when the lung simulator operates at 4 seconds per cycle

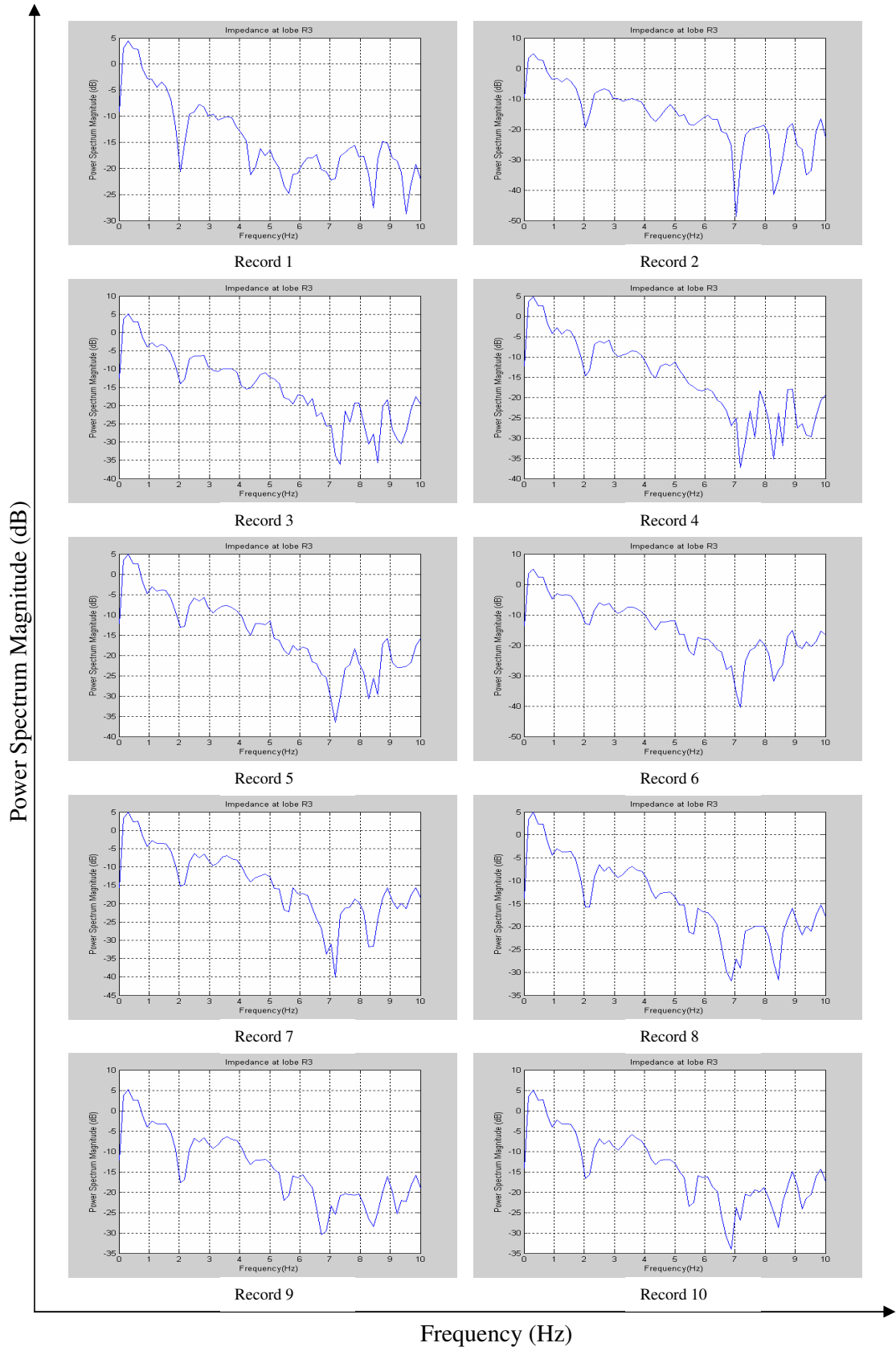


Figure D 22: Power Spectrum of Impedance at lobe R3 when the lung simulator operates at 4 seconds per cycle

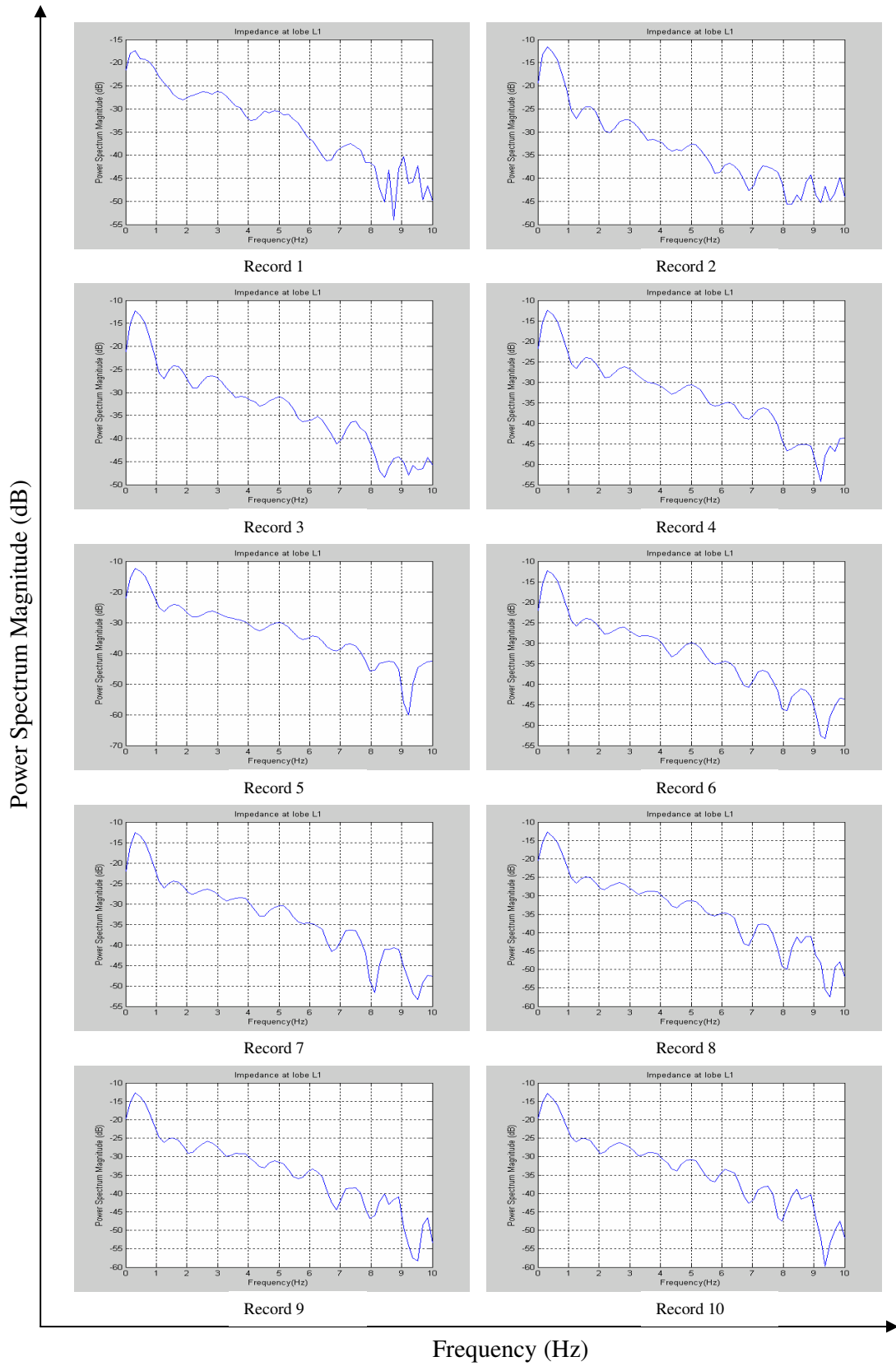


Figure D 23: Power Spectrum of Impedance at lobe L1 when the lung simulator operates at 4 seconds per cycle

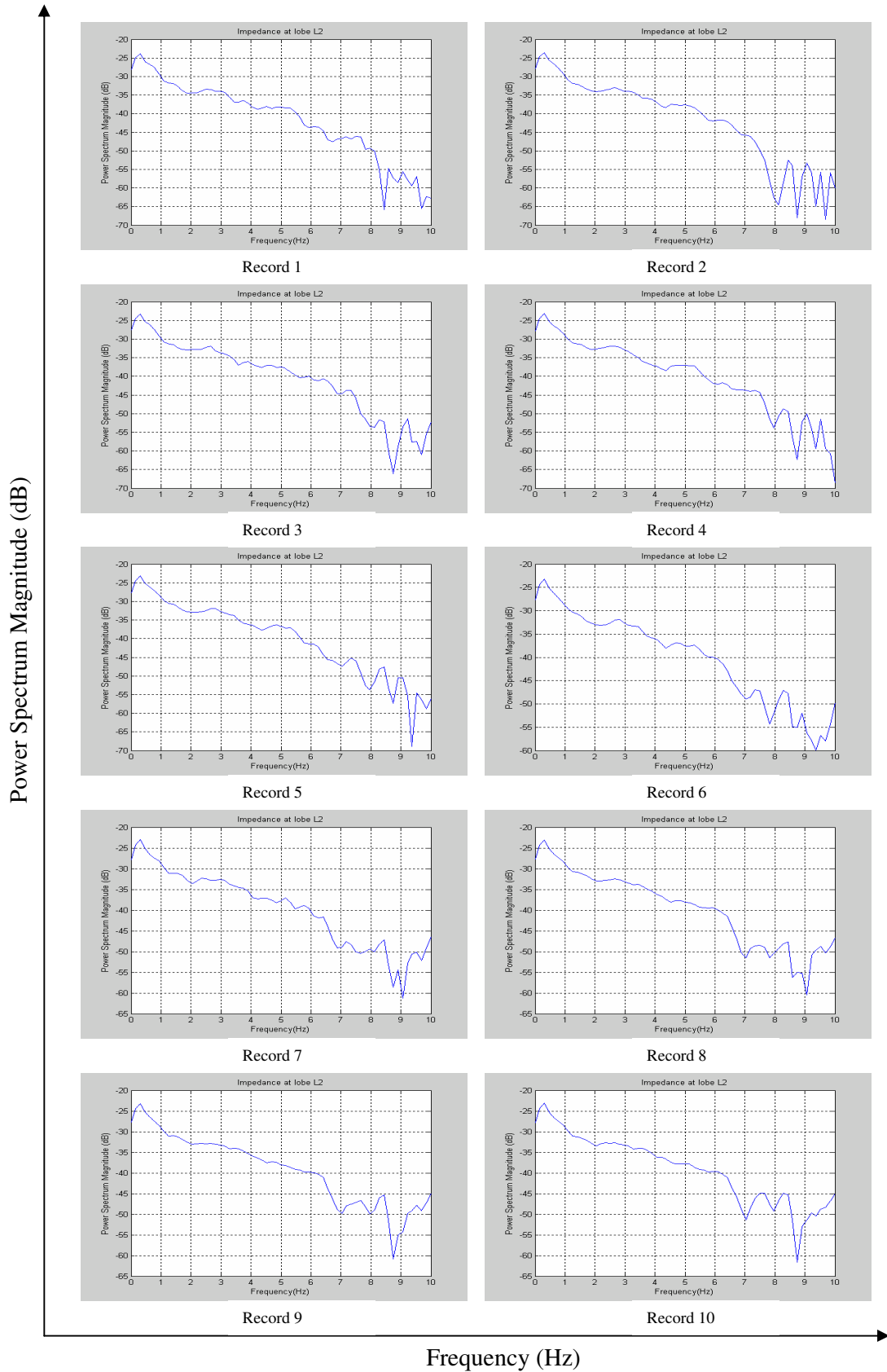


Figure D 24: Power Spectrum of Impedance at lobe L2 when the lung simulator operates at 4 seconds per cycle

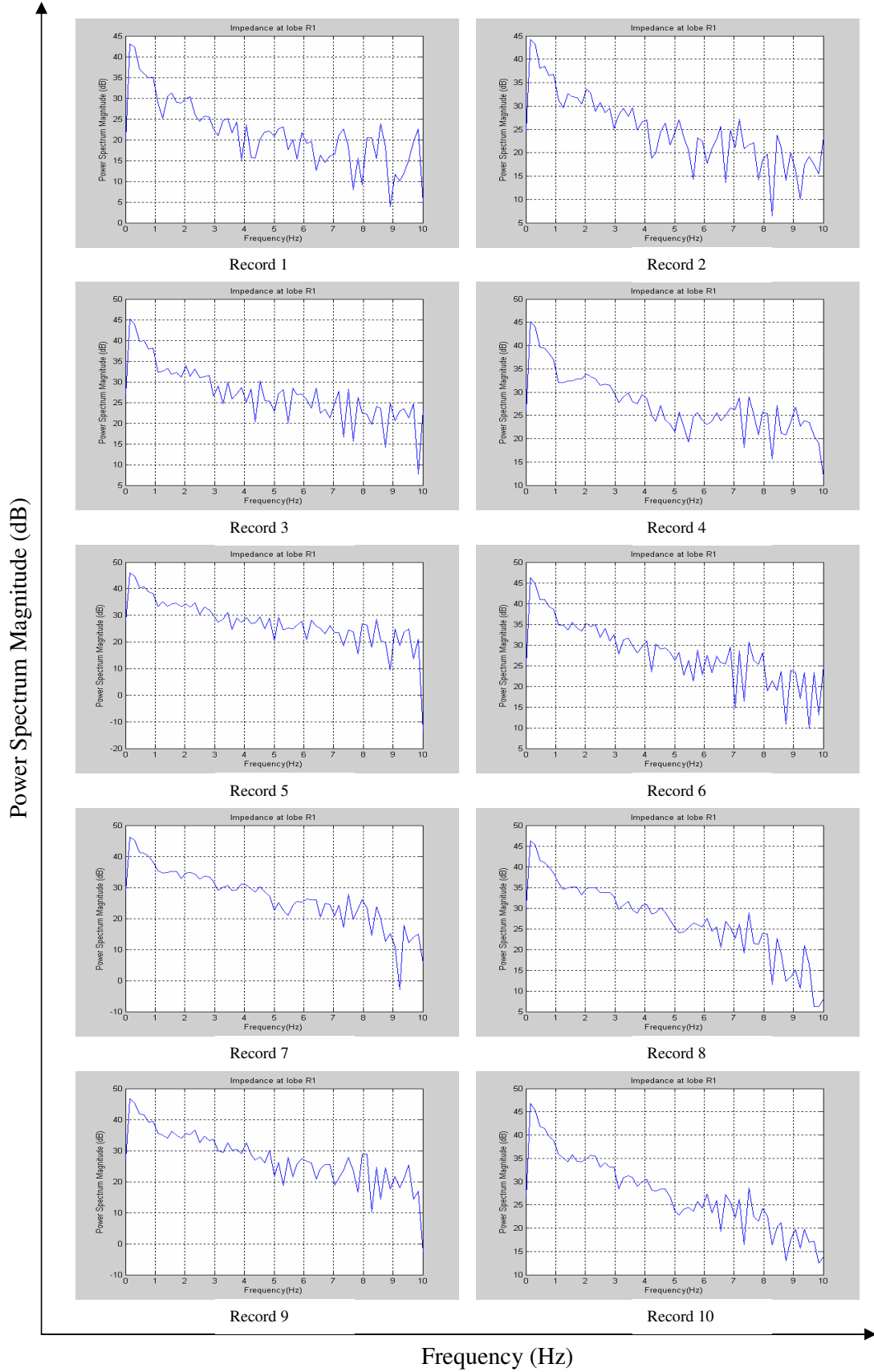


Figure D 25: Power Spectrum of Impedance at lobe R1 when the lung simulator operates at 5 seconds per cycle

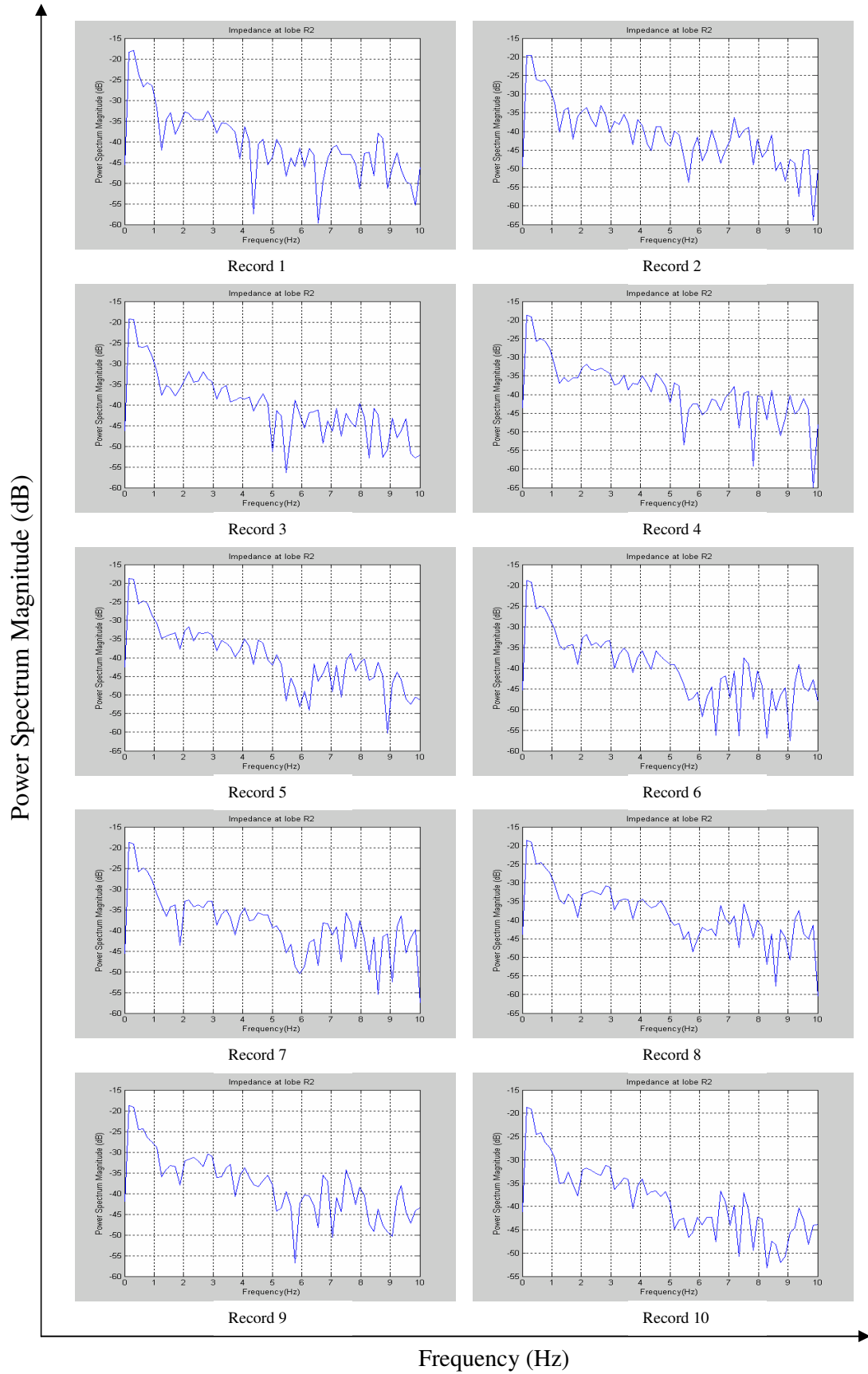


Figure D 26: Power Spectrum of Impedance at lobe R2 when the lung simulator operates at 5 seconds per cycle

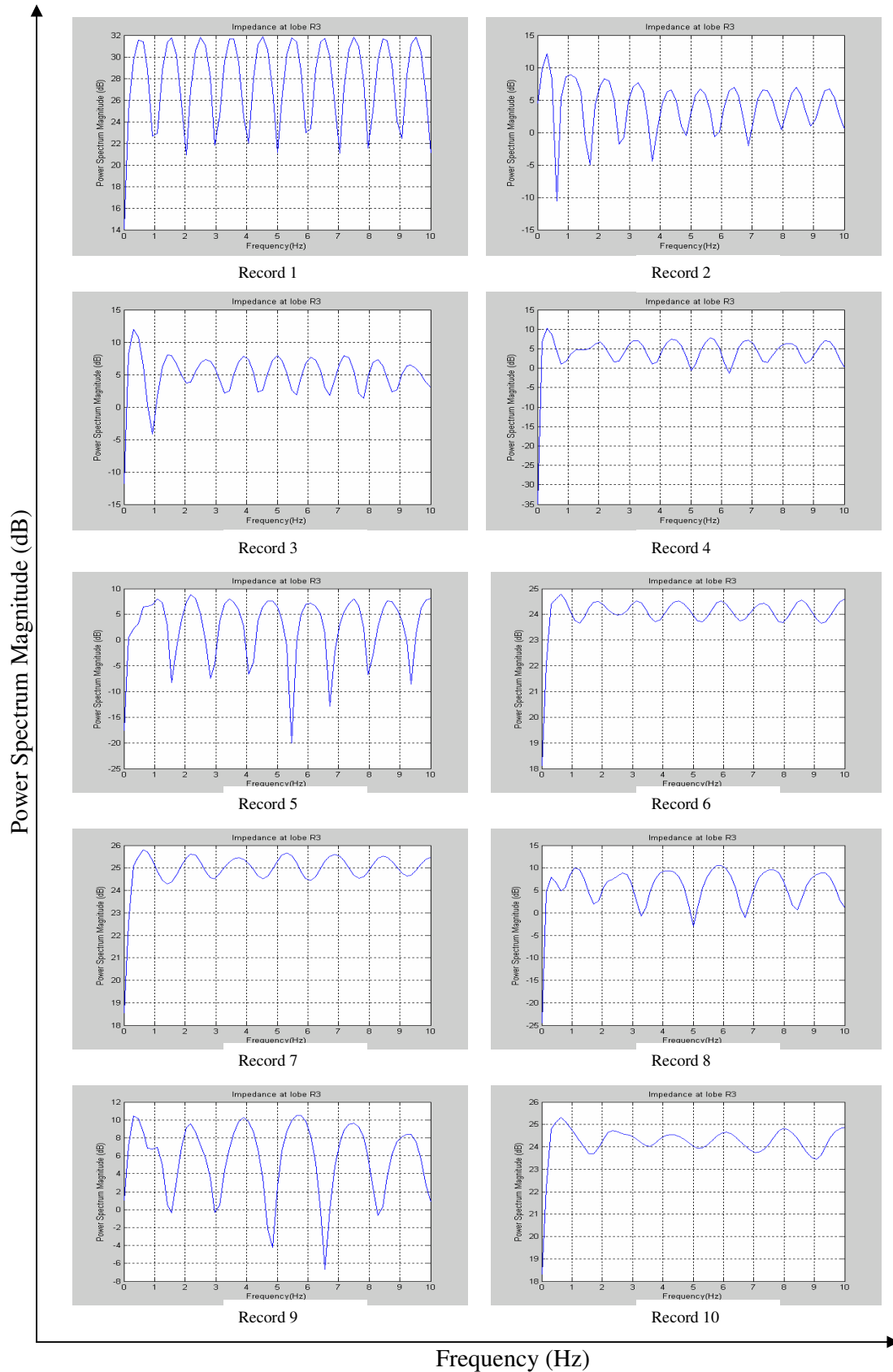


Figure D 27: Power Spectrum of Impedance at lobe R3 when the lung simulator operates at 5 seconds per cycle

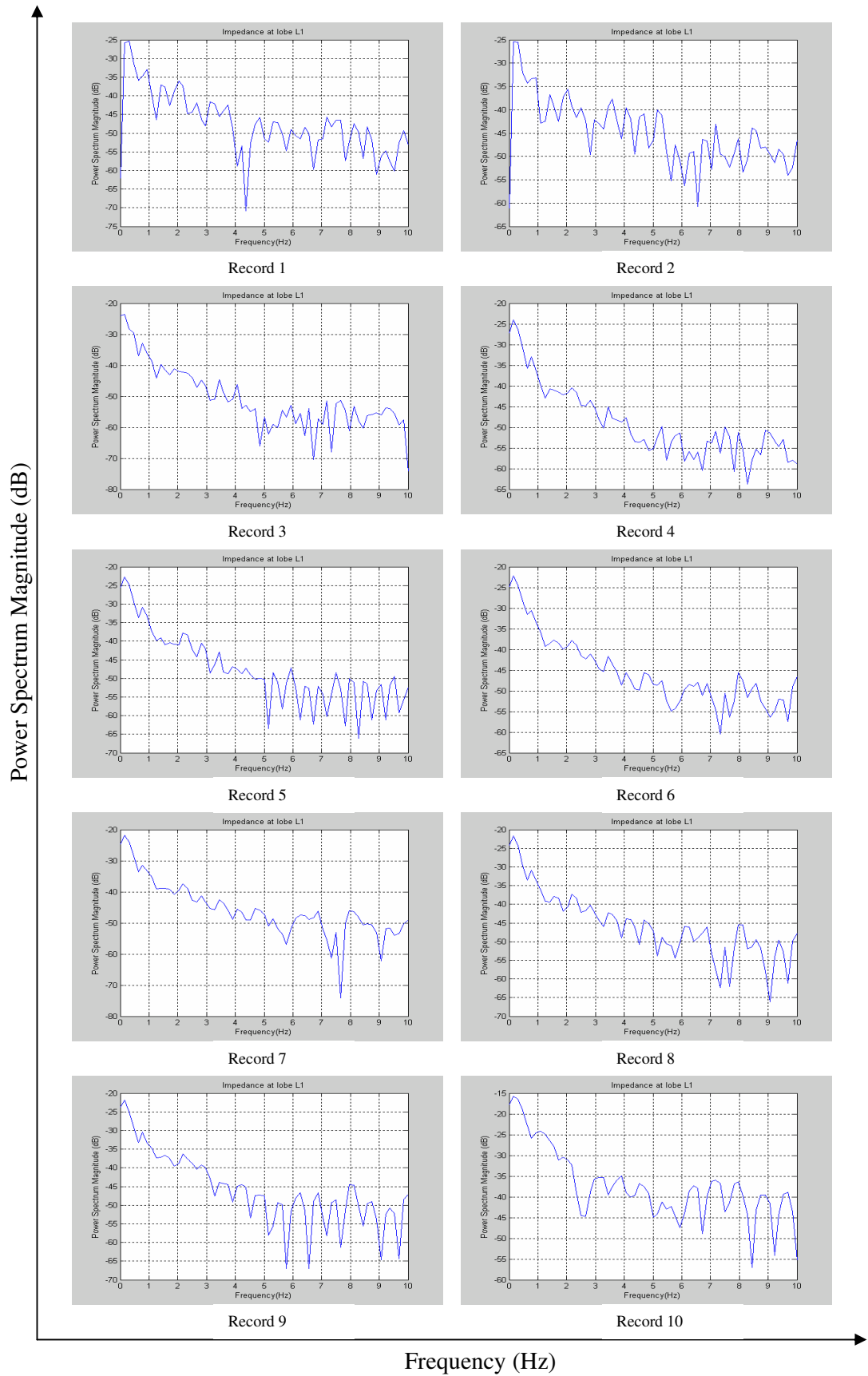


Figure D 28: Power Spectrum of Impedance at lobe L1 when the lung simulator operates at 5 seconds per cycle

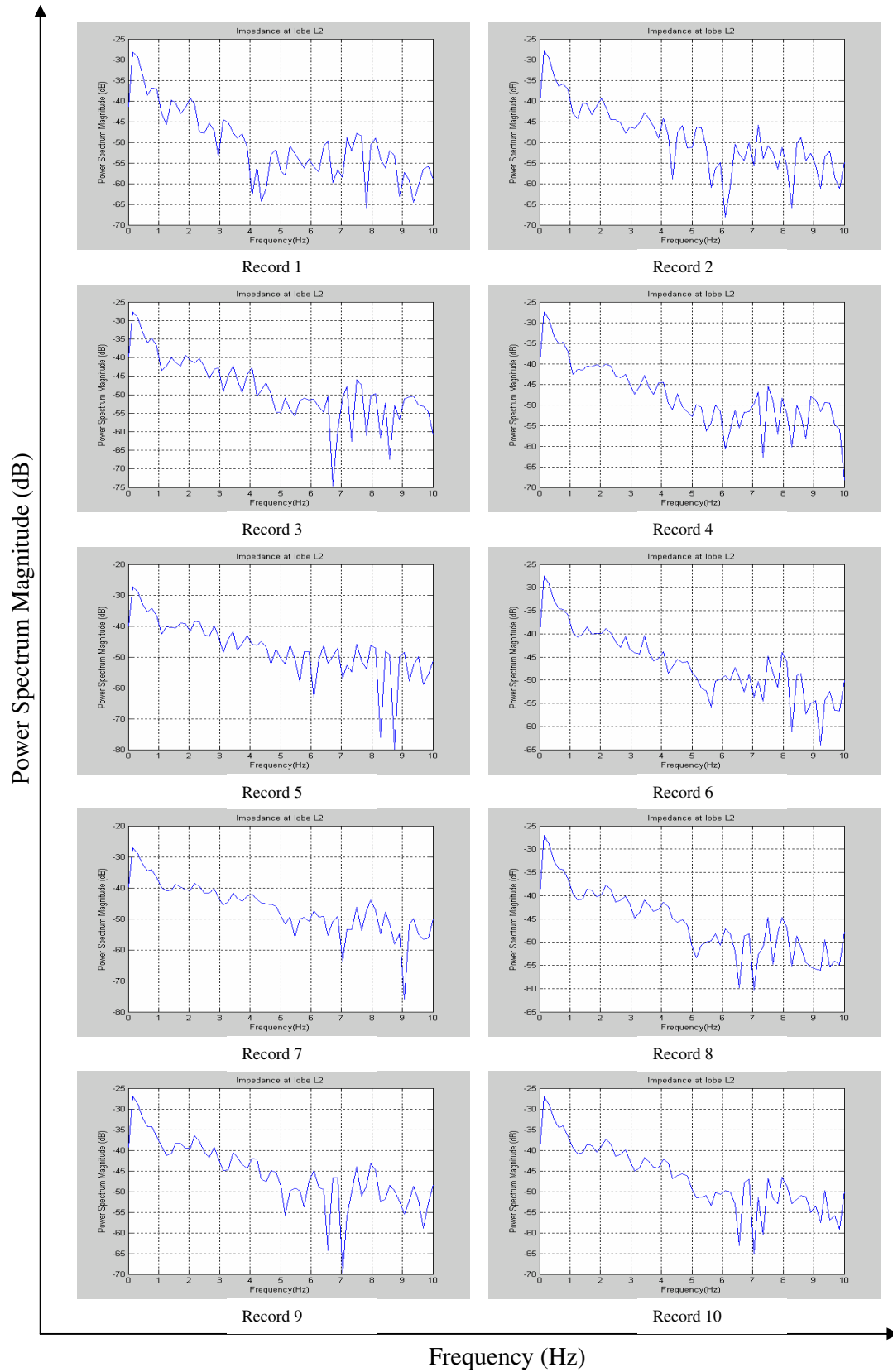


Figure D 29: Power Spectrum of Impedance at lobe L2 when the lung simulator operates at 5 seconds per cycle

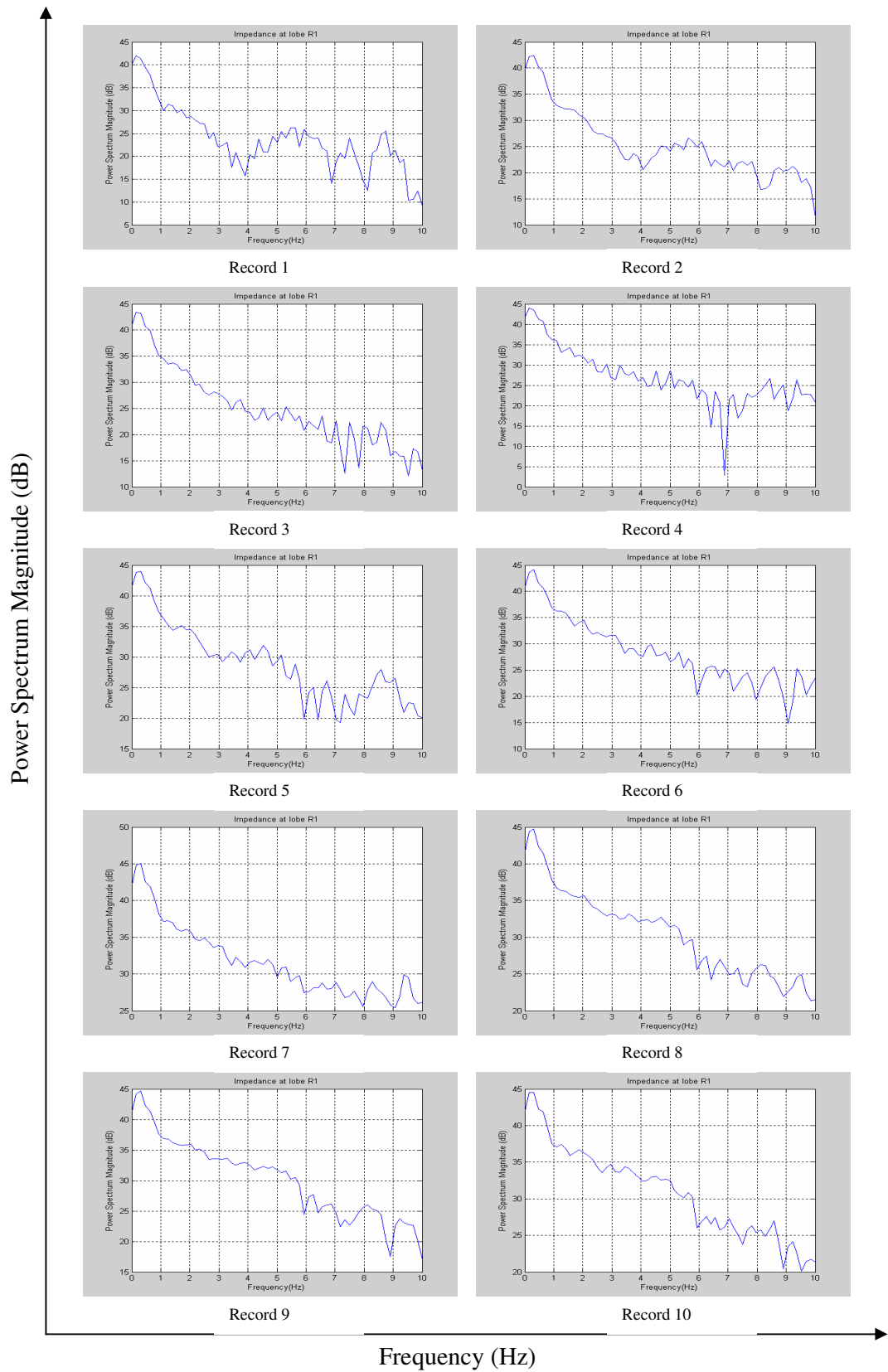


Figure D 30: Power Spectrum of Impedance at lobe R1 when the lung simulator operates at 6 seconds per cycle

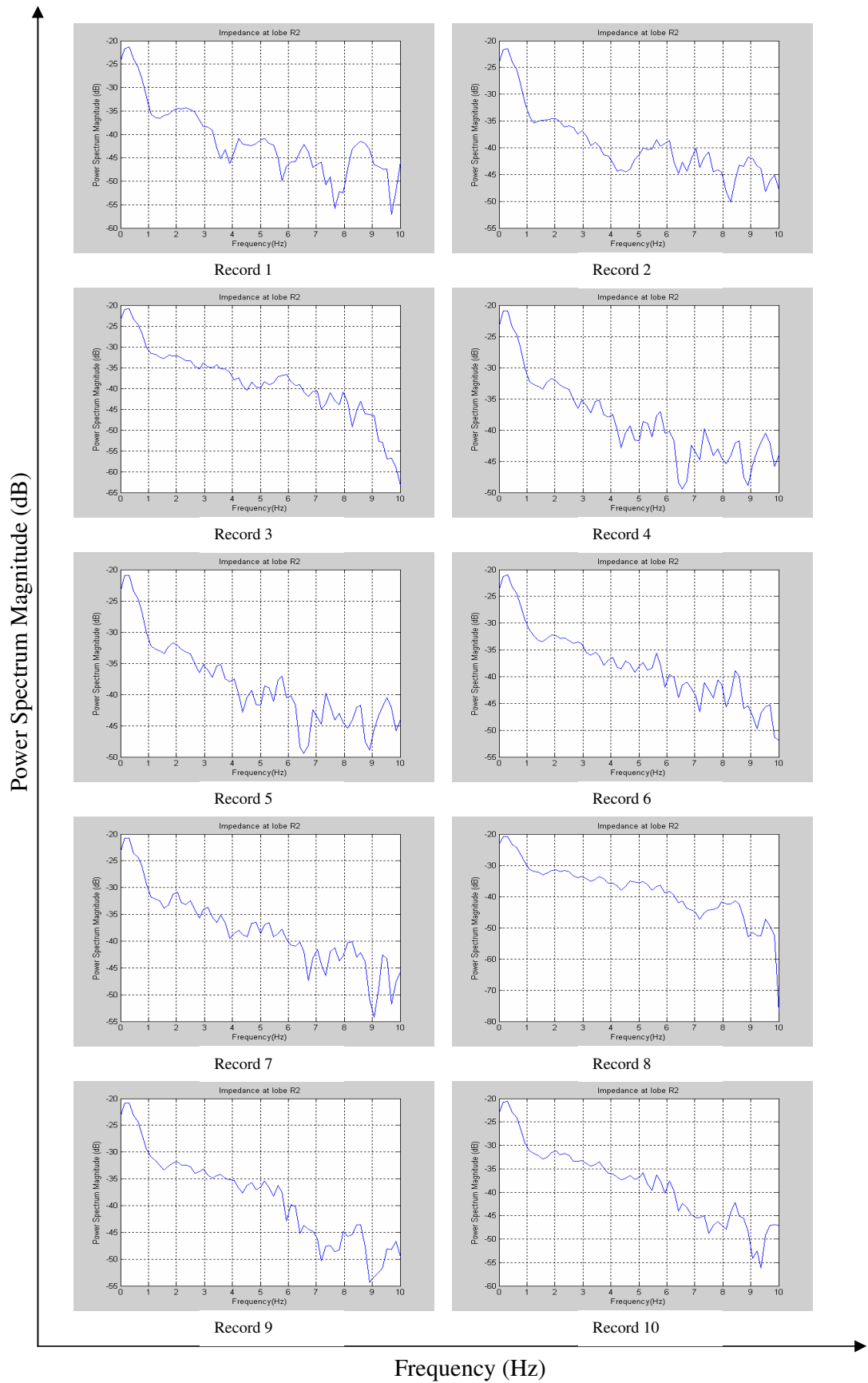


Figure D 31: Power Spectrum of Impedance at lobe R2 when the lung simulator operates at 6 seconds per cycle

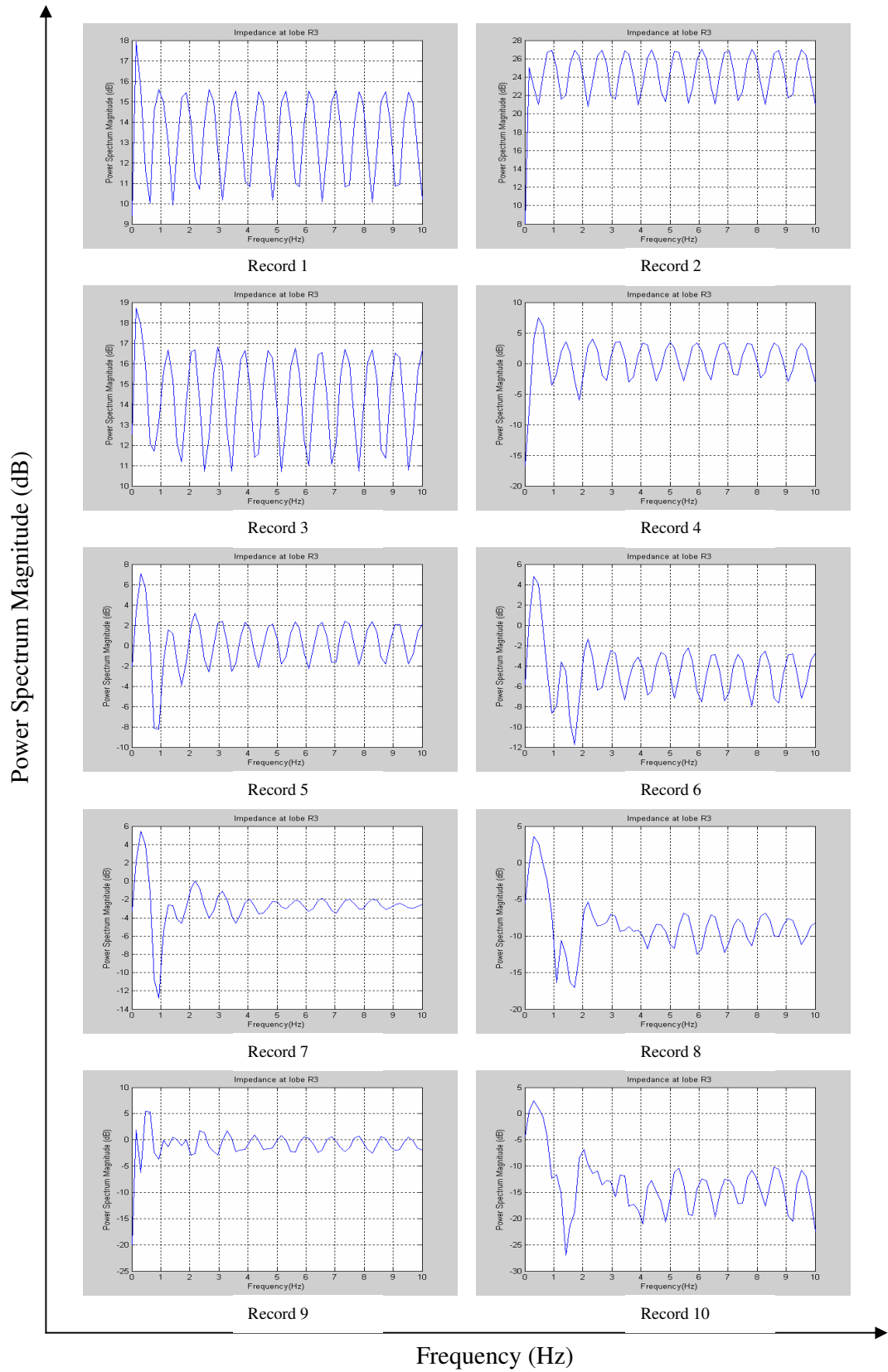


Figure D 32: Power Spectrum of Impedance at lobe R3 when the lung simulator operates at 6 seconds per cycle

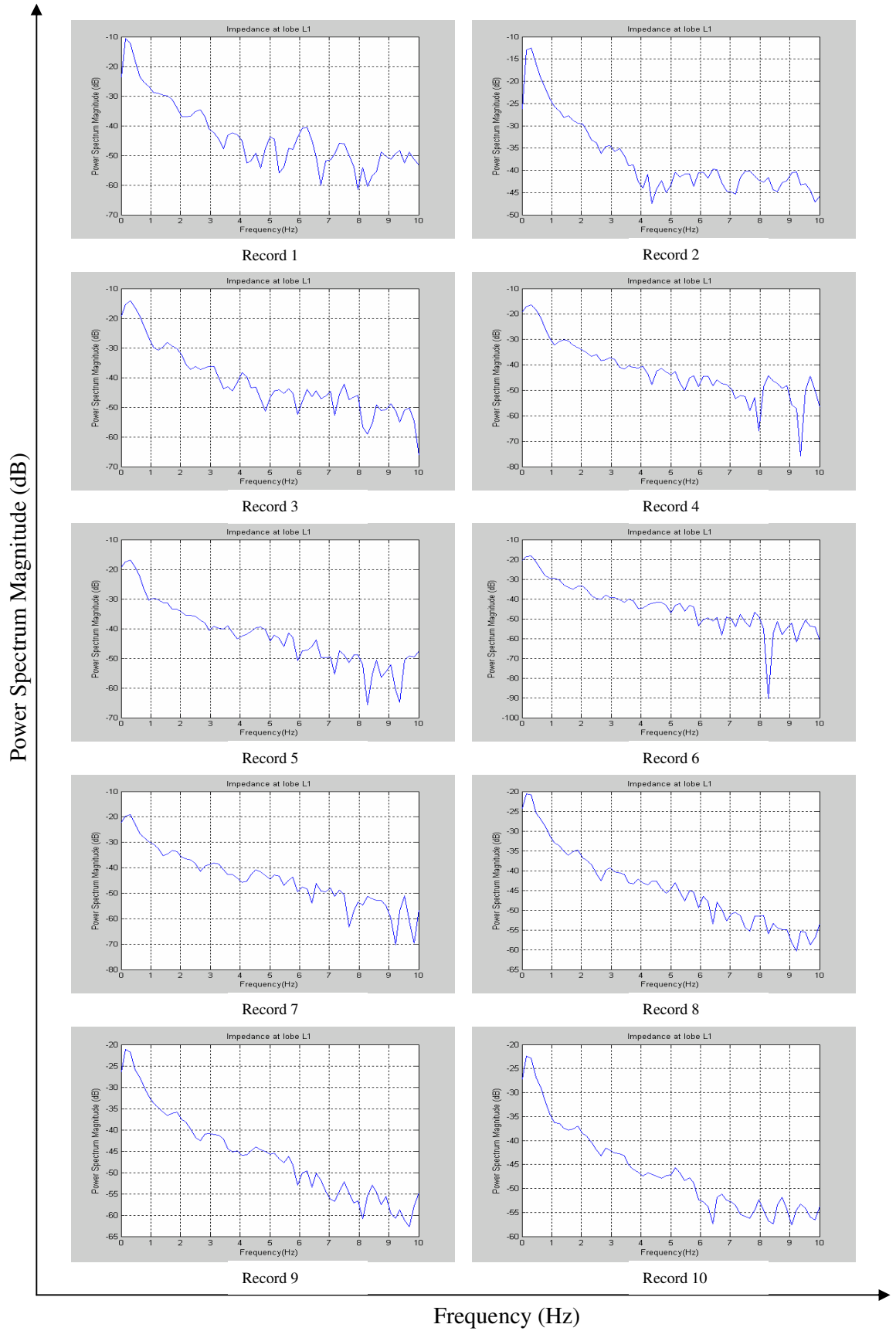


Figure D 33: Power Spectrum of Impedance at lobe L1 when the lung simulator operates at 6 seconds per cycle

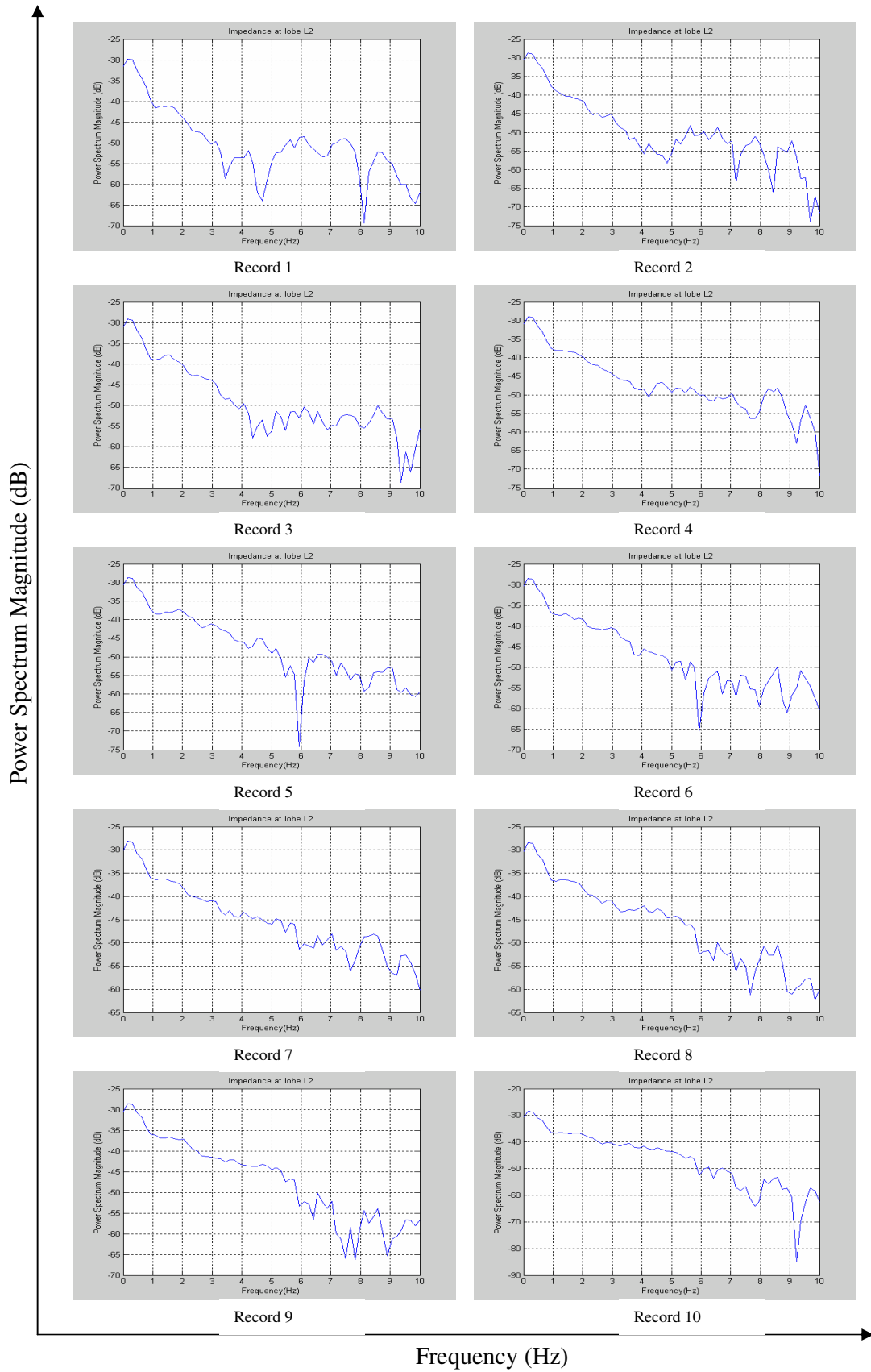


Figure D 34: Power Spectrum of Impedance at lobe L2 when the lung simulator operates at 6 seconds per cycle

APPENDIX E EXPERIMENT INPUT IMPEDANCE RESULTS

For the experiment input impedance of the 5-lobe model, 10 short records for each experiment were done, as discussed in Chapter 3. The results are presented in this Appendix E.

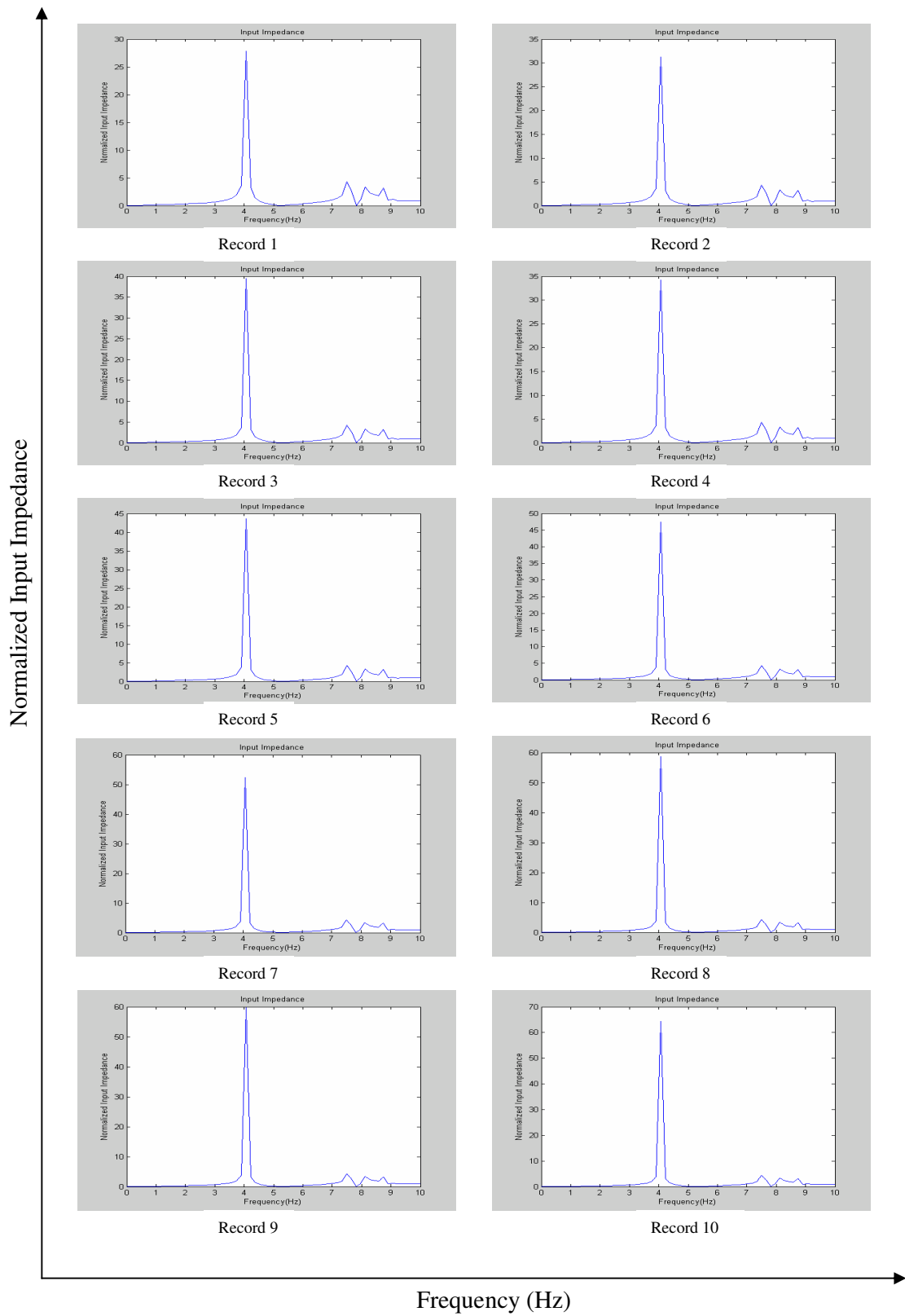


Figure E 1: Input Impedance determined when the lung simulator operates at 1 second per cycle

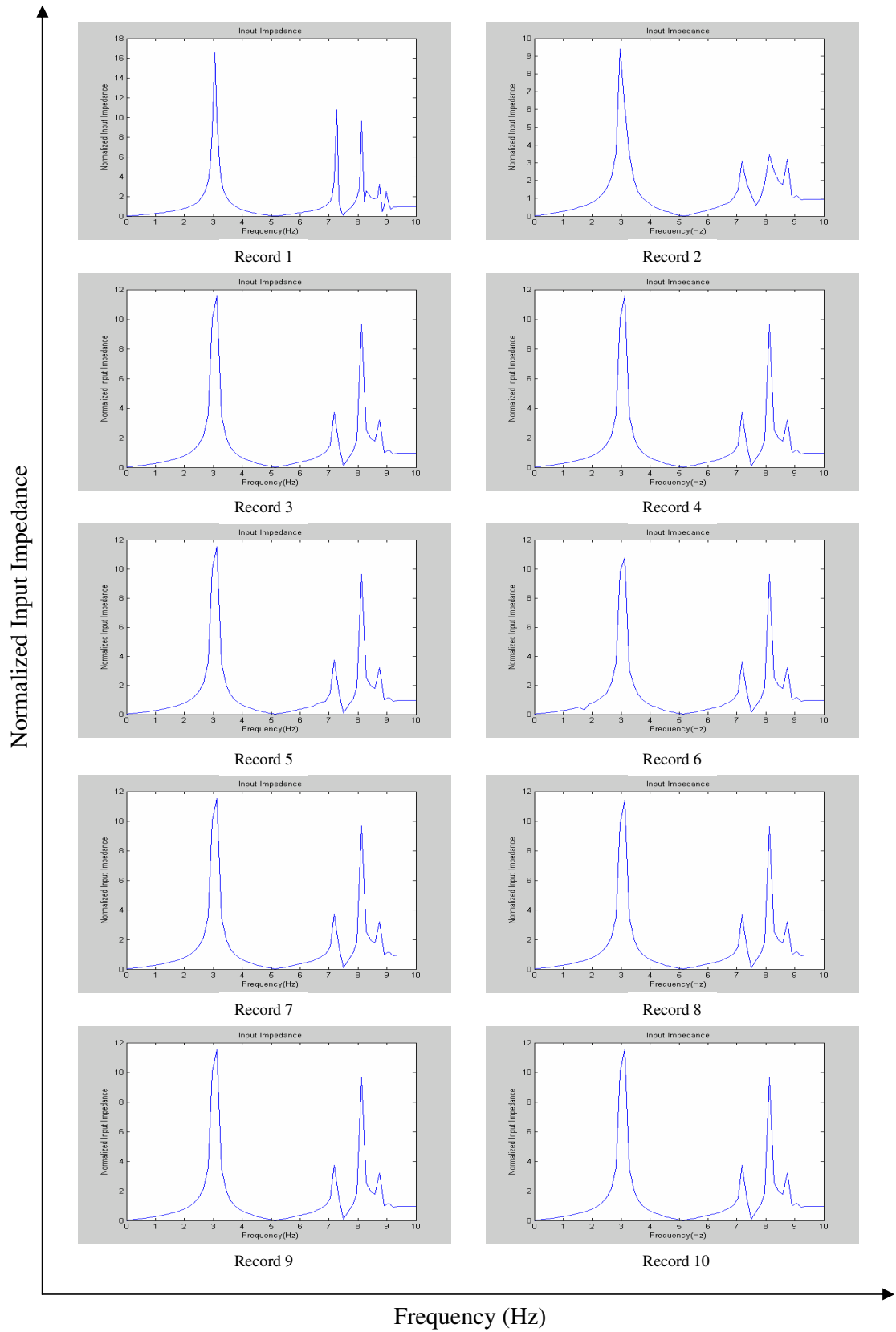


Figure E 2: Experiment Input Impedance determined when the lung simulator operates at 2 seconds per cycle

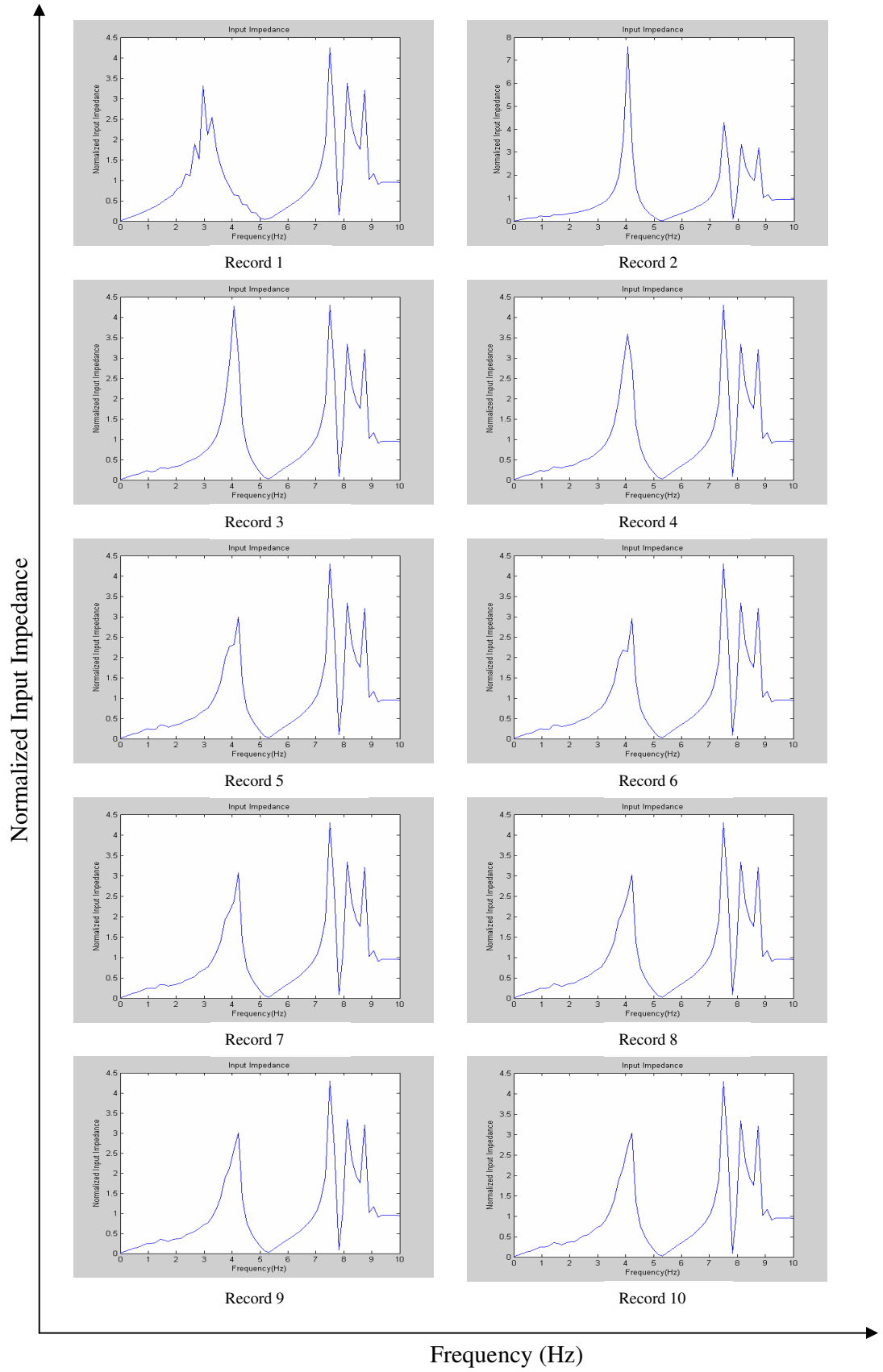


Figure E 3: Experiment Input Impedance determined when the lung simulator operates at 3 seconds per cycle

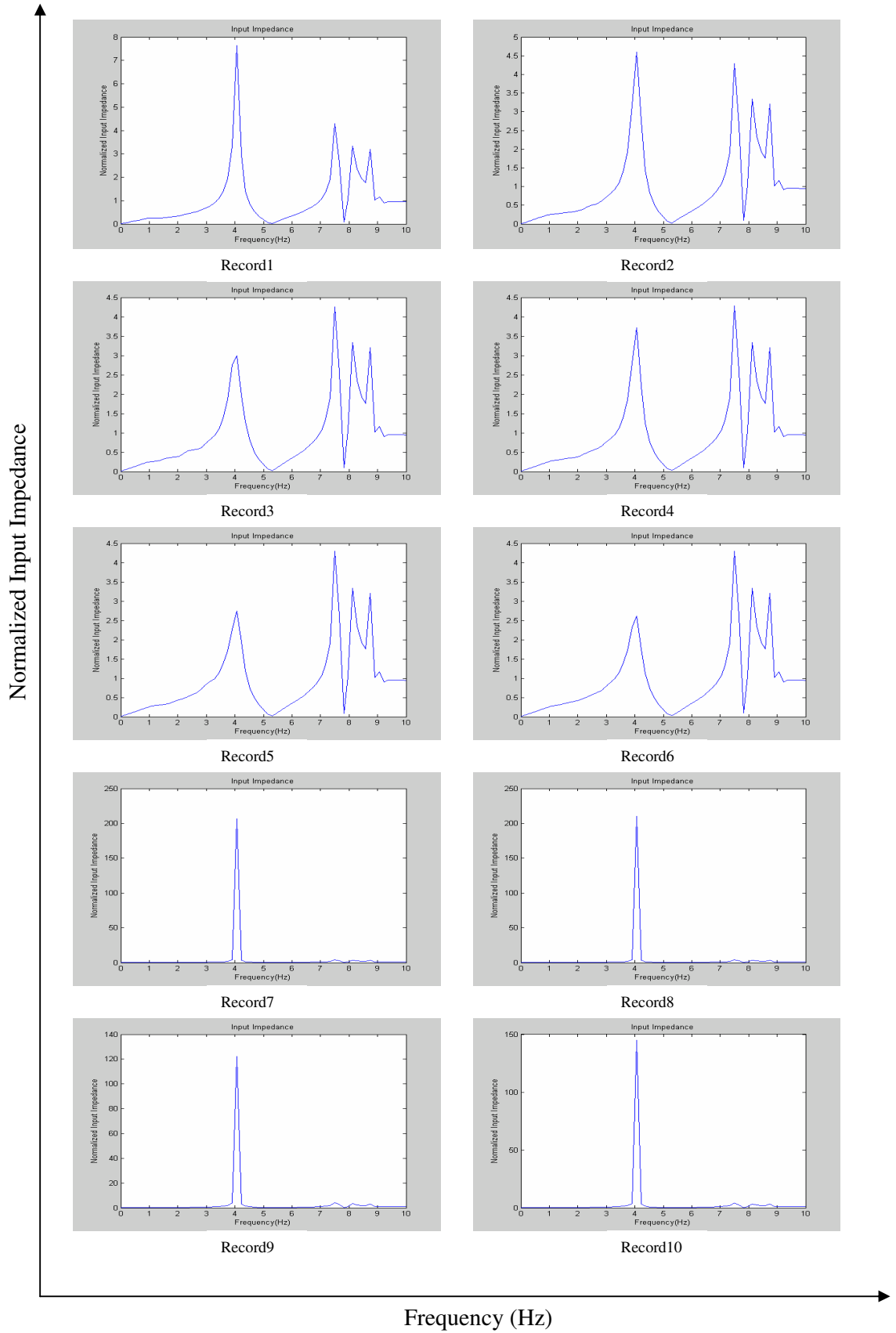


Figure E 4: Experiment Input Impedance determined when the lung simulator operates at 4 seconds per cycle

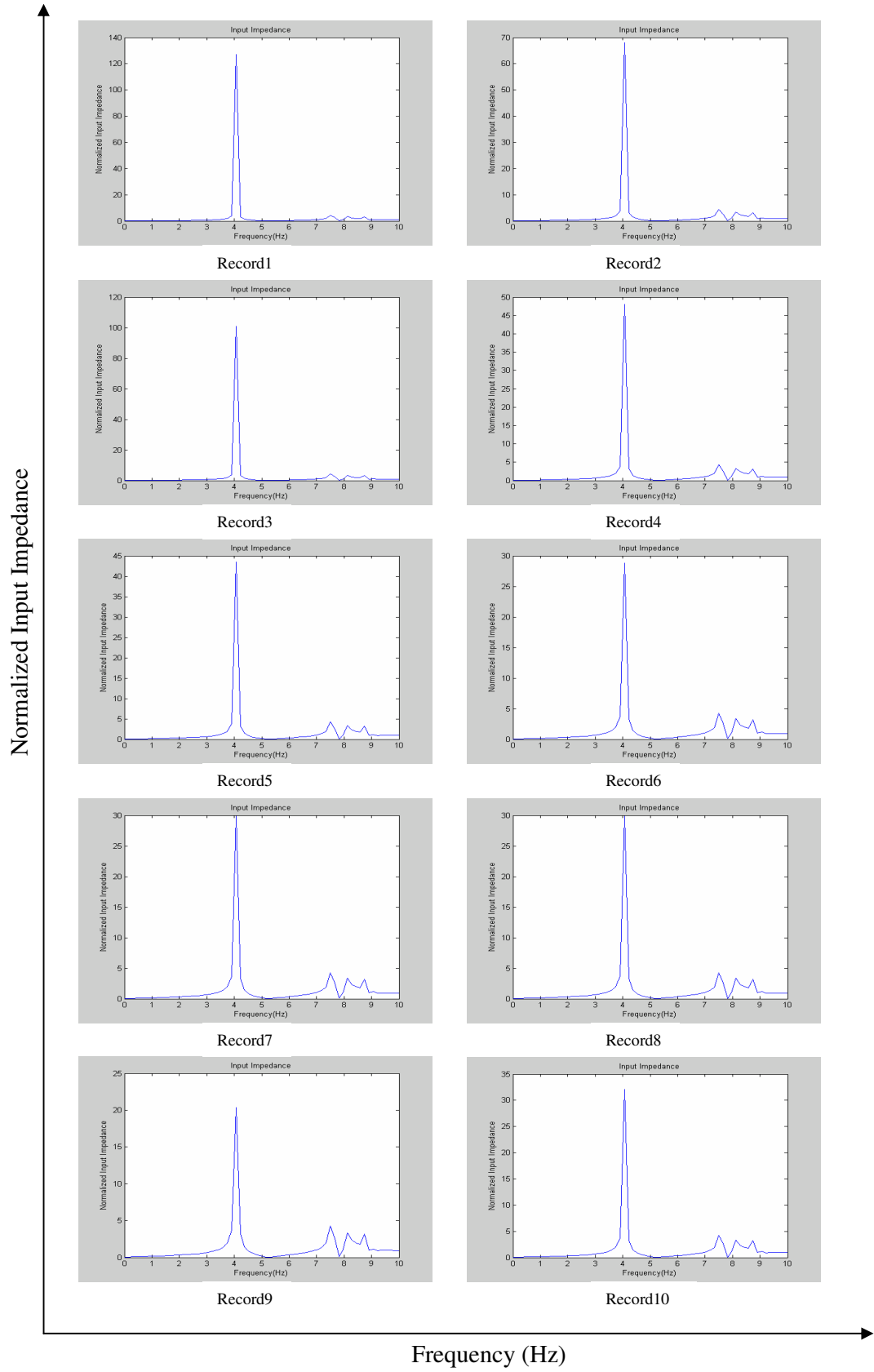


Figure E 5: Experiment Input Impedance determined when the lung simulator operates at 5 seconds per cycle

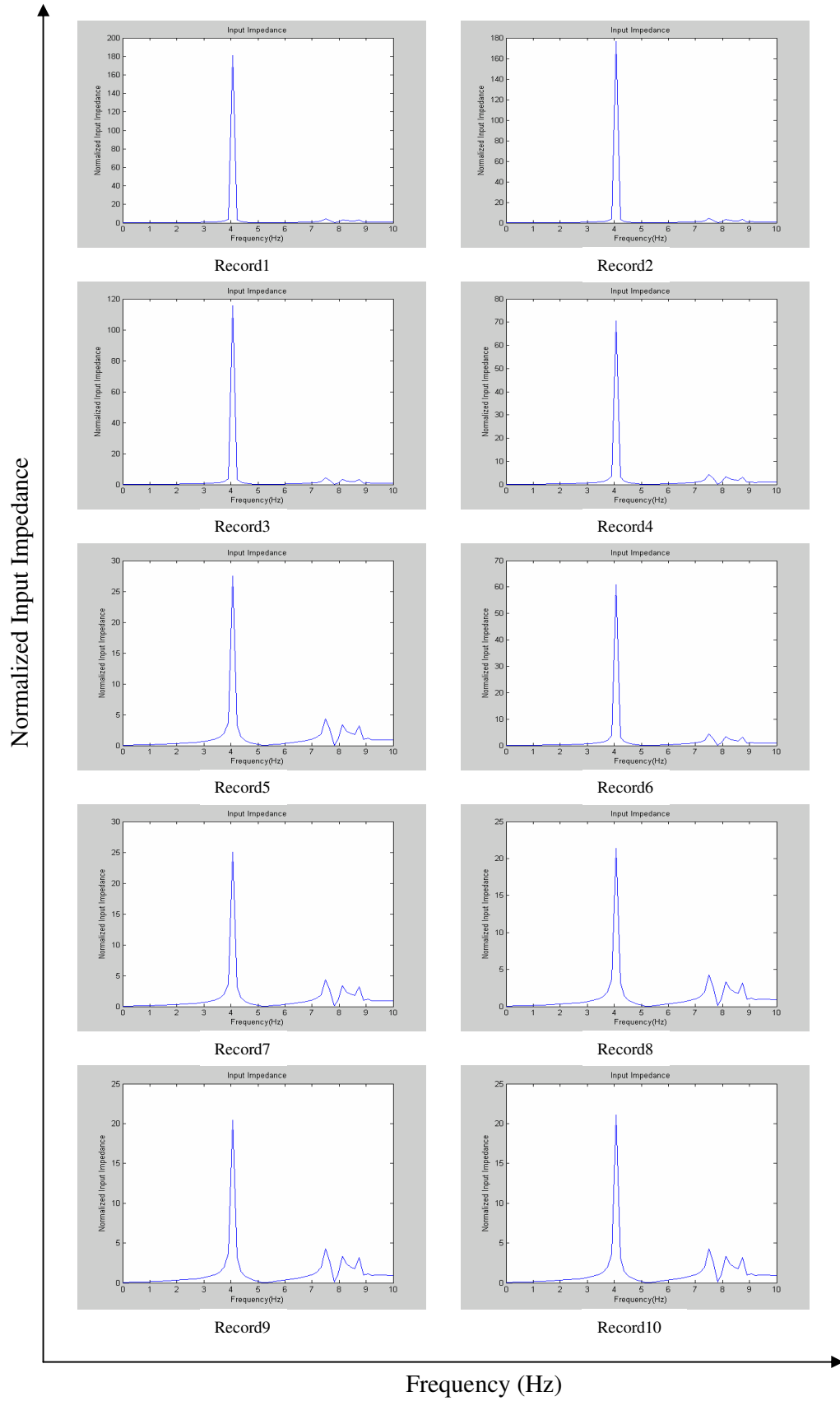


Figure E 6: Experiment Input Impedance determined when the lung simulator operates at 6 seconds per cycle